

**RATIONAL DESIGN OF NANOCARRIERS WITH ENHANCED CARRIER-DRUG
INTERACTION FOR IMPROVED CANCER THERAPY**

by

Peng Zhang

B. Eng. in Pharmaceutical Preparation, Nanjing University of Technology, 2005

M.S. in Medicinal Chemistry, China Pharmaceutical University, 2008

Submitted to the Graduate Faculty of
School of Pharmacy in partial fulfillment
of the requirements for the degree of
Doctor of Philosophy

University of Pittsburgh

2015

UNIVERSITY OF PITTSBURGH
SCHOOL OF PHARMACY

This dissertation was presented

by

Peng Zhang

It was defended on

July 9, 2015

and approved by

Lisa C. Rohan, Ph.D., Associate Professor
Department of Pharmaceutical Sciences, School of Pharmacy
Department of Obstetrics, Gynecology, and Reproductive Sciences, School of Medicine,
Magee-Womens Research Institute, University of Pittsburgh Medical Center
Clinical and Translational Science Institute, University of Pittsburgh

Shilpa Sant, Ph.D., Assistant Professor
Department of Pharmaceutical Sciences, School of Pharmacy
Departments of Bioengineering, Swanson School of Engineering, University of Pittsburgh

Y.P. Peter Di, Ph.D. MBA, Assistant Professor
Director, Inhalation Exposure Facility
Chair, Chemical and Hygiene Safety Committee
Department of Environmental and Occupational Health, University of Pittsburgh

Dissertation Advisor: **Song Li**, M.D., Ph.D., Professor
Center for Pharmacogenetics, Department of Pharmaceutical Sciences, School of Pharmacy
University of Pittsburgh Cancer institute
University of Pittsburgh

Copyright © by Peng Zhang

2015

**RATIONAL DESIGN OF NANOCARRIERS WITH ENHANCED CARRIER-DRUG
INTERACTION FOR IMPROVED CANCER THERAPY**

Peng Zhang, Ph.D.

University of Pittsburgh, 2015

Micelles are simple and effective nanocarriers in formulating hydrophobic agents. However, limited drug loading capacity and intrinsic poor formulation stability of micelles represent two major issues in the bench-to-bedside translation, which are largely attributed to the insufficient carrier-drug interaction. The aim of my dissertation study is to gain more insight into the molecular basis of carrier-drug interactions, and develop effective strategies to improve the compatibility of nanomicelles with chemotherapeutic agents for more efficient *in vivo* delivery.

Firstly, we demonstrated that introduction of additional mechanisms of carrier-drug interaction is an effective strategy to improve drug loading and stability of nanomicelles. We interfacially decorated micelle-forming PEG-lipids with Fmoc motifs that can effectively interact with drug molecules through π - π stacking and hydrogen bonding interactions. The resulting lipid vector showed dramatically enhanced effectiveness in formulating paclitaxel (PTX) and several other agents with diverse structures.

To clearly address the molecular basis of Fmoc/drug interaction, a new model was established by using a simple PEG-Fmoc conjugate without lipid chains. Interestingly, this system demonstrated a significant improvement in PTX encapsulation (36%, w/w). Our data indicated a strong Fmoc/PTX intermolecular π - π stacking, which may play a major role in the overall

carrier-drug interaction, and high effectiveness of PEG-Fmoc in delivery of PTX to tumor cells *in vitro* and *in vivo*.

A further SAR study was conducted to investigate the impact of Fmoc neighboring group on the overall carrier-drug interactions. This study identified several factors that may impact the performance of micelles, which led to the discovery of Cbz as a favored neighboring group of Fmoc for effective interaction with a broad range of drugs. Based on this discovery, a nanocarrier with expanded interior volume was developed for co-delivery of multi-agents in combination chemotherapy. A dramatically enhanced anti-tumor activity over single agent therapy was achieved in both cultured cancer cells and tumor-bearing animal models.

In summary, incorporation of additional mechanisms of carrier-drug interactions significantly enhanced *in vitro* and *in vivo* performance of nanomicelles. Comprehensive SAR studies of carrier-drug interactions led to the discovery of several simple and effective nanocarriers for improved delivery of chemotherapeutic agents to tumors.

TABLE OF CONTENTS

| | |
|--|--------------|
| PREFACE..... | XXIII |
| 1.0 INTRODUCTION..... | 1 |
| 1.1 NANOMEDICINE IN CANCER CHEMOTHERAPY | 1 |
| 1.1.1 Current issues in cancer chemotherapy..... | 1 |
| 1.1.2 Advantages of nanomedicine in cancer chemotherapy | 2 |
| 1.2 MICELLES AS AN EFFECTIVE NANOCARRIER FOR CHEMOTHERAPEUTIC AGENTS | 3 |
| 1.2.1 An overview of micellar system | 3 |
| 1.2.2 Advances in improvement of carrier/drug compatibility..... | 6 |
| 1.2.3 Discovery of 9-Fluorenylmethoxycarbonyl (Fmoc) as interfacial drug-interactive motif | 8 |
| 2.0 DESIGN AND EVALUATION OF A PEGYLATED LIPOPEPTIDE EQUIPPED WITH DRUG-INTERACTIVE MOTIFS AS AN IMPROVED DRUG CARRIER | 11 |
| 2.1 BACKGROUND | 11 |
| 2.2 METHODS | 13 |
| 2.2.1 Materials | 13 |
| 2.2.2 Cell culture | 13 |
| 2.2.3 Synthesis of PEG₅₀₀₀-Lys-(α-Fmoc-ϵ-oleoyl lysine)₂ (PEG₅₀₀₀-(Fmoc-OA)₂) | 14 |
| 2.2.4 Synthesis of PEG₅₀₀₀-OA₂..... | 16 |
| 2.2.5 Preparation and characterization of drug-loaded micelles..... | 16 |

| | | |
|--------|--|----|
| 2.2.6 | Determination of the critical micelle concentration (CMC) | 17 |
| 2.2.7 | Fluorescence quenching study | 17 |
| 2.2.8 | Changes of particle sizes before and after lyophilization/reconstitution | 18 |
| 2.2.9 | <i>In vitro</i> drug release | 18 |
| 2.2.10 | <i>In vitro</i> cytotoxicity | 18 |
| 2.2.11 | Animals | 19 |
| 2.2.12 | <i>In vivo</i> tumor inhibition study | 19 |
| 2.2.13 | Statistical analysis | 20 |
| 2.3 | RESULTS | 21 |
| 2.3.1 | Synthesis and characterization of PEG ₅₀₀₀ -lipopeptide with drug- interactive motifs..... | 21 |
| 2.3.2 | Biophysical characterization of drug-free and PTX-loaded PEG- lipopeptide micelles..... | 24 |
| 2.3.3 | Release kinetics of PTX-loaded mixed micelles..... | 28 |
| 2.3.4 | <i>In vitro</i> cytotoxicity study | 30 |
| 2.3.5 | <i>In vivo</i> antitumor activity | 31 |
| 2.3.6 | Effectiveness of PEG ₅₀₀₀ -(Fmoc-OA) ₂ micelles in formulating 7 other drugs of differents..... | 32 |
| 2.4 | DISCUSSION | 33 |
| 3.0 | A PEG-FMOC CONJUGATE AS A NANOCARRIER FOR PACLITAXEL..... | 37 |
| 3.1 | BACKGROUND | 37 |
| 3.2 | METHODS | 39 |
| 3.2.1 | Materials | 39 |

| | | |
|--------|---|----|
| 3.2.2 | Synthesis of PEG ₅₀₀₀ -lysyl-(α -Fmoc- ϵ -t-Boc-lysine) ₂ (PEG-Fmoc) | 40 |
| 3.2.3 | Preparation and biophysical characterization of PTX/PEG-Fmoc mixed micelles | 40 |
| 3.2.4 | Effect of lyophilization/reconstitution on particle sizes..... | 41 |
| 3.2.5 | Differential scanning calorimetry (DSC) analysis | 42 |
| 3.2.6 | Fluorescence quenching..... | 42 |
| 3.2.7 | <i>In vitro</i> drug release kinetics | 42 |
| 3.2.8 | Cell culture | 43 |
| 3.2.9 | <i>In vitro</i> cytotoxicity study | 43 |
| 3.2.10 | Animals | 44 |
| 3.2.11 | Maximum tolerated dose (MTD) study..... | 44 |
| 3.2.12 | Fluorescence optical imaging | 44 |
| 3.2.13 | <i>In vivo</i> therapeutic efficacy | 45 |
| 3.2.14 | Statistical analysis | 46 |
| 3.3 | RESULTS AND DISCUSSION | 46 |
| 3.3.1 | Design, preparation, and characterization of PEG-Fmoc/PTX mixed micelles | 46 |
| 3.3.2 | Mechanism of carrier/drug interactions..... | 52 |
| 3.3.3 | Effect of lyophilization/reconstitution on PEG-Fmoc/PTX mixed micelles | 57 |
| 3.3.4 | Release kinetics of PTX from PEG-Fmoc/PTX mixed micelles..... | 58 |
| 3.3.5 | <i>In vitro</i> cytotoxicity of PEG-Fmoc/PTX..... | 59 |

| | | |
|--------|---|----|
| 3.3.6 | Biodistribution of PEG-Fmoc/PTX micelles through NIR fluorescent optical imaging | 60 |
| 3.3.7 | Maximum tolerated dose (MTD) study..... | 62 |
| 3.3.8 | <i>In vivo</i> therapeutic efficacy of PEG-Fmoc/PTX..... | 63 |
| 3.3.9 | Summary..... | 65 |
| 4.0 | PEGYLATED FMOC-AMINO ACID CONJUGATES AS EFFECTIVE NANOCARRIERS FOR IMPROVED DRUG DELIVERY | 66 |
| 4.1 | BACKGROUND | 66 |
| 4.2 | METHODS | 68 |
| 4.2.1 | Materials | 68 |
| 4.2.2 | Synthesis of PEG ₂₀₀₀ -Fmoc-amino acid conjugates (PFA) | 68 |
| 4.2.3 | Preparation and biophysical characterization of PTX/PFA mixed micelles | 69 |
| 4.2.4 | Fluorescence quenching..... | 70 |
| 4.2.5 | Reconstituability of PTX/PFA mixed micelles following lyophilization | 70 |
| 4.2.6 | PTX release kinetics..... | 70 |
| 4.2.7 | Cell culture | 71 |
| 4.2.8 | <i>In vitro</i> cytotoxicity study | 71 |
| 4.2.9 | Animals | 72 |
| 4.2.10 | Maximum tolerated dose (MTD) study..... | 72 |
| 4.2.11 | <i>In vivo</i> therapeutic efficacy | 72 |
| 4.2.12 | Statistical analysis | 73 |
| 4.3 | RESULTS | 73 |

| | | |
|--------|--|----|
| 4.3.1 | Synthesis and characterization of PFA conjugates..... | 73 |
| 4.3.2 | Effectiveness of PFA in formulating PTX | 74 |
| 4.3.3 | Further biophysical characterization of drug-free and PTX-loaded PFA micelles | 77 |
| 4.3.4 | Effect of PFA structure on the carrier-drug and carrier-carrier interactions | 79 |
| 4.3.5 | Reconstituability of PTX/PFA mixed micelles following lyophilization | 81 |
| 4.3.6 | PTX release kinetics..... | 82 |
| 4.3.7 | <i>In vitro</i> cytotoxicity | 83 |
| 4.3.8 | Maximum tolerated dose (MTD) study..... | 84 |
| 4.3.9 | <i>In vivo</i> therapeutic efficacy | 85 |
| 4.3.10 | Effectiveness of PFA ₂ micelles in formulating a broad variety of drug molecules..... | 86 |
| 4.4 | DISCUSSION | 87 |
| 5.0 | EFFECTIVE CO-DELIVERY OF DOXORUBICIN AND DASATINIB USING A PEG-FMOC NANOCARRIER FOR COMBINATION CANCER CHEMOTHERAPY... | 92 |
| 5.1 | BACKGROUND | 92 |
| 5.2 | METHODS | 94 |
| 5.2.1 | Materials | 94 |
| 5.2.2 | Synthesis of PEG ₅₀₀₀ -lysyl-(α -Fmoc- ϵ -Cbz-lysine) ₂ (PLFCL) | 95 |
| 5.2.3 | Preparation and biophysical characterization of drug-free and drug-loaded PLFCL micelles..... | 96 |
| 5.2.4 | Fluorescence quenching..... | 97 |

| | | |
|--------|--|-----|
| 5.2.5 | UV absorbance spectroscopy | 97 |
| 5.2.6 | <i>In vitro</i> drug release kinetics | 97 |
| 5.2.7 | Cell culture | 98 |
| 5.2.8 | Intracellular trafficking..... | 98 |
| 5.2.9 | <i>In vitro</i> cytotoxicity study | 99 |
| 5.2.10 | Cell migration inhibition | 99 |
| 5.2.11 | Animals | 99 |
| 5.2.12 | <i>In vivo</i> therapeutic efficacy | 100 |
| 5.2.13 | Histochemical staining..... | 101 |
| 5.2.14 | Statistical analysis | 101 |
| 5.3 | RESULTS | 102 |
| 5.3.1 | Combinational effect of DOX&DAS on cancer cell proliferation | 102 |
| 5.3.2 | Design, synthesis, and characterization of PLFCL conjugate | 103 |
| 5.3.3 | Fabrication and biophysical characterization of PLFCL micelles for co-encapsulation of DOX&DAS | 106 |
| 5.3.4 | Demonstration of carrier-drug intermolecular interaction | 109 |
| 5.3.5 | Release kinetics of DOX & DAS from PLFCL micelles..... | 112 |
| 5.3.6 | Intracellular trafficking..... | 112 |
| 5.3.7 | Inhibition of cancer cell proliferation and migration by DOX&DAS/PLFCL micelles..... | 114 |
| 5.3.8 | <i>In vivo</i> therapeutic efficacy and histochemical staining | 116 |
| 5.4 | DISCUSSION | 119 |
| 6.0 | SUMMARY AND PERSPECTIVES | 123 |

BIBLIOGRAPHY..... 127

LIST OF TABLES

| | |
|--|-----|
| Table 1. Biophysical characterization of drug-free and PTX-loaded PEG ₅₀₀₀ -OA ₂ and PEG ₅₀₀₀ -(Fmoc-OA) ₂ micelles. | 26 |
| Table 2. Effectiveness of PEG ₅₀₀₀ -(Fmoc-OA) ₂ micelles in formulating drugs of diverse structures. | 33 |
| Table 3. Characterization of drug-free and PTX-loaded PEG-Fmoc nanomicelles..... | 51 |
| Table 4. Maximum tolerated dose of PEG-Fmoc/PTX and Taxol..... | 63 |
| Table 5. Effectiveness of PFA conjugates in PTX encapsulation..... | 77 |
| Table 6. Characterization of drug-free and PTX-loaded PFA micelles. | 79 |
| Table 7. Maximum tolerated dose of PTX/PFA ₂ micelles..... | 85 |
| Table 8. Effectiveness of PFA ₂ micelles in formulating various therapeutic agents..... | 87 |
| Table 9. Biophysical characterization of drug-free and drug-loaded PLFCL micelles. | 105 |
| Table 10. Broad utility of PLFCL as a nanocarrer for a panel of chemotherapeutic agents..... | 121 |

LIST OF FIGURES

| | |
|--|----|
| Figure 1. Synthetic route of PEG ₅₀₀₀ -(Fmoc-OA) ₂ and PEG ₅₀₀₀ -OA ₂ | 14 |
| Figure 2. Structure of PEG ₅₀₀₀ -(Fmoc-OA) ₂ and the postulated modes of carrier-drug and carrier-carrier interactions. | 22 |
| Figure 3. ¹ H NMR spectrum of PEG ₅₀₀₀ -(Fmoc-OA) ₂ | 22 |
| Figure 4. ¹ H NMR spectrum of PEG ₅₀₀₀ -OA ₂ | 23 |
| Figure 5. MALDI-TOF Mass Spectrum of PEG ₅₀₀₀ -(Fmoc-OA) ₂ | 23 |
| Figure 6. MALDI-TOF Mass Spectrum of PEG ₅₀₀₀ -OA ₂ | 24 |
| Figure 7. Size distribution of PEG ₅₀₀₀ -OA ₂ (A) and PEG ₅₀₀₀ -(Fmoc-OA) ₂ (D) measured by dynamic light scattering (DLS); and transmission electron microscopy (TEM) of PEG ₅₀₀₀ -OA ₂ (B) and PEG ₅₀₀₀ -(Fmoc-OA) ₂ (E) micelles. The spherical particles with a diameter around 20 nm were observed for PEG ₅₀₀₀ -OA ₂ micelles, while filamentous micelles with tubular structure were observed for PEG ₅₀₀₀ -(Fmoc-OA) ₂ micelles. CMC measurements of the PEG ₅₀₀₀ -OA ₂ (C) and PEG ₅₀₀₀ -(Fmoc-OA) ₂ (F) micelles using pyrene as a fluorescence probe. The fluorescence intensity was plotted as a function of logarithmic concentration of micelles..... | 25 |
| Figure 8. Fluorescence quenching of PEG ₅₀₀₀ -(Fmoc-OA) ₂ . The concentration of PEG ₅₀₀₀ -(Fmoc-OA) ₂ was fixed at 1.5 mg/mL, and mixed with PTX and Chol at designated molar ratios in PBS. Intensity of fluorescence emitted between 300-460 nm was recorded with excitation wavelength at 270 nm. | 27 |

Figure 9. ¹H NMR spectra of PTX/PEG₅₀₀₀-(Fmoc-OA)₂ in D₂O and CDCl₃. Carrier/drug molar ratio was retained at 2.5:1. 28

Figure 10. Particle size distribution before (A) and after (B) lyophilization and reconstitution of PTX-loaded PEG₅₀₀₀-(Fmoc-OA)₂ micelles. No obvious size change was observed. PTX concentration in micelles was at 1 mg/mL. 29

Figure 11. Cumulative PTX release profile from PTX-loaded PEG₅₀₀₀-(Fmoc-OA)₂ micelles (Fmoc-OA/PTX), PEG₅₀₀₀-OA₂ micelles (OA/PTX) and Taxol. PTX concentration was kept at 1 mg/mL in all the formulations, and DPBS (pH 7.4) containing 0.5% (w/v) Tween 80 was utilized as release medium. 29

Figure 12. Cytotoxicity of PTX-loaded PEG₅₀₀₀-(Fmoc-OA)₂ micelles, drug-free PEG₅₀₀₀-(Fmoc-OA)₂ micelles, and Taxol to 4T1.2 mouse breast cancer cell line (A), human prostate cancer cell lines PC-3 (B), and DU145 (C). Cells were treated for 72 h and cytotoxicity was determined by MTT assay. 30

Figure 13. (A) Tumor inhibitory activity of PTX-loaded PEG₅₀₀₀-(Fmoc-OA)₂ micelles. BALB/c mice were inoculated s.c. with 4T1.2 cells (2×10⁵ cells/mouse). Five days later, mice received various treatments on days 1, 3, 5, 7 and 9, and tumor growth was monitored and plotted as relative tumor volume. **P* < 0.05 (PEG₅₀₀₀-(Fmoc-OA)₂/PTX at 10 mg/kg vs. Taxol at 10 mg/kg). ***P* < 0.01 (PEG₅₀₀₀-(Fmoc-OA)₂/PTX at 10 mg/kg vs. Taxol at 10 mg/kg). N=4. (B) Changes of body weight in mice in different treatment groups. 31

Figure 14. Chemical structure of seven drug candidates effectively formulated in PEG₅₀₀₀-(Fmoc-OA)₂ micelles. A, probucol; B, niclosamide; C, JP4-039; D, progesterone; E, cyclosporin A; F, nifedipine; and G, griseofulvin. 32

| | |
|---|----|
| Figure 15. Synthetic route of PEG-Fmoc (A), and schematic representation of self-assembled PEG-Fmoc/PTX mixed micelle based on carrier/drug intermolecular π - π stacking (B)..... | 47 |
| Figure 16. $^1\text{H-NMR}$ spectrum of PEG-Fmoc..... | 48 |
| Figure 17. MALDI-TOF mass spectrum of PEG-Fmoc. | 48 |
| Figure 18. TEM image of PEG-Fmoc micelles at 5 mg/mL in DPBS using negative staining... | 49 |
| Figure 19. Biophysical characterization of PEG-Fmoc nanomicelles. (A) Particle size distribution of PEG-Fmoc/PTX nanomicelles at 1 mg PTX/mL in DPBS with a carrier/drug ratio of 0.75:1 (m/m) via DLS measurement; (B) TEM image of PEG-Fmoc/PTX nano-micelles with PTX concentration at 1 mg/mL using negative staining; (C) Critical micelle concentration (CMC) measurement of PEG-Fmoc using pyrene as a fluorescence probe. | 50 |
| Figure 20. $^1\text{H-NMR}$ spectra of PEG-Fmoc/PTX in CDCl_3 and D_2O . The suppressed proton signals of Fmoc motifs and PTX in D_2O indicated the self-assembly of PEG-Fmoc micelles in aqueous solution and entrapment of PTX into the interior core of PEG-Fmoc micelles. | 51 |
| Figure 21. DSC thermograms of PTX alone, PEG-Fmoc/PTX mixed micelles, and drug-free PEG-Fmoc micelles. | 53 |
| Figure 22. Fluorescence quenching study. Fluorescence intensity of PEG-Fmoc (A) at 300- 460 nm was recorded with an excitation wavelength at 270 nm, and compared with its lipid-bearing counterpart PEG-Fmoc-OA (B). Both PEG-Fmoc and PEG-Fmoc-OA were kept at 0.88 mM for comparison, and all carrier/drug ratios were reported as molar ratios..... | 54 |
| Figure 23. Chemical structures of paclitaxel (PTX) (A), docetaxel (DTX) (B), and cholesterol (CHOL) (C)..... | 54 |
| Figure 24. Fluorescence quenching caused by different hydrophobic molecules. PEG-Fmoc micelles loaded with different hydrophobic drugs (PTX, DTX, and CHOL) were prepared, | |

respectively, at a carrier/drug molar ratio of 5:1 and PEG-Fmoc concentration of 1.17 mM, and the emission fluorescence intensity was detected at 305 nm. The fluorescence quenching ratio (%) was calculated as: $(1 - (\text{fluorescence intensity of drug-loaded PEG-Fmoc} / \text{fluorescence intensity of drug-free PEG-Fmoc})) \times 100\%$ 55

Figure 25. ^{13}C -NMR of carrier-mixed (A & B) and carrier-free PTX (C) in CDCl_3 . PTX was mixed with PEG_{550} - α -Fmoc- ϵ -t-Boc-lysine at a drug/carrier molar ratio of 1:10 (A) and 1:3 (B), respectively. Average shift index (Δ) was calculated as the average absolute value of chemical shift changes of all the six carbon atoms on the same aromatic ring compared with free PTX (C). 56

Figure 26. ^{13}C NMR of free PTX and PTX/Fmoc-Lys (Boc)-OH in CDCl_3 . PTX was mixed with Fmoc-Lys (Boc)-OH at a drug/carrier molar ratio of 1:10 (A), 1:3 (B) and 1:1 (C), and then subjected to ^{13}C NMR analysis. Free PTX (D) was used as a control. 57

Figure 27. Size distribution of PEG-Fmoc/PTX mixed micelles with PTX concentration at 1 mg/mL before (A) and after (B) lyophilization/reconstitution. 58

Figure 28. PTX release kinetics of PEG-Fmoc/PTX examined via a dialysis method. PTX concentrations in PEG-Fmoc/PTX and Taxol were kept at 1 mg/mL, and DPBS containing 0.5% (w/v) Tween 80 was utilized as release medium. PTX concentration was analyzed at 0, 1, 2, 4, 8, 24, 48 and 72 h using HPLC at 227 nm. 59

Figure 29. *In vitro* cytotoxicity of PEG-Fmoc/PTX. 4T1.2 mouse breast cancer cell line (A), human prostate cancer cell lines PC-3 (B), and DU145 (C) were treated with PEG-Fmoc/PTX, drug-free PEG-Fmoc and Taxol for 72 h, and tumor cell inhibition was determined by MTT assay. * $P < 0.05$ or ** $P < 0.01$ (PEG-Fmoc/PTX vs Taxol). 60

| | |
|---|----|
| Figure 30. Biodistribution of PEG-Fmoc/Cy5.5-PTX in tumor-bearing mouse as examined by NIR fluorescence imaging. Mouse bearing PC-3 cancer xenograft was scanned at 0.2 h, 24 h, 48 h, 72 h, and 96 h after i.v. injection of PEG-Fmoc/Cy5.5-PTX; and ex vivo imaging of tumors and major organs was performed 96 h after injection..... | 62 |
| Figure 31. <i>In vivo</i> therapeutic efficacy of PEG-Fmoc/PTX. Groups of 5 BALB/c mice bearing 4T1.2 murine breast cancer grafts were injected with PEG-Fmoc/PTX (10, 20, or 40 mg PTX/kg body weight), Taxol (10 mg PTX/kg body weight) and saline on days 0, 2, 4, 7, 10 and 12, respectively. Tumor growth was monitored and plotted as relative tumor volume (A). *P < 0.05; **P < 0.01 (vs Taxol). Tumor weights were measured after excision and plotted as average tumor weight, and tumor growth inhibition rate (IR) was calculated (B). | 64 |
| Figure 32. Changes of body weight in mice treated with PEG-Fmoc/PTX (10, 20, or 40 mg PTX/kg) or Taxol (10 mg PTX/kg). | 65 |
| Figure 33. Structures and synthetic route of PFA conjugates..... | 75 |
| Figure 34. ¹ H NMR spectra of PFA ₂ in CDCl ₃ (A), and PTX/PFA ₂ in CDCl ₃ (B) and D ₂ O (C). The greatly suppressed proton signals of Fmoc, Cbz, and PTX in D ₂ O indicated the encapsulation of PTX into inner core of self-assembled PFA ₂ micelles in aqueous phase. | 75 |
| Figure 35. MALDI-TOF mass spectrum of PFA ₁ (A), PFA ₂ (B), and PFA ₄ (C)..... | 76 |
| Figure 36. ¹ H NMR spectrum of PFA ₁ (A), PFA ₃ (B), PFA ₄ (C), PFA ₅ (D), PFA ₆ (E), PFA ₇ (F), and PFA ₈ (G)..... | 76 |
| Figure 37. Critical micelle concentration (CMC) measurement of PFA ₁ (A), PFA ₂ (B), and PFA ₄ (C) with pyrene as a fluorescence probe..... | 78 |
| Figure 38. Negative staining TEM images of drug-free (A) and PTX-loaded (B) PFA ₂ micelles. Scale bar is 100 nm. | 78 |

Figure 39. Fluorescence quenching study. Drug-free and PTX/PFA mixed micelles were prepared at a fixed PFA concentration of 1.17 mmol/L. PTX/PFA ratios were reported as molar ratios. The samples were excited at 270 nm and the fluorescence intensity at 300 to 460 nm was recorded. % Fluorescence quenching was calculated as: $(1 - \text{fluorescence intensity of PTX/PFA} / \text{fluorescence intensity of drug-free PFA}) \times 100\%$ 80

Figure 40. ^{13}C NMR of PTX mixed with FA₁, FA₂, and FA₄ in CDCl₃. PTX was mixed with FA at a molar ratio of 1:5. Signal shift (Δ) indicates the signal shift of carbon atom on aromatic rings of PTX before and after mixing with FA, and SUM indicates a cumulative shift of all the atoms (absolute values)..... 81

Figure 41. Size distribution of PTX/PFA₂ micelles before (A) and after (B) lyophilization/reconstitution. PTX concentration in the mixed micelles was kept at 1 mg/mL... 82

Figure 42. The kinetics of PTX release from PTX/PFA₂ as examined via a dialysis method. PTX concentration in PTX/PFA₂ and Taxol was kept at 1 mg/mL, and DPBS containing 0.5% (w/v) Tween 80 was used as release medium. PTX concentration was analyzed by HPLC at 0, 1, 2, 4, 8, and 24 h..... 83

Figure 43. *In vitro* cytotoxicity. PC-3 androgen-independent human prostate cancer cells (A), 4T1-2 mouse metastatic breast cancer cells (B), HCT-116 human colonic carcinoma cells (C), and A549 human lung adenocarcinoma epithelial cells (D) were treated with PTX/PFA₂, drug-free PFA₂, and Taxol for 72 h, and cancer cell inhibition was determined by MTT assay. Panel E summarizes the IC₅₀ of PTX/PFA₂ and Taxol in different cell lines..... 84

Figure 44. *In vivo* antitumor activity of PTX/PFA₂. BALB/c mice (n=5) bearing 4T1.2 murine breast cancer grafts were i.v. injected with PTX/PFA₂ (10 and 25 mg PTX/kg body weight), Taxol (10 mg PTX/kg body weight), and saline on days 0, 2, 4, 7, 10 and 13, respectively.

Tumor growth was monitored and plotted as relative tumor volume (A). * $P < 0.05$; ** $P < 0.01$ (vs Taxol). No significant changes of body weight in mice were observed (B)..... 86

Figure 45. Schematic representation of proposed mechanisms of intermolecular interaction between PFA₂ conjugate and PTX..... 90

Figure 46. Proliferation inhibition of 4T1-2 mouse metastatic breast cancer cell line (A), PC 3 androgen-independent human prostate cancer cell line (B), and HCT-116 human colonic carcinoma cell line (C) treated with combination of DOX and DAS for 72 h. Synergy of DOX with DAS was indicated by combination index (CI) (D). 103

Figure 47. Synthetic route of PLFCL and schematic representation of PLFCL-mediated combination cancer therapy. (A) Self-assembly of PLFCL into nano-sized micelles in aqueous environment and co-encapsulation of DOX&DAS into core area of formed micelles; (B) Internalization of DOX&DAS/PLFCL micelles by cancer cells through endocytosis, and induction of cancer cell death as consequences of released DAS binding to tyrosine kinase (TK) and accumulation of DOX inside nucleus. 105

Figure 48. ¹H NMR spectra of PLFCL (A), DOX (B), DAS (C), DOX&DAS/PLFCL (D) in DMSO-*d*₆, and DOX&DAS/PLFCL in D₂O (E). The suppression of proton signals from Fmoc, Cbz, and both drug molecules in D₂O indicated the self-assembly of PLFCL micelles in aqueous medium and encapsulation of drug molecules into inner core of formed micelles. 106

Figure 49. MALDI-TOF mass spectrum of PLFCL. 107

Figure 50. Critical micelle concentration (CMC) measurement of PLFCL using pyrene as a fluorescence probe. 107

Figure 51. TEM images of drug-free (A), DOX-loaded (B), DAS-loaded (C), and DOX&DAS-loaded (D) PLFCL micelles using negative staining. Scale bar is 100 nm..... 108

Figure 52. Fluorescence emission of Fmoc at 300-450 nm was recorded with an excitation wavelength at 270 nm (A). Fluorescence of DOX was measured using an excitation wavelength of 480 nm and emission wavelength from 510-650 nm (B). Both Fmoc and DOX showed significant fluorescence quenching in mixed micelles. 110

Figure 53. Chemical structures of (A) doxorubicin and (B) dasatinib..... 110

Figure 54. UV-spectrum of DOX and DAS before and after encapsulation into PLFCL micelles. 111

Figure 55. The kinetics of DOX (A) and DAS (B) release from DOX&DAS/PLFCL micelles as examined through a dialysis method. DPBS containing 0.5% (w/v) Tween 80 was used as release medium. Drug concentration was analyzed by HPLC at 0, 1, 2, 4, 8, 24 and 48 h. 111

Figure 56. Intracellular trafficking of DOX in 4T1.2 cells. Cells were treated with DOX&DAS/PLFCL, DOX/PLFCL micelles, or free DOX at 10 $\mu\text{mol/L}$ for 0.5 h (A), 2 h (B), and 4 h (C). The nuclei were stained with Hoechst 33342, and endo/lysosomes were stained by LysoTracker DND-26. The intracellular distribution of DOX in various formulations was observed under a confocal laser scanning microscope (CLSM)..... 113

Figure 57. *In vitro* cytotoxicity. 4T1-2 mouse metastatic breast cancer cell line (A), PC 3 androgen-independent human prostate cancer cell line (B), and HCT-116 human colonic carcinoma cell line (C) were treated with different formulations for 72 h, and cancer cell inhibition was determined by MTT assay..... 114

Figure 58. Wound healing assay of 4T1-2 mouse metastatic breast cancer cells 0 and 16 h after treated by drug-free or drug-loaded PLFCL micelles with each drug concentration at 100 nmol/L. Bright field images were obtained under microscope and relative cell migration was quantified using cells without treatment as control..... 115

Figure 59. *In vivo* therapeutic efficacy of DOX&DAS/PLFCL micelles. Groups of 5 BALB/c mice bearing 4T1.2 murine breast cancer grafts were injected with DOX&DAS/PLFCL, DOX/PLFCL, DAS/PLFCL micelles (5 mg each agent/kg body weight) and saline on days 0, 3, and 6, respectively. Free DOX+DAS combination dissolved in 50% propylene glycol was used for comparison. Tumor growth was monitored and plotted as relative tumor volume (A). *P < 0.05; **P < 0.01 (DOX&DAS/PLFCL micelles vs other treatment). Tumor weights were measured after excision and % tumor growth inhibition was calculated as: 1- (mean tumor weight of drug treated group/mean tumor weight of saline treated group) * 100% (B). Significant difference in tumor size was observed between groups (C), and changes of body weight in mice was also monitored (D)..... 117

Figure 60. Kaplan-Meier survival curves for BALB/c mice (n=7) bearing 4T1.2 murine breast cancer grafts. Mice were treated with DOX&DAS/PLFCL, DOX/PLFCL, DAS/PLFCL micelles, free DOX+DAS combination (5 mg each agent/kg body weight), and saline on days 0, 3, and 6, respectively. 118

Figure 61. *In vivo* therapeutic efficacy of DOX&DAS/PLFCL micelles with long follow-up time. Groups of 7 BALB/c mice bearing 4T1.2 murine breast cancer grafts were injected with DOX&DAS/PLFCL, DOX/PLFCL, DAS/PLFCL micelles (5 mg each agent/kg body weight) and saline on days 0, 3, and 6, respectively. Free DOX+DAS combination dissolved in 50% propylene glycol was used for comparison. Tumor growth was monitored and plotted as relative tumor volume (A). Changes of body weight in mice was also monitored (B). 118

Figure 62. Histological analyses of tumor tissues using H&E staining and TUNEL assay. 119

PREFACE

The research work described in this Ph.D. dissertation was accomplished under the supervision of my advisor, Dr. Song Li, in the Center for Pharmacogenetics, Department of Pharmaceutical Sciences at the University of Pittsburgh School of Pharmacy.

To embark on a new journey of pursuing a Ph.D. degree on another continent which I had never been to is one of the most crucial and critical decisions that I ever make in my life. This journey per se, though fairly challenging and difficult, is also filled with warm and sweet memories. I feel quite fortunate to have met an amazing group of scientists and colleagues who have guided me on this academic journey and helped me grow up as a qualified doctoral student. Simultaneously, my family and friends, whether on the same continent or far apart in China, have been tremendously supporting me and standing by me over these years. My most sincere and heartfelt thanks go to all of them. Had I not met them and got their invaluable help or advice, I could not make this far and even have finished this journey.

First of all, I would like to express my sincere gratitude and appreciation to my advisor, Dr. Song Li, for his generous support throughout my Ph.D. study. Dr. Li is an impressively knowledgeable scientist and extremely nice mentor who is always ready to give me positive advice and

encouragement with endless patience and kindness. In Dr. Li's laboratory, I have an excellent environment to receive a comprehensive training in chemical synthesis, formulation development, and molecular biology, which equipped me with multi-disciplinary expertise to explore a broad academic area. Besides, Dr. Li also kindly extended me a variety of opportunities to improve my professional expertise in scientific writing, communication, and presentation, which will greatly facilitate my future career development. Grateful thanks to his tremendous help and support that make me grow up academically and personally.

Meanwhile, I am sincerely grateful to my committee members, Dr. Lisa Rohan, Dr. Shilpa Sant, and Dr. YP Peter Di, for their considerable support and expert guidance in my research. I would also like to thank all my colleagues and friends in Dr. Song Li's lab. Special thanks to Dr. Xiang Gao, a dedicated scientist full of passion and willingness to take new adventures in science, for his wholehearted support and critical thinking which have guided me this far running on the right track; to Dr. Jiang Li for his generous help in my studies as well as my life; to Dr. Yixian Huang for his kind instruction in chemical synthesis; and to all my friends in Dr. Li's laboratory (Yifei Zhang, Jianqin Lu, Mohammed Ghazwani, Xiaolan Zhang, Yichao Chen, Jieni Xu, Jingjing Sun, Yukun Huang, and Min Zhao). Had I not met them, the journey would be much less fascinating.

My sincere and hearty thanks also go to all the members at the Center for Pharmacogenetics, particularly to Dr. Wen Xie, Dr. Yong Tae Kwon, Dr. Xiaochao Ma, Dr. Da Yang, William Smith, and Meishu Xu for their helpful advice and generous help. I feel supremely fortunate having joined this warm family to enrich myself with a wide range of expertise and make me always feel at home. Further, grateful thanks to the faculty, staffs, and students in the

Department of Pharmaceutical Sciences at the University of Pittsburgh School of Pharmacy. Special thanks to Dr. Patricia D Kroboth, Dr. Randall B Smith, Dr. Barry Gold, Dr. Robert B Gibbs, Dr. Raman Venkataramanan, Dr. Sean Xie, Dr. Maggie Folan, and Lori Schmotzer for their enormous help and support over these years. Many thanks to our extremely supportive and friendly cooperators Dr. Donna B Stolz, Ming Sun, Dr. Peijun Zhang, Dr. Alexander M. Makhov, Dr. Liang Xu, Dr. Rebecca Marquez, Hao Liu, Douglas E. Nelson, Wenchen Zhao, Dr. Peng Yang, Galit R Frenkel, and Dr. Wei Zhang for their lab equipment and expert insights.

This dissertation is dedicated to my parents, Jing Yang and Guangchun Zhang, and my grandparents, Zhiqing Sun and Shengyu Zhang, who have been instilling into me endless love, courage, and hope in my life. It is their unconditional love and belief that constantly keep me forging ahead on the path towards success with determination and confidence in my heart.

1.0 INTRODUCTION

1.1 NANOMEDICINE IN CANCER CHEMOTHERAPY

1.1.1 Current issues in cancer chemotherapy

Currently, cancer is still one of the leading causes of death all over the world. Approximately 14.1 million new cases of cancer were reported globally in 2012 and resulted in 8.2 million deaths (World Cancer Report 2014 from World Health Organization). Breast, prostate, lung, and colorectal cancers are the most common types of cancers with about 617,000 new cases expected in the United States in 2014 (data reported by American Cancer Society). Typically, cancers are caused by mutations in oncogenes and/or tumor suppressor genes resulting from genetic or environmental factors [1, 2]. These genetic mutations give cancer cells malignant characteristics of uncontrolled growth, invasion and metastasis [3].

Chemotherapy represents one of the most potent and commonly used cancer treatments in clinic. Most chemotherapeutics are cytotoxic agents targeting rapidly proliferating cells, either causing DNA damage or inhibiting other cellular machinery to induce programmed cell death known as apoptosis [4, 5]. However, clinical translation of a variety of promising anticancer agents was beleaguered by many issues associated with physiochemical or pharmacokinetic properties of these drugs [6]. Firstly, most of the chemotherapeutic agents are poorly water

soluble. This limited aqueous solubility brings tremendous difficulties to clinical administration of these agents, and are usually coupled with low absorption and bioavailability [7]. Secondly, chemotherapeutic agents are usually small molecules, rapidly metabolized and excreted through the liver and kidneys. This short circulation time results in an inadequate accumulation of these agents in tumor sites, which may account for ineffective cancer therapy and sometimes the development of tumor resistance against anti-cancer agents. Furthermore, as mentioned above, chemotherapeutic agents are typically cytotoxic and act through killing fast-growing cells. Although cancer cells are more sensitive to these agents due to their high proliferation rates, non-specific tissue distribution of anti-cancer drugs causes severe toxicity to other fast-dividing cells in normal tissues such as bone marrow, gastrointestinal tract and hair follicles [8, 9].

1.1.2 Advantages of nanomedicine in cancer chemotherapy

Since last century, tremendous efforts have been made to circumvent the limitations of chemotherapy and maximize its clinical outcomes in cancer treatment. Among them, nanomedicine has gained popularity as an attractive strategy to improve physiochemical/pharmacokinetic properties, enhance therapeutic efficacy, and reduce systemic toxicity of a broad variety of anticancer agents [10, 11]. A number of nanocarriers, such as polymeric conjugates, liposomes, micelles, dendrimers, nano-crystals, and many others, have been developed, and some of them have already been successfully put into market or under clinical trials [12-14].

The advantages of nanomedicine over the administration of free anti-cancer agents include enhanced water-solubility of hydrophobic agents, increased absorption and bioavailability,

protection from degradation by the degrading enzymes before reaching target area, and prolonged blood circulation allowing increased accumulation in tumor site. It has been well established that newly-formed vasculatures at a tumor site are usually leaky and abnormal in architecture. At the same time, lymphatic drainage is usually ineffectively developed in solid tumor. Therefore, nanoparticles with a size of 20-200 nm, given adequate circulating time, preferentially extravasate into solid tumor tissues, and are retained at tumor at a higher concentration over normal tissues. This phenomenon, first discovered by Maeda and Matsumura [15, 16], is well known as the enhanced permeability and retention (EPR) effect and is the physiological basis of the preferential accumulation of nanoparticles in tumor site or “passive targeting”. In addition to passive targeting, the efficiency of selective delivery can be further enhanced by attaching a targeting ligand, such as an antibody, small peptide, aptamer, or others, onto the surface of nanoparticles. Based on high affinity between ligands and receptors highly expressed on target cells, this “active targeting” strategy further enhances recognition and uptake of drug-loaded particles by cancer cells [17-19].

1.2 MICELLES AS AN EFFECTIVE NANOCARRIER FOR CHEMOTHERAPEUTIC AGENTS

1.2.1 An overview of micellar system

Among a variety of nanocarriers developed in recent decades, micelles are unique and appealing due to their high capability to solubilize hydrophobic agents and ease of manipulation. More

importantly, the small size of micelles, typically below 100 nm, allows for preferential accumulation in a solid tumor through passive targeting. Micellar systems are usually formed by amphipathic molecules, or surfactants, composed of two distinct domains, one being hydrophilic and the other hydrophobic. Upon exposure to an aqueous environment, the hydrophobic segments are self-assembled into a hydrophobic inner core, surrounded by a corona formed by hydrated hydrophilic domains. This unique core-shell architecture of micelles provides both a hydrophobic loading zone for the encapsulation of hydrophobic drugs as well as a hydrophilic outer layer to effectively diminish the binding of plasma proteins, nonspecific uptake by the reticuloendothelial system (RES), and unwanted self-aggregation with other micelles [20-22]. A minimum concentration of micelle-forming surfactants is required for micelle formation in an aqueous medium, which is termed as critical micelle concentration (CMC). Micelle-forming amphipathic molecules remain as monomers in solution when below CMC; while above CMC, they are self-assembled into micelles. CMC is an important parameter of the stability of micelles upon dilution. Generally, larger hydrophobic segments lead to a lower CMC value.

Poly (ethylene glycol) (PEG) is the most commonly utilized hydrophilic polymer to construct micelle-forming surfactants. The advantages of PEG in pharmaceutical application include high water solubility, neutral charge, low polydispersity index (PDI), non-toxicity, low immunogenicity, commercial availability, high solubility in most organic solvents, and ease to conjugate with other segments [23]. It has been demonstrated that PEGylation effectively stabilizes micellar systems, diminishes undesired binding with blood components, and prolongs circulation time. Besides micelles, PEG is also widely applied to other delivery systems as liposomes, polymer-drug conjugates, and PEGylated proteins/peptides [24-26].

For most of the current micellar systems, drug loading largely relies on hydrophobic interactions between their core-forming hydrophobic segments and the poorly water-soluble drugs. Commonly used hydrophobic segments include hydrophobic copolymers, lipids, or other small hydrophobic molecules. Due to good biocompatibility and biodegradability, polyester and polyamide are two widely used copolymers in micelle formulation, such as poly (lactic acid) (PLA), poly (lactic-co-glycolic acid) (PLGA), and poly (L-lysine) (PLL) [27-30]. These materials are able to be gradually degraded *in vivo* through enzyme-assisted hydrolysis of ester or amide bond, and finally excreted out of body without causing toxicity. The disadvantage of these types of micelles is the relatively large particle size, usually above 100 nm. Besides copolymers, lipids are also used as hydrophobic segments in micelle formation. Torchilin's group has developed a lipid-core micellar system using PEG–phosphatidylethanolamine (PE) conjugate as surfactant [31-33]. In these systems, strong hydrophobic interaction provided by double acyl chains of PE facilitated the formation of stable micelles and encapsulation of a broad spectrum of anti-cancer agents including paclitaxel (PTX), tamoxifen, and camptothecin (CPT) [31, 34-37].

As for cases of using small molecules as hydrophobic segments of surfactants, the PEG-dendritic oligo-cholic acid system would be an excellent example. This so-called amphiphilic telodendrimer system was first developed by Lam's group [38]. In their studies, multiple cholic acids (CA), one of the major bile acids produced in the human liver, was conjugated to the terminal of PEG chain to construct a biocompatible copolymer with linear-dendritic architecture. Distinct from other hydrophobic molecules, CA has unique facial amphiphilicity, making it an efficient functional building block for caging other hydrophobic molecules [38-41]. Using dendritic oligo-CA as hydrophobic core, a PEG conjugate coupled with eight CA molecules

(PEG₅₀₀₀-CA₈) exhibited excellent loading capacity with PTX. Combined with its small particle size (20-60 nm) and superior stability, this micellar system acts as an promising delivery vector for PTX with specific tumor accumulation, low toxicity profiles, and excellent therapeutic efficacy in a nude mice model with human ovarian cancer xenograft when compared to two clinically used FDA-approved formulation of PTX, Taxol (PTX in 1:1 (v/v) of Cremophor EL/ethanol) and Abraxane (albumin-bound PTX). Subsequent studies further demonstrated the potential of the PEG-CA system as a promising nanocarrier for PTX and other anti-cancer agents [42-47].

1.2.2 Advances in improvement of carrier/drug compatibility

In the past decades, polymeric micelles, using either hydrophobic copolymers or lipids as hydrophobic segments, have been intensively studied. The inner core of micelles formed by these segments provides a highly hydrophobic area for drug entrapment. For most of current micellar systems, drug encapsulation heavily relies on hydrophobic/hydrophobic interaction. While working well for highly hydrophobic/lipophilic agents, these systems have limited effectiveness for moderately hydrophobic drugs due to carrier/drug incompatibility. The inadequate mixing of core-forming segments with payload drugs severely diminishes drug loading capacity and formulation stability of micelles.

A number of advances have been made to improve the carrier/drug compatibility of micelles based on structural optimization of the core-forming segments. One of the most effective strategies was the incorporation of less hydrophobic and hydrogen bond-forming functional building blocks, termed as “hydrotropic motifs” or “hydrotropes”. Typically, hydrotropes consist

of aromatic rings substituted with heteroatoms such as nitrogen. Aromatic rings strongly interact with other hydrophobic drugs via hydrophobic and π - π stacking interaction, while hydrogen bonding provided by polar groups further strengthens interaction with drug molecules. This strategy was firstly described by Kinam Park's group [48-50].

In one of their studies, the solubilizing ability of two aromatic hydrotropes, N,N-dimethylbenzamide (DMBA) and N, N-diethylnicotinamide (DENA) was evaluated by using 13 agents with limited water solubility and diverse structures [51]. The data demonstrated a nonspecific solubilization capacity of DMBA, a more hydrophobic hydrotrope with higher self-association tendency, to dissolve a broad panel of drugs with a solubility enhancement ranging from 1,000 to 10,000-fold. Interestingly, although less hydrophobic and potent than DMBA, DENA showed a specific solubilization capacity to PTX. It is likely that this more polar hydrotrope exhibits higher hydrogen bonding ability with PTX, which strongly facilitated carrier/drug intermolecular interaction.

Using DENA as a functional motif to strengthen carrier/drug interaction, an amphiphilic block copolymer, PEG-block-poly (2-(4-vinylbenzyloxy)-N,N-diethylnicotinamide) (PEG-b-P(VBODENA)) effectively solubilized PTX [52]. An impressively high loading capacity of PTX (37.4 wt%) was achieved with long-term stability for weeks. In addition, these micelles showed enhanced efficacy in inhibition of cancer cell proliferation in four different cancer cell lines over the control formulation without drug-interactive motifs.

Besides hydrotropes, entire drug molecules were also used as functional building blocks in nanocarriers for enhanced entrapment of the same drug. Park's group has developed a doxorubicin-polyethylene glycol-folate (DOX-PEG-FOL) conjugate for targeted delivery of DOX to tumor site [53, 54]. Deprotonated DOX was physically entrapped into micelles formed

by polymeric carriers with covalently conjugated DOX as hydrophobic segments, and folate was decorated to the surface of micelles for active targeting to folate-receptor-positive cancer. These micelles exhibited enhanced cellular uptake and cytotoxicity in *in vivo* studies. Stronger tumor inhibition was also observed in a human tumor xenograft nude mouse model.

Furthermore, lipid-based micellar systems with improved stability and drug loading capacity have also been developed. These are PEGylated surfactants with cholic acid, vitamin E, EB, or FTS, instead of simple lipids as a hydrophobic domain. Vitamin E, EB, and FTS all have an aromatic ring linked to an acyl chain, which may strongly stack with benzene rings in drug molecules for additional carrier/drug interaction. These studies highlight the benefits of introducing additional structural variables as drug-interactive motifs into traditional micellar system.

1.2.3 Discovery of 9-Fluorenylmethoxycarbonyl (Fmoc) as interfacial drug-interactive motif

Our group recently discovered an unusual propensity of 9-Fluorenylmethoxycarbonyl (Fmoc) to interact with hydrophobic drugs [55]. Fmoc is a widely used amine protection group. It has a compact fused aromatic ring structure of fluorenyl group capable of forming hydrophobic and π - π stacking interactions with compounds carrying one or more aromatic rings. In addition, the carbamate linkages in Fmoc also facilitate hydrogen bonding interactions. Such interactions are believed to be much stronger than the van der Waals interaction between alkyl chains, and introduction of these extra mechanisms of interactions into micellar systems or other carriers shall significantly strengthen overall carrier/carrier and carrier/drug interactions.

Initially, this discovery was made in optimization of emulsion and micellar formulations of JP4-039, a peptide-based antioxidant [55-57]. Due to its moderate hydrophobicity and strong crystalline tendency, JP4-039 showed strong tendency to precipitate out from these formulations. Over time, drug/lipid phase separates and the drug migrates to interface and crystallizes. This poor formulation stability can be attributed to the incompatibility of highly lipophilic/hydrophobic lipid chains with moderately hydrophobic drug molecules, a challenge encountered by most of the conventional colloidal systems.

In colloidal systems, it is widely believed that hydrophobic core region is the key drug-loading region. Although it is true for highly hydrophobic/lipophilic agents, it may also account for incompatibility of carriers with hydrophobic molecules with hydrophilic structural elements. For these moderately hydrophobic molecules, the interface, neither too hydrophobic as deep in the core nor too hydrophilic as outer shell formed by PEG, would be a thermodynamically favored destination. However, the significance of interfacial region is usually not appropriately appreciated. Mostly, it is either missing or compact in size relative to the rest of the surfactant molecules. Gao hypothesized that an expanded interfacial region equipped with functional motifs capable of interacting with drug molecules shall significantly improve the compatibility of nanocarrier with moderately hydrophobic agents [55].

For selection of drug-interactive motifs, a panel of lysine derivatives was screened for their ability to block the crystallization of JP4-039 [55]. Among all the lysine derivatives tested, α -Fmoc- ϵ -t-Boc-lysine showed the most potent capability to prevent JP4-039 from forming crystals, which may indicate the critical role of α -Fmoc motif in interaction with JP4-039. Incorporation of Fmoc into the interfacial region of a PEG-lipid surfactant led to a significant improvement in loading JP4-039 as both emulsion and micellar formulations.

The work by Gao in our laboratory represented a new approach to solving the problems of limited drug loading capacity and poor stability that are associated with many of current formulations. However, much more needs to be understood about the underlying carrier/drug interactions and the optimal structures for the Fmoc-containing micellar formulations. It is also important to investigate if this strategy can be readily applied to a broad variety of therapeutics, especially chemotherapeutics. In the 1st part of my dissertation work, I demonstrated the effectiveness of Fmoc as an effective interfacial drug-interactive motif in enhancing drug loading and retention of micellar system. A PEG-lipopeptide conjugate equipped with interfacial Fmoc motifs (PEG₅₀₀₀-lysyl-(α -Fmoc- ϵ -oleoyl lysine)₂) effectively solubilized a panel of drugs with diverse chemical structures and water solubility [58]. To clearly address the molecular basis of Fmoc/drug interaction, a new model was established by using a simple PEG-Fmoc conjugate without lipid chains. Interestingly, this simple PEG-Fmoc conjugate (PEG₅₀₀₀-lysyl-(α -Fmoc- ϵ -t-Boc-lysine)₂) works more effectively than the lipopeptide counterparts in formulating anti-cancer agent PTX, which is attributed to a strong Fmoc/PTX intermolecular π - π stacking [59]. Inspired by this discovery, a structure-activity relationship (SAR) study was performed to gain better insights into the effects of neighboring structures of Fmoc on the overall carrier-drug interactions [60]. This study further led to the design of a nanocarrier with enhanced carrier-drug interactions and expanded drug-binding pocket for effective co-delivery of multi-agents in combination cancer chemotherapy [61].

2.0 DESIGN AND EVALUATION OF A PEGYLATED LIPOPEPTIDE EQUIPPED WITH DRUG-INTERACTIVE MOTIFS AS AN IMPROVED DRUG CARRIER

2.1 BACKGROUND

Drug discovery and development is an extremely time-consuming and costly process, during which only very few candidates survive the screening process and eventually become clinical drugs. Many promising candidates are eliminated due to poor solubility and bioavailability [62]. Drug formulations have gained increasing attention as a strategy to maximize the success of drug development process and to improve the performance of existing drugs [63].

Micelles are an attractive delivery system due to the ease of application and their small particle sizes, which allow effective passive targeting to tissues with leaky vasculature such as tumors and inflammatory tissues based on the enhanced penetration and retention (EPR) effect [15, 16]. However, there are several issues with conventional micellar systems such as low drug loading capacity and limited colloidal stability, which limit their successful *in vivo* applications [64]. Incorporation of drugs into hydrophobic core of typical micelle formulations is largely based on hydrophobic-hydrophobic interactions. While these micellar formulations are effective in formulating very few drugs that are highly hydrophobic or lipophilic, they have limited effectiveness in formulating many drugs that are only moderately hydrophobic.

Studies from Park's group have shown that inclusion of hydrotropic motifs into the

hydrophobic domain of polymeric micelles significantly improves the compatibility of the core-forming blocks with the drugs that are not entirely hydrophobic/lipophilic [48, 51]. Hydrotropes are small molecular amphiphiles that increase the aqueous solubility of poorly soluble agents. This strategy has led to significant improvement in both drug loading capacity and the colloidal stability of drug-loaded micelles. The study by Yoo et al showed that covalent coupling of a drug molecule (doxorubicin, DOX) into the hydrophobic domain of polymeric micelles resulted in an improved system for loading of the same drug, e.g., DOX [53, 54]. These studies highlight the benefit of introducing additional structural variables to the traditional polymeric micellar systems.

The idea of including an additional drug-interactive domain in lipidic micellar systems has not been studied before. However, the importance of such approach has been suggested by recent studies with several “unconventional” pegylated surfactants with Vitamin E, embelin, or farnesylthiosalicylic acid (FTS, a Ras inhibitor), instead of simple lipids as a hydrophobic domain [65-68]. Vitamin E, embelin, and FTS all have an interfacial aromatic ring linked to an acyl chain, which may contribute significantly to the improved formulation properties over the surfactants with simple lipid chains. We hypothesized that expansion of the interfacial region to purposely include motifs that have drug interaction potential could result in further improved lipidic micellar systems. We have experimentally demonstrated that such motif can be identified via a screening process, and then incorporated into the interfacial region of a pegylated surfactant to add a drug interactive functionality. With JP4-039, a mitochondria-targeted antioxidant featuring a peptide derivative carrying a nitroxide group, we have shown that such approach is both feasible and significant. We have found that 9-Fluorenylmethoxycarbony (Fmoc) moiety, a functional group that is routinely used for amino acid protection, was the best among several

motifs examined [55].

The aim of the present study is to examine the broad applicability of our new micellar system in formulating different drugs of diverse structures. The potential of the new formulation in delivery of paclitaxel to tumor cells was also investigated *in vitro* and *in vivo*.

2.2 METHODS

2.2.1 Materials

Paclitaxel (PTX, 98%) was purchased from AK Scientific Inc. (CA, USA). α -Fmoc- ϵ -Boc-lysine, di-Boc-lysine, N, N'-dicyclohexylcarbodiimide (DCC), N-hydroxysuccinimide (NHS), trifluoroacetic acid (TFA), and triethylamine (TEA) were obtained from Acros Organic (NJ, USA), and oleic acid (OA) was from Alfa Aesar (MA, USA). Monomethoxy PEG₅₀₀₀, 4-dimethylaminopyridine (DMAP), ninhydrin, and other unspecified chemicals were all purchased from Sigma-Aldrich (MO, USA). Dulbecco's phosphate buffered saline (DPBS), Dulbecco's Modified Eagle's Medium (DMEM), fetal bovine serum (FBS), 100X Penicillin-streptomycin solution were all purchased from Invitrogen (NY, USA). All solvents used in this study were HPLC grade.

2.2.2 Cell culture

4T1-2 is a mouse metastatic breast cancer cell line. PC-3 and DU145 are two androgen-

independent human prostate cancer cell lines. The cell lines were kindly provided by Dr. You and Dr. Fan at University of Pittsburgh School of Medicine, and they were all cultured at 37 °C in DMEM containing 10% FBS and 1% penicillin-streptomycin in a humidified environment with 5% CO₂.

2.2.3 Synthesis of PEG₅₀₀₀-Lys-(α -Fmoc- ϵ -oleoyl lysine)₂ (PEG₅₀₀₀-(Fmoc-OA)₂)

The synthetic route of PEG₅₀₀₀-(Fmoc-OA)₂ and PEG₅₀₀₀-di-oleoyl lysine (PEG₅₀₀₀-OA₂) was depicted in **Figure 1**.

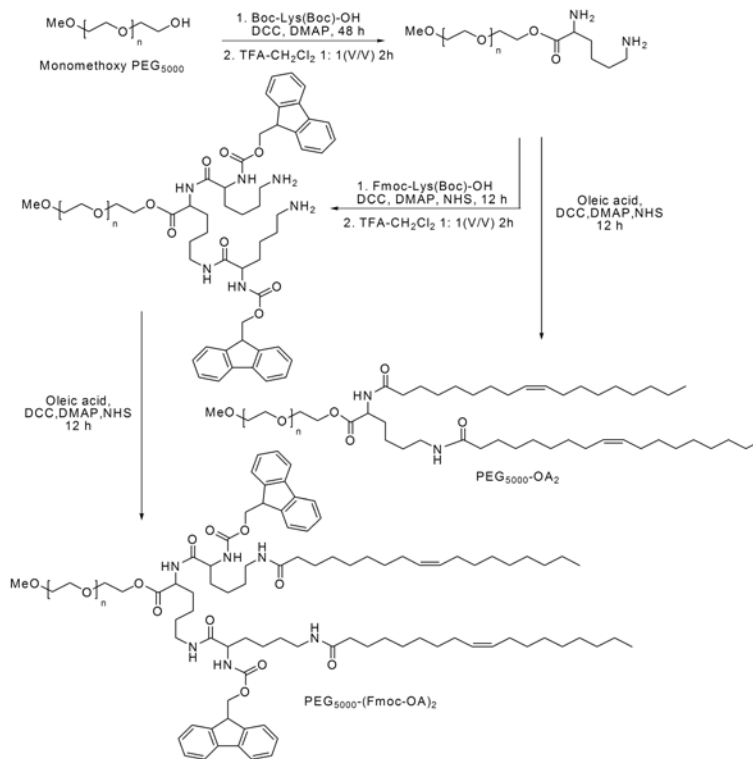


Figure 1. Synthetic route of PEG₅₀₀₀-(Fmoc-OA)₂ and PEG₅₀₀₀-OA₂.

Monomethoxy PEG₅₀₀₀ (1 eq.) was dissolved in CH₂Cl₂ and mixed with di-Boc-lysine (1.5 eq.), DCC (1.8 eq.) and DMAP (0.3 eq.). After stirring at room temperature for 24 h, another portion of di-Boc-lysine (1.5 eq.) and DCC (1.8 eq.) was added into reaction mixture and the reaction was allowed for another 24 h. White solid precipitate was then removed by filtration, and the filtrate was added into 10-fold volume of cold ethyl ether to precipitate the PEG derivative, followed by three washes with cold ethanol and ether. The obtained PEG₅₀₀₀-di-Boc-lysine ester was dissolved in CH₂Cl₂/TFA (1:1, v/v) at the concentration of 0.3 g/mL, and stirred for 2 h at room temperature to remove the Boc moiety. After removal of most of the solvent, the PEG derivative was precipitated in cold ether, and washed three times with cold ethanol and ether.

α -Fmoc- ϵ -Boc-lysine (3 eq.), NHS (3.6 eq.), DCC (4 eq.) and DMAP (0.8 eq.) were dissolved in CH₂Cl₂ and activated at 37°C for 4 h, followed by mixing with PEG₅₀₀₀-di-NH₂-lysine (1 eq.) and TEA (3 eq.). The reaction was allowed at 37 °C overnight till completion as indicated by the negative results in the ninhydrin tests. The white solid precipitate was removed by filtration, and the PEG derivative was precipitated in cold ether and washed by cold ethanol and ether. The PEG₅₀₀₀-Lys-(α -Fmoc- ϵ -Boc lysine)₂ obtained was dissolved in CH₂Cl₂/TFA (1:1, v/v), and stirred for 2 h at room temperature to remove the Boc moiety. The resulting PEG₅₀₀₀-Lys-(α -Fmoc- ϵ -NH₂ lysine)₂ was then purified by cold ether and ethanol precipitation.

The NH₂-terminated PEG₅₀₀₀-Lys-(α -Fmoc- ϵ -NH₂ lysine)₂ (1 eq.) was conjugated with oleic acid (OA, 3 eq.) that was pre-activated with NHS (3.6 eq.), DCC (4 eq.) and DMAP (0.8 eq.) for 4 h at 37 °C. The conjugating reaction was allowed overnight until negative results were shown in the ninhydrin tests. After filtration and precipitation, the obtained PEG₅₀₀₀-Lys-(α -Fmoc- ϵ -oleoyl lysine)₂ (PEG₅₀₀₀-(Fmoc-OA)₂) was purified via three washes with cold ethanol and ether.

2.2.4 Synthesis of PEG₅₀₀₀-OA₂

The PEG₅₀₀₀-di-NH₂-lysine was synthesized as described above and the di-NH₂-terminated PEG was reacted with OA (3 eq.) that was pre-activated with NHS (3.6 eq.), DCC (4 eq.) and DMAP (0.8 eq.) for 4 h at 37 °C. The reaction was completed as indicated by the negative results in the ninhydrin tests. After filtration and precipitation, the obtained PEG₅₀₀₀-OA₂ was purified by three washes with cold ethanol and ether.

2.2.5 Preparation and characterization of drug-loaded micelles

All of the drugs were dissolved in chloroform (10 mg/mL) and were mixed with PEG₅₀₀₀-(Fmoc-OA)₂ (100 mg/mL in chloroform) at various carrier/drug molar ratios. The organic solvent was removed by a stream of nitrogen to generate a thin film at the bottom of a glass tube, and the trace amount of solvent was further removed under vacuum for 2 h. DPBS was added to hydrate and suspend the thin film to form drug-loaded micelles as clear solution, followed by filtration through 220 nm PVDF syringe filter to remove any unincorporated drug. The drug-free micelles were prepared via a same procedure without the addition of drug. Drug-free or drug-loaded PEG₅₀₀₀-OA₂ micelles were also similarly prepared as described above.

The diameter and size distribution of the micelles were examined via a Malvern Zeta Nanosizer. The morphology of both drug-free and drug-loaded micelles was observed by transmission electron microscopy (TEM) after negative staining. Drug in micelles was extracted by methanol, and detected by Waters Alliance 2695-2998 high-performance liquid chromatography (HPLC) system with a Lichrospher® 100 RP-18 column (250 mm × 4.6 mm)

equipped with a UV detector at 227 nm at room temperature, and 80:20 (v/v) of methanol/water was used as mobile phase at the flow rate at 0.8 mL/min. The drug loading capacity and efficiency were calculated according to the formula listed below:

$$\text{Drug loading capacity\%} = \frac{\text{weight of drug}}{\text{weight of polymer} + \text{weight of drug}} \times 100\%$$

$$\text{Drug loading efficiency\%} = \frac{\text{weight of drug loaded into micelles}}{\text{weight of drug used}} \times 100\%$$

2.2.6 Determination of the critical micelle concentration (CMC)

The fluorescence probe pyrene was employed to measure the critical micelle concentrations of PEG₅₀₀₀-(Fmoc-OA)₂ and PEG₅₀₀₀-OA₂ micelles. Various amounts of the conjugates in chloroform were mixed with pyrene (4×10^{-5} M in chloroform). The organic solvent was completely removed, and 2 mL of DPBS was added to each tube to form the micelles with the conjugate concentrations ranging from 1×10^{-4} to 0.5 mg/mL and a final pyrene concentration of 6×10^{-7} M. The fluorescence intensity of each sample was detected at 334/390 nm (excitation/emission) via Synergy H1 Hybrid Multi-Mode Microplate Reader (Winooski, VT), and the CMC value was determined from the threshold concentration, where the sharp increase in pyrene fluorescence intensity is observed.

2.2.7 Fluorescence quenching study

PTX-loaded PEG₅₀₀₀-(Fmoc-OA)₂ micelles and cholesterol (Chol) /PEG₅₀₀₀-(Fmoc-OA)₂ were prepared according to the procedure described above, and the carrier concentration was retained at 1.5 mg/mL in all the samples. The fluorescence intensity of sample solutions at the wavelength between 300-460 nm was recorded with an excitation wavelength at 270 nm by

using a Synergy H1 Hybrid Multi-Mode Microplate Reader.

2.2.8 Changes of particle sizes before and after lyophilization/reconstitution

One mL of PTX-loaded PEG₅₀₀₀-(Fmoc-OA)₂ micelles (PTX concentration at 1 mg/mL) was prepared according to the procedure described above. The micelle solution was frozen at -80 °C and then lyophilized overnight to obtain white powder. The obtained powder was suspended in 1 mL of distilled water to reconstitute the micelle solution. Particle sizes of the micelles before and after lyophilization/reconstitution were measured by dynamic light scattering method using a Zetasizer (Malvern).

2.2.9 *In vitro* drug release

Two mL of PTX-loaded PEG₅₀₀₀-(Fmoc-OA)₂ micelles, PEG₅₀₀₀-OA₂ micelles, or Taxol formulation (6 mg/mL PTX in Cremophor EL/ethanol 1:1, diluted to 1 mg PTX/mL with DPBS) was placed in a dialysis tube (MWCO 12 kDa, Spectrum Laboratories) that was incubated in 200 mL DPBS (PH = 7.4) containing 0.5% (w/v) Tween 80 at 37 °C with gentle shaking. The concentration of PTX remaining in the dialysis bags at scheduled times was detected by HPLC at the condition expressed above.

2.2.10 *In vitro* cytotoxicity

4T1.2 (1000 cells/well), PC-3 (3000 cells/well), or DU145 (2000 cells/well) cells were seeded in

96-well plates and incubated in DMEM containing 10% FBS and 1% streptomycin-penicillin at 37 °C for 24 h. PTX/PEG₅₀₀₀-(Fmoc-OA)₂ mixed micelles or Taxol formulation were added to cells in triplicate at the PTX concentrations from 6.25 to 200 ng/mL and cells were further incubated for 72 h. Then 20 µL of 3-(4, 5-dimethylthiazol-2-yl)-2,5-diphenyltetrazoliumbromide (MTT) in DPBS (5 mg/mL) was added to each well. Four h later, the medium was removed and 150 µL of DMSO was added to each well to solubilize the formazan crystal. The absorbance was measured at a wavelength of 550 nm and a reference wavelength at 630 nm with a microplate reader. Untreated cells were included as a control. Cell viability was calculated according to the following formula:

$$\% \text{ cytotoxicity} = [1 - (\text{OD}_{\text{treat}} - \text{OD}_{\text{blank}})/(\text{OD}_{\text{control}} - \text{OD}_{\text{blank}})] \times 100\%$$

2.2.11 Animals

Female BALB/c mice (10 to 12 weeks) were purchased from Charles River (Davis, CA), and were housed under pathogen-free conditions according to AAALAC guidelines. All animal-related experiments were performed in full compliance with institutional guidelines and approved by the Animal Use and Care Administrative Advisory Committee at the University of Pittsburgh.

2.2.12 *In vivo* tumor inhibition study

An aggressive syngeneic murine breast cancer model (4T1.2) was employed to evaluate the tumor inhibition effect of PTX-loaded PEG₅₀₀₀-(Fmoc-OA)₂ micelles. For establishment of the

tumor model, 2×10^5 of 4T1.2 cells in 100 μL of DPBS were inoculated s.c. at the right flank of female BALB/c mice, and treatments were initiated (Day 1) when the tumor volume reached $\sim 50 \text{ mm}^3$. Mice were randomly divided into four groups ($n=4$) and received i.v. administration of PTX/PEG₅₀₀₀-(Fmoc-OA)₂ micelles (10 mg PTX/kg), PTX/PEG₅₀₀₀-(Fmoc-OA)₂ micelles (20 mg PTX/kg), Taxol (10 mg PTX/kg), and saline, respectively on days 1, 3, 5, 7, and 9. Tumor sizes were monitored by a digital caliper and calculated based on the formula: $(L \times W^2)/2$, where L is the longest and W is the shortest tumor diameters (mm). Data were presented as relative tumor volume (RTV, the tumor volume at a given time point divided by the tumor volume prior to first treatment). Mice were sacrificed when tumors reached 2000 mm^3 or developed ulceration. The change of body weights of all mice was monitored during the entire course of treatment to evaluate the potential toxicity of different formulations.

2.2.13 Statistical analysis

In all statistical analysis, Student's t-test was performed between two groups, and the significance level was set at a probability of $p < 0.05$ and $p < 0.01$. All results were reported as the mean \pm standard error unless otherwise indicated.

2.3 RESULTS

2.3.1 Synthesis and characterization of PEG₅₀₀₀-lipopeptide with drug-interactive motifs

We have previously shown that inclusion of Fmoc motifs into PEG-lipid conjugates at the interfacial region significantly improved the drug-loading capacity and the formulation stability with JP4-039 as a model drug [55]. Our data showed that PEG-lipopeptides with 2 or 4 Fmoc motifs were more active than the one with one Fmoc motif in formulating JP4-039. This study is focused on the PEG-lipopeptide with 2 Fmoc motifs due to its relative simplicity. PEG₅₀₀₀ was chosen to construct the hydrophilic motif as the resulting PEG₅₀₀₀-lipopeptide performed better than the counterpart with PEG₂₀₀₀ or PEG₁₀₀₀ in formulating several compounds in a preliminary study (data not shown).

Figure 2 shows the structure of PEG₅₀₀₀-(Fmoc-OA)₂, in which two oleic acids and two Fmoc moieties were conjugated to PEG₅₀₀₀ using lysine-(lysine)₂ as a bridge. Scheme 1 shows the procedures for the synthesis of both PEG₅₀₀₀-(Fmoc-OA)₂ and PEG₅₀₀₀-OA₂, a control PEG-lipopeptide without Fmoc motifs. ¹H NMR spectrum of PEG₅₀₀₀-(Fmoc-OA)₂ shows signals at 3.63 ppm attributed to the methylene protons located at the terminal of PEG backbone, the Fmoc proton signals at 7.9-7.3 ppm, the signals attributed to the double bond at the carbon chain of OA at 5.25 ppm, the signals attributed to the methyl of OA at 0.89 ppm, and the carbon chain signals of OA at 1.25-1.05 ppm (**Figure 3**). The ¹H NMR spectrum for PEG₅₀₀₀-OA₂ shows similar proton signals except lack of proton signals for Fmoc (**Figure 4**). The molecular weights of the PEG₅₀₀₀-(Fmoc-OA)₂ and PEG₅₀₀₀-OA₂ conjugates measured by MALDI-TOF Mass Spectrum are close to the theoretical values (**Figures 5&6**).

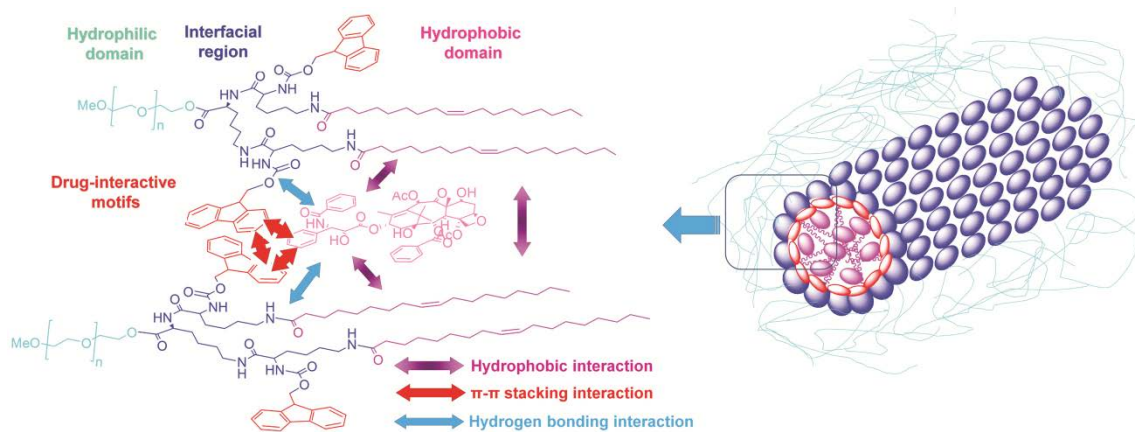


Figure 2. Structure of PEG₅₀₀₀-(Fmoc-OA)₂ and the postulated modes of carrier-drug and carrier-carrier interactions.

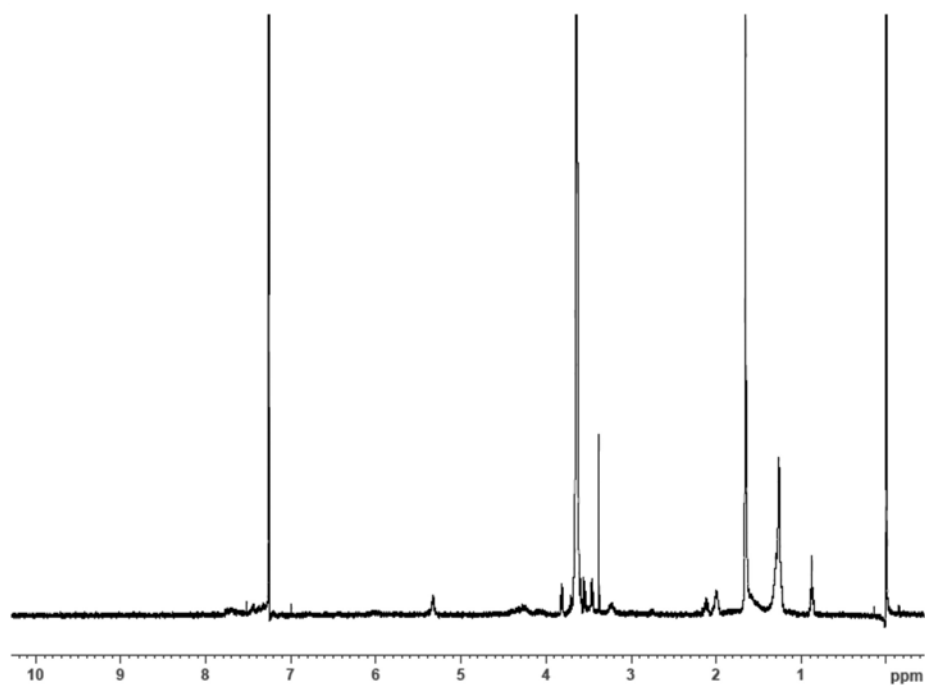


Figure 3. ¹H NMR spectrum of PEG₅₀₀₀-(Fmoc-OA)₂.

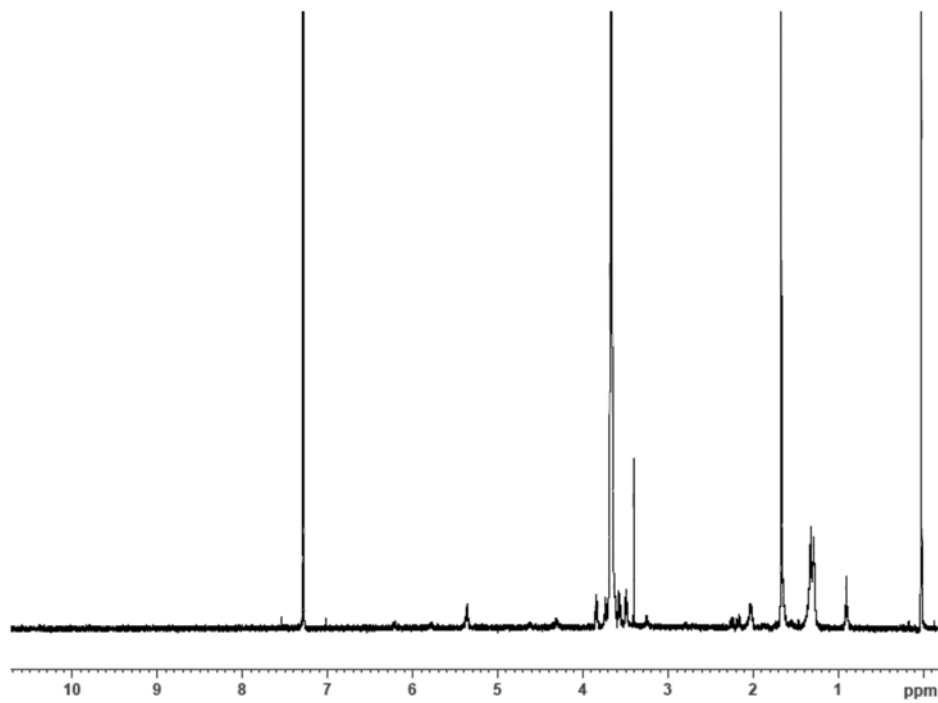


Figure 4. ^1H NMR spectrum of $\text{PEG}_{5000}\text{-OA}_2$.

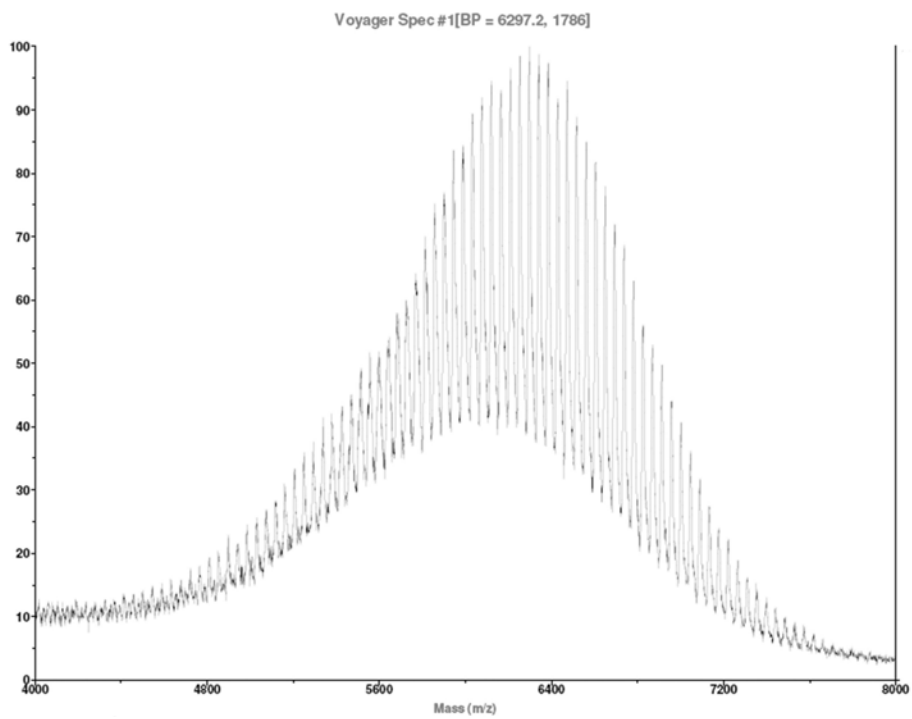


Figure 5. MALDI-TOF Mass Spectrum of $\text{PEG}_{5000}\text{-(Fmoc-OA)}_2$.

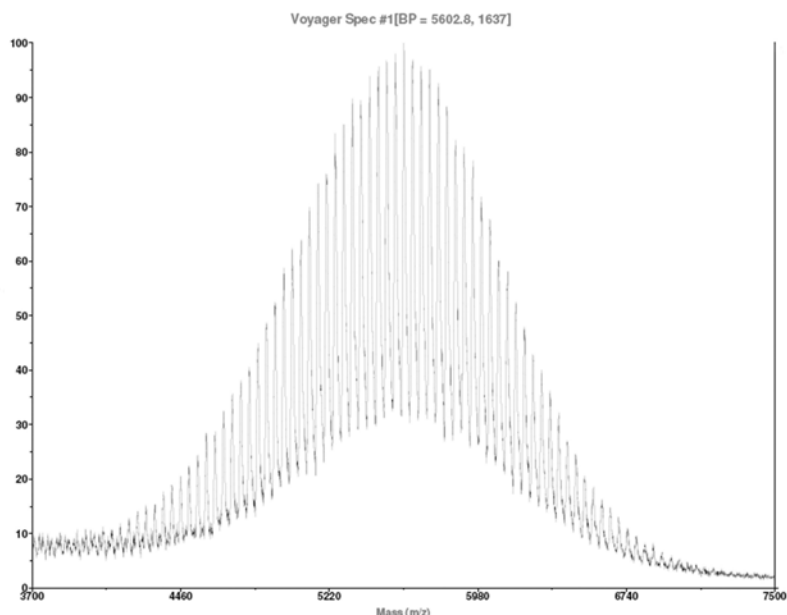


Figure 6. MALDI-TOF Mass Spectrum of PEG₅₀₀₀-OA₂.

2.3.2 Biophysical characterization of drug-free and PTX-loaded PEG-lipopeptide micelles

As an initial step to examine the general applicability of our PEG-lipopeptide in formulating different drugs of diverse structures, we examined the efficiency of PEG₅₀₀₀-(Fmoc-OA)₂ in delivering PTX to tumor cells *in vitro* and *in vivo*. PEG₅₀₀₀-OA₂ was used as a control formulation.

Both PEG₅₀₀₀-(Fmoc-OA)₂ and PEG₅₀₀₀-OA₂ readily formed micelles in DPBS. **Figure 7** shows the size distribution and TEM images of PEG₅₀₀₀-(Fmoc-OA)₂ and PEG₅₀₀₀-OA₂ micelles. The size of PEG₅₀₀₀-OA₂ is around 20 nm as determined by DLS (**Figure 7A**). TEM images show spherical particles for PEG₅₀₀₀-OA₂ micelles (**Figure 7B**) and the sizes of the particles on TEM were consistent with that determined by DLS. PEG₅₀₀₀-(Fmoc-OA)₂ formed particles of slightly larger size (~ 60 nm) as determined by DLS (**Figure 7D**). TEM revealed mostly tubular structures (**Figure 7E**), suggesting formation of filamentous micelles.

The CMC values of PEG₅₀₀₀-(Fmoc-OA)₂ and PEG₅₀₀₀-OA₂ micelles were measured using pyrene as a fluorescence probe. As shown in **Figure 7C&F**, the CMC of PEG₅₀₀₀-(Fmoc-OA)₂ is 0.626 μM, which is lower than those of PEG₅₀₀₀-OA₂ (0.994 μM) and many reported surfactants [69-71].

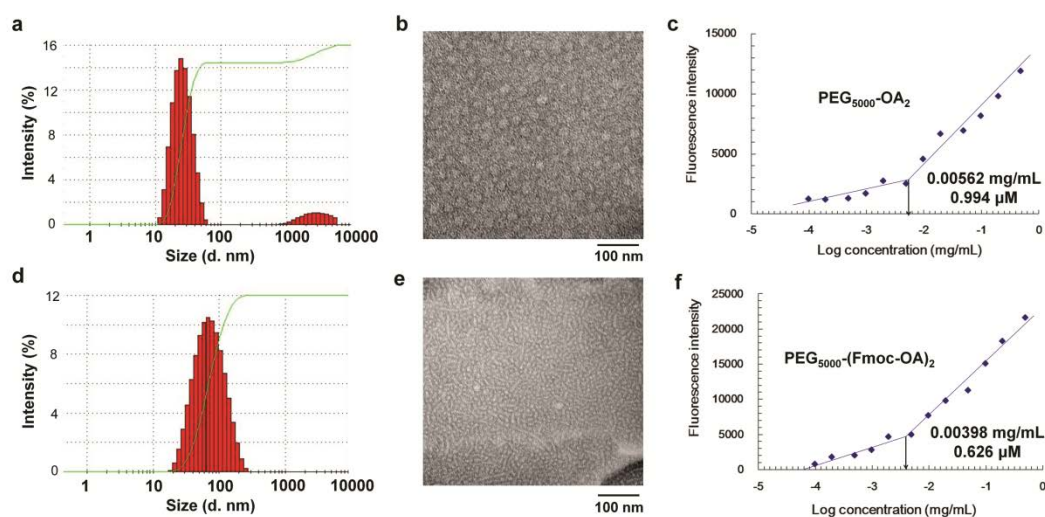


Figure 7. Size distribution of PEG₅₀₀₀-OA₂ (A) and PEG₅₀₀₀-(Fmoc-OA)₂ (D) measured by dynamic light scattering (DLS); and transmission electron microscopy (TEM) of PEG₅₀₀₀-OA₂ (B) and PEG₅₀₀₀-(Fmoc-OA)₂ (E) micelles. The spherical particles with a diameter around 20 nm were observed for PEG₅₀₀₀-OA₂ micelles, while filamentous micelles with tubular structure were observed for PEG₅₀₀₀-(Fmoc-OA)₂ micelles. CMC measurements of the PEG₅₀₀₀-OA₂ (C) and PEG₅₀₀₀-(Fmoc-OA)₂ (F) micelles using pyrene as a fluorescence probe. The fluorescence intensity was plotted as a function of logarithmic concentration of micelles.

Table 1 shows the size, drug loading capacity (DLC), and drug loading efficiency (DLE) for PEG₅₀₀₀-(Fmoc-OA)₂/PTX mixed micelles in comparison with PEG₅₀₀₀-OA₂ formulation. PTX could be formulated in PEG₅₀₀₀-(Fmoc-OA)₂ micelles at a carrier/drug molar ratio as low as 0.75/1 although the resulting PTX-loaded micelles stayed stable for only 1.5 h. There was little change in the particle sizes before and after the incorporation of PTX. Under this condition, the DLC and DLE were 15.19% and 56.29%, respectively. An increase in the carrier/drug input ratio was associated with an increase in the DLE and significantly improved stability of the PEG₅₀₀₀-(Fmoc-OA)₂/PTX mixed micelles. The particles stayed stable for more than 20 h at carrier/drug

ratios of 5/1 and above.

On the contrary, a minimal carrier/drug ratio of 2.5/1 was needed to load PTX into PEG₅₀₀₀-OA₂ micelles and the resulting mixed micelles were only stable for 1 h. The PEG₅₀₀₀-OA₂/PTX mixed micelles were also significantly less stable than PEG₅₀₀₀-(Fmoc-OA)₂/PTX mixed micelles at other carrier/drug ratios examined.

Table 1. Biophysical characterization of drug-free and PTX-loaded PEG₅₀₀₀-OA₂ and PEG₅₀₀₀-(Fmoc-OA)₂ micelles.

| Micelles | Molar ratio | Size (nm) | PDI ^a | DLC ^b (%) | DLE ^c (%) | Stability (h) |
|---|-------------|------------|------------------|----------------------|----------------------|---------------|
| PEG ₅₀₀₀ -OA ₂ | - | 26.76±0.44 | 0.262 | - | - | - |
| PEG ₅₀₀₀ -OA ₂ /PTX ^d | 2.5:1 | 23.52±0.21 | 0.103 | 5.70 | ND ^e | 1 h |
| | 5:1 | 22.62±0.33 | 0.102 | 2.93 | ND | 1.5 h |
| | 7.5:1 | 23.93±0.33 | 0.098 | 1.97 | ND | 3.5 h |
| PEG ₅₀₀₀ -(Fmoc-OA) ₂ | - | 58.72±1.06 | 0.220 | - | - | - |
| PEG ₅₀₀₀ -(Fmoc-OA) ₂ /PTX ^d | 0.75:1 | 66.26±0.46 | 0.233 | 15.19 | 56.29 | 1.5 h |
| | 1:1 | 70.28±1.25 | 0.256 | 11.84 | 88.73 | 2 h |
| | 2.5:1 | 69.42±1.91 | 0.248 | 5.10 | 80.50 | 3.5 h |
| | 5:1 | 73.55±1.26 | 0.258 | 2.62 | 92.95 | 22 h |
| | 7.5:1 | 73.13±1.29 | 0.245 | 1.76 | 97.73 | 70 h |

^a PDI, polydispersity index. ^b DLC, drug loading capacity. ^c DLE, drug loading efficiency.

^d PTX concentration in micelles were kept at 1 mg/mL, drug-free micelle concentration was 20 mg/mL.

^e ND, not determined.

The above data clearly demonstrated that the inclusion of Fmoc motifs into PEG₅₀₀₀-OA₂ micelles significantly improved the PTX loading capacity and the stability of PTX-loaded micelles. This improvement is likely due to strong Fmoc/PTX π - π stacking interaction. With the attempt to obtain more insight into this intermolecular interaction, fluorescence quenching of PEG₅₀₀₀-(Fmoc-OA)₂ was investigated. As shown in **Figure 8**, with an excitation at wavelength of 270 nm, PEG₅₀₀₀-(Fmoc-OA)₂ exhibited a maximum fluorescence at 305 nm, while the fluorescence intensity was decreased with the addition of PTX, and the extent of this quenching was apparently correlated to amount of PTX. However, no quenching was observed with the

presence of the same amount of cholesterol (Chol), a hydrophobic molecule lack of aromatic rings. It has been proved that intermolecular π - π stacking between aromatic rings can efficiently cause fluorescence quenching through energy transfer [72]. This may solidify the presence of π - π stacking interaction occurred between Fmoc and PTX.

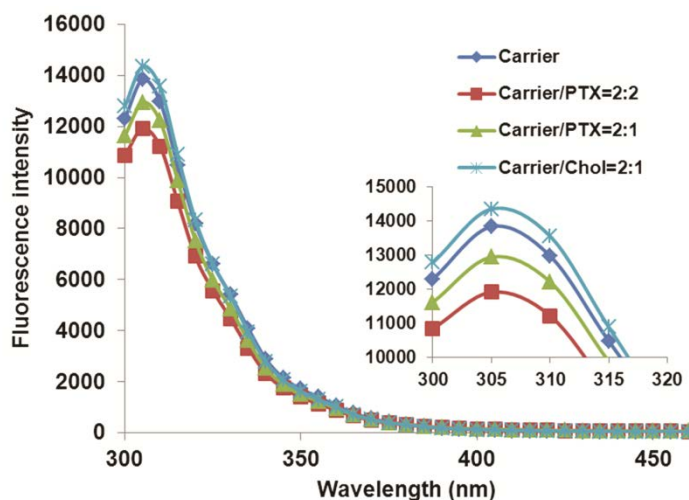


Figure 8. Fluorescence quenching of PEG₅₀₀₀-(Fmoc-OA)₂. The concentration of PEG₅₀₀₀-(Fmoc-OA)₂ was fixed at 1.5 mg/mL, and mixed with PTX and Chol at designated molar ratios in PBS. Intensity of fluorescence emitted between 300-460 nm was recorded with excitation wavelength at 270 nm.

As revealed by ¹H-NMR spectra of PEG₅₀₀₀-(Fmoc-OA)₂/PTX (**Figure 9**), all the proton signals of PTX were suppressed in deuterated water, indicating a complete entrapment of PTX inside self-assembled micelle surrounded by PEG shell, while when presence as polymer/drug mixture in CDCl₃, signals from both carrier and PTX were clearly observed.

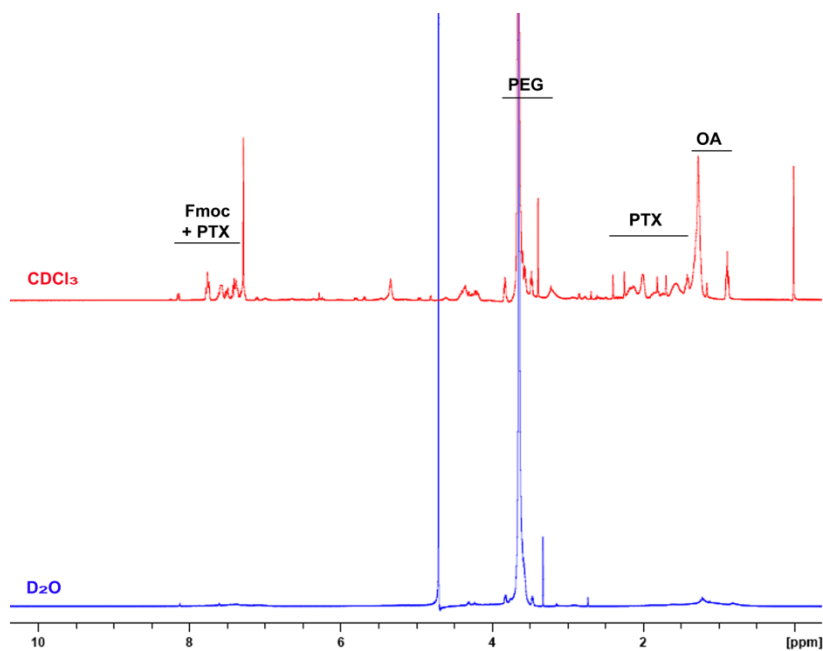


Figure 9. ^1H NMR spectra of PTX/PEG₅₀₀₀-(Fmoc-OA)₂ in D₂O and CDCl₃. Carrier/drug molar ratio was retained at 2.5:1.

We then examined the effect of freezing and lyophilization on the stability of PEG₅₀₀₀-(Fmoc-OA)₂/PTX mixed micelles. As shown in **Figure 10**, there were essentially no changes in the size distribution for PEG₅₀₀₀-(Fmoc-OA)₂/PTX mixed micelles following lyophilization and reconstitution of the lyophilized power with water.

2.3.3 Release kinetics of PTX-loaded mixed micelles

The kinetics of PTX release from PTX-loaded PEG₅₀₀₀-(Fmoc-OA)₂ micelles was examined via dialysis method, and compared to PEG₅₀₀₀-OA₂/PTX micelles and Taxol formulation. As shown in **Figure 11**, the PTX-loaded PEG₅₀₀₀-(Fmoc-OA)₂ micelles showed much enhanced stability. After first 24 h, only 27.88% of formulated PTX was released from PTX/PEG₅₀₀₀-(Fmoc-OA)₂ mixed micelles, while 55.90% and 62.88% of PTX was released from PEG₅₀₀₀-OA₂/PTX micelles and Taxol formulation, respectively. The $T_{1/2}$ of PTX release is 19.8 h and 14.4 h for

PEG₅₀₀₀-OA₂/PTX and Taxol formulation, respectively, while only 33% of PTX was released from PEG₅₀₀₀-(Fmoc-OA)₂ micelles even after 72 h.

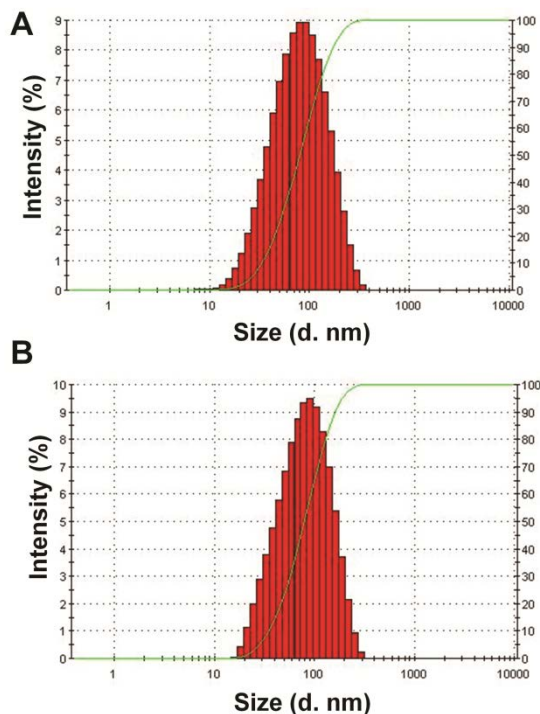


Figure 10. Particle size distribution before (A) and after (B) lyophilization and reconstitution of PTX-loaded PEG₅₀₀₀-(Fmoc-OA)₂ micelles. No obvious size change was observed. PTX concentration in micelles was at 1 mg/mL.

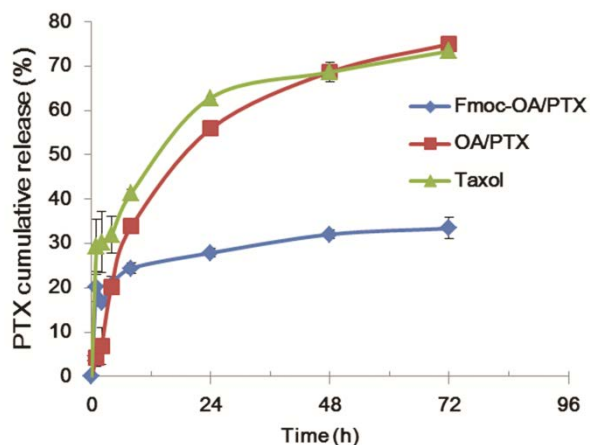


Figure 11. Cumulative PTX release profile from PTX-loaded PEG₅₀₀₀-(Fmoc-OA)₂ micelles (Fmoc-OA/PTX), PEG₅₀₀₀-OA₂ micelles (OA/PTX) and Taxol. PTX concentration was kept at 1 mg/mL in all the formulations, and DPBS (pH 7.4) containing 0.5% (w/v) Tween 80 was utilized as release medium.

2.3.4 *In vitro* cytotoxicity study

The *in vitro* cytotoxicity of PTX-loaded PEG₅₀₀₀-(Fmoc-OA)₂ micelles was evaluated with three different tumor cell lines, 4T1.2, PC-3, and DU145, and compared to that of Taxol, a clinical PTX formulation. PTX-loaded PEG₅₀₀₀-(Fmoc-OA)₂ micelles exhibited higher levels of cytotoxicity than Taxol in all three cell lines tested (**Figure 12A, B & C**). Interestingly, PEG₅₀₀₀-(Fmoc-OA)₂ micelles alone showed modest cytotoxicity towards 4T1.2 cells (**Figure 12A**) while they showed minimal effect on the growth of prostate cancer cells PC-3 and DU145 (**Figure 12B & C**).

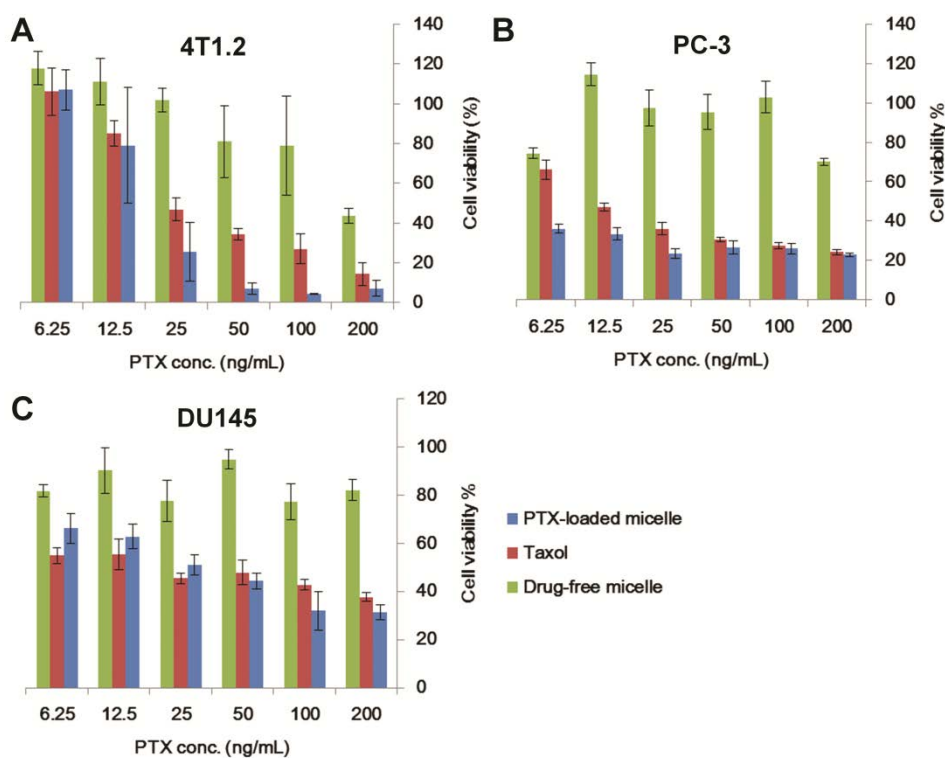


Figure 12. Cytotoxicity of PTX-loaded PEG₅₀₀₀-(Fmoc-OA)₂ micelles, drug-free PEG₅₀₀₀-(Fmoc-OA)₂ micelles, and Taxol to 4T1.2 mouse breast cancer cell line (A), human prostate cancer cell lines PC-3 (B), and DU145 (C). Cells were treated for 72 h and cytotoxicity was determined by MTT assay.

2.3.5 *In vivo* antitumor activity

The *in vivo* therapeutic activity of PTX formulated in PEG₅₀₀₀-(Fmoc-OA)₂ micelles was investigated in a syngeneic murine breast cancer model (4T1.2). As shown in **Figure 13**, compared with saline treated mice (control), Taxol dosed at 10 mg/kg exhibited modest effects in inhibiting the tumor growth. At the same PTX dosage, PTX formulated in PEG₅₀₀₀-(Fmoc-OA)₂ micelles was more effective than Taxol in inhibiting the tumor growth ($p < 0.05$). PTX/PEG₅₀₀₀-(Fmoc-OA)₂ micelles with an increased dose at 20 mg/kg clearly exhibited a dramatically elevated therapeutic efficacy than Taxol ($p < 0.01$). No apparent weight change was observed in both 10 and 20 mg/kg treatment groups.

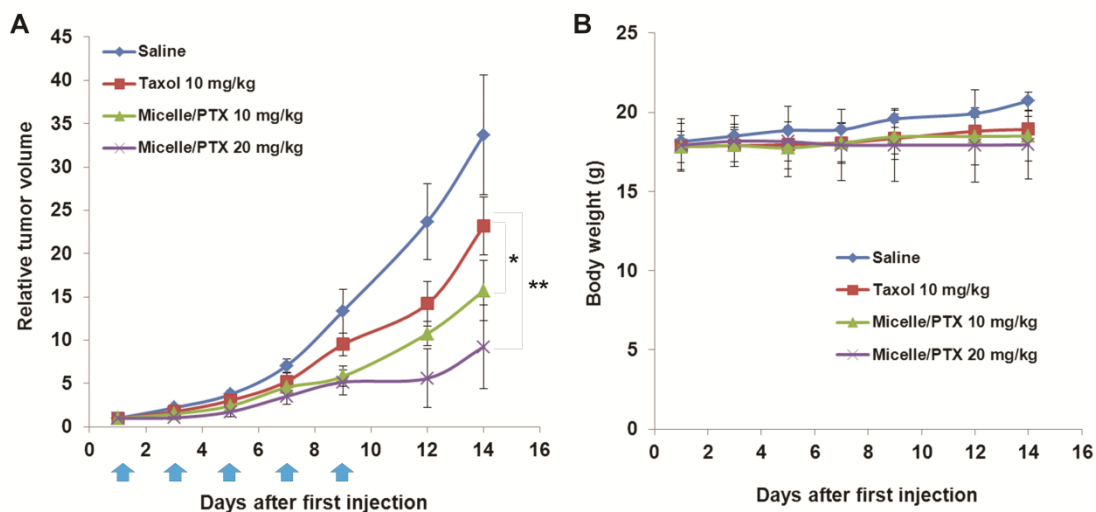


Figure 13. (A) Tumor inhibitory activity of PTX-loaded PEG₅₀₀₀-(Fmoc-OA)₂ micelles. BALB/c mice were inoculated s.c. with 4T1.2 cells (2×10^5 cells/mouse). Five days later, mice received various treatments on days 1, 3, 5, 7 and 9, and tumor growth was monitored and plotted as relative tumor volume. * $P < 0.05$ (PEG₅₀₀₀-(Fmoc-OA)₂/PTX at 10 mg/kg vs. Taxol at 10 mg/kg). ** $P < 0.01$ (PEG₅₀₀₀-(Fmoc-OA)₂/PTX at 10 mg/kg vs. Taxol at 10 mg/kg). N=4. (B) Changes of body weight in mice in different treatment groups.

2.3.6 Effectiveness of PEG₅₀₀₀-(Fmoc-OA)₂ micelles in formulating 7 other drugs of differents

The above study clearly demonstrated that the inclusion of Fmoc motifs into PEG-lipid micelles improved PTX loading capacity and facilitates its delivery to tumor cells *in vitro* and *in vivo*. We then went on to test the effectiveness of our improved system in formulating seven additional model drugs of different structures (**Figure 14**) to test the general utility of our formulation. These include probucol (cholesterol-lowering drug), niclosamide (antiparasitic agent), JP4-039 (antioxidant), progesterone (female hormone), cyclosporin A (immunosuppressant), nifedipine (Ca²⁺ channel blocker), and griseofulvin (antifungal agent). The structural features of these compounds were summarized in **Table 2** and they were loaded into PEG₅₀₀₀-(Fmoc-OA)₂ micelles at the concentration of 1 mg drug/mL, respectively, which represents a 71 ~ 1.7×10⁵-fold increase in solubility compared with the original aqueous solubility of each compound.

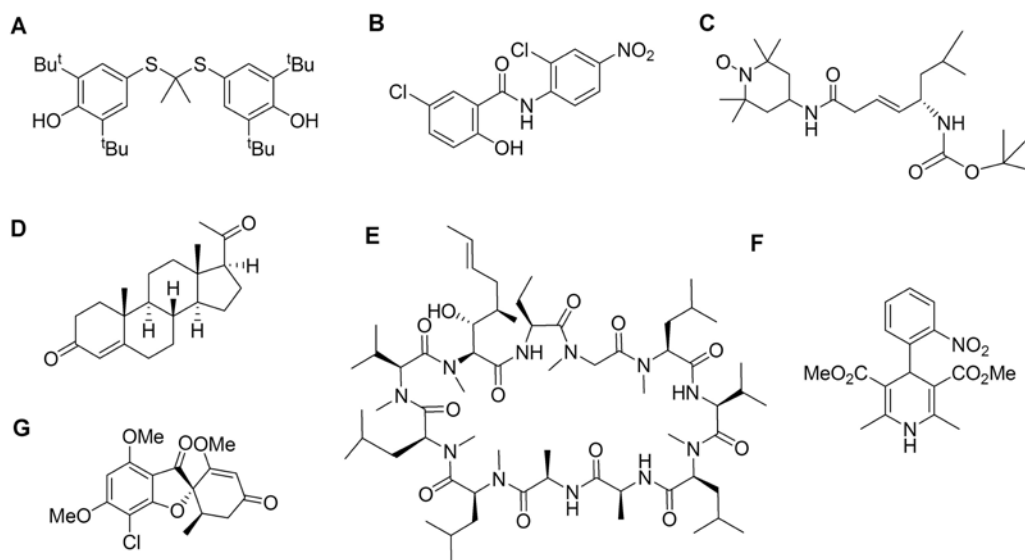


Figure 14. Chemical structure of seven drug candidates effectively formulated in PEG₅₀₀₀-(Fmoc-OA)₂ micelles. A, probucol; B, niclosamide; C, JP4-039; D, progesterone; E, cyclosporin A; F, nifedipine; and G, griseofulvin.

Table 2. Effectiveness of PEG₅₀₀₀-(Fmoc-OA)₂ micelles in formulating drugs of diverse structures.

| Drug candidate | Biologic activities | Number of aromatic rings | Structural features | Log P | Free drug solubility (μg/mL) | Carrier/drug molar ratio ^a | DLC ^b (%) | Particle size (nm) |
|----------------|----------------------------------|--------------------------|---|-------------------|------------------------------|---------------------------------------|----------------------|--------------------|
| probucol | cholesterol-lowering drug | 2 | dimerized di-tert-butylthiophenol | 8.08 ^c | 0.006 ^d | 2.5 | 3.15 | 74.22±2.57 |
| niclosamide | antiparasitic agent | 2 | salicylanilide | 4.56 ^c | 0.23 ^f | 2.5 | 2.02 | 81.94±4.37 |
| JP4-039 | antioxidant | 0 | peptide | N/A | N/A | 2.5 | 3.13 | 55.90±0.75 |
| progesterone | female hormone | 0 | steroid hormone | 3.87 ^e | 7 ^h | 0.25 | 16.52 | 70.57±0.73 |
| cyclosporin A | immunosuppressant | 0 | 11 amino acids cyclic peptide | 3.0 ^f | 6.6 ^f | 2.5 | 7.04 | 72.79±1.62 |
| nifedipine | Ca ²⁺ channel blocker | 2 | nitrophenyl dihydropyridine dicarboxylate | 2.5 ^f | 5 ^h | 0.5 | 9.83 | 63.75±1.22 |
| griseofulvin | antifungal agent | 1 | methoxy benzofuran, cyclohexene-dione | 2.0 ^f | 14 ^h | 2.5 | 2.17 | 66.79±0.96 |

^a Carrier/drug molar ratio to efficiently solubilize drug at 1 mg/mL in DPBS. ^b DLC, drug loading capacity. ^{c-m} Log P and solubility of listed drugs refer to [58].

2.4 DISCUSSION

We have confirmed and extended our previous work that the inclusion of a drug-interactive motif at the interfacial region of surfactants significantly improves the drug-loading capacity and formulation stability. PEG-lipopeptides were originally developed to formulate JP4-039, a peptide-based antioxidant [55]. Data from the present study suggest that our concept is applicable to various types of therapeutic agents of diverse structures.

One of the key findings of our study is the unusual propensity of Fmoc motif in interacting with many types of drugs, ranging from PTX, steroids, to hydrophobic peptide drugs with linear or cyclic configuration (**Table 2**). These agents have one or more aromatic or heterocyclic ring structures or multiple hydrophobic side chain groups if it is a peptide derivative, and can form hydrogen bond with other molecules. These features are quite ubiquitous among many drugs and drug candidates, suggesting that this motif may have the utility for a broad spectrum of compounds. These data strongly suggest that α-Fmoc behaves as a “formulation chemophor” or

a structural unit capable of interacting with many pharmaceutical agents. The molecular basis for such propensity of interactions is likely due to a combination of the fused aromatic ring structure of fluorenyl group and its carbamate and amide linkages. Fluorenyl group is a compact hydrophobic motif capable of forming hydrophobic π - π interactions with compounds carrying one or more aromatic ring structures. Such interaction is normally stronger than the van der Waals interaction between alkyl chains. The carbamate and other amine linkages in the conjugate are known to facilitate hydrogen bonding interactions, which shall also contribute to both carrier/carrier and carrier/drug interactions (**Figure 2**). The importance of Fmoc was supported by the observations that the performance of the PEG-lipopeptides was significantly compromised if it was replaced by other motifs such as Boc (Gao et al., unpublished data).

Similar to a PEG-lipopeptide with 4 Fmoc motifs, PEG₅₀₀₀-(Fmoc-OA)₂ formed tubular structures, suggesting the formation of filamentous micelles (**Figure 7E**). These structures were well retained following the incorporation of PTX. This is likely due to strong interaction among the Fmoc-containing PEG-lipopeptides. It is known that Fmoc-containing short peptides tend to show strong interaction among themselves to form tubular structures that resulted in formation of hydrogels [73]. However, the lipid motif may also contribute to the formation of tubular structures as a PEG₅₀₀₀-Fmoc counterpart without OA chains formed spherical particles in the absence or presence of loaded PTX (data not shown). It has been reported that filamentous polymeric micelles exhibit substantially longer half-life in the blood compared to the spherical counterparts [74]. More studies are needed to examine the *in vivo* pharmacokinetics profiles of our PEG-lipopeptides as well as the mechanisms involved in various modes of self-assemblies.

In addition to examining the general utility of our system in formulating different types of drugs of diverse structures, we further explored its potential in the delivery of PTX to tumor

cells. PTX is a first-line therapeutic agent for various types of cancers; however its clinical application is limited by the toxicity and poor water solubility [75-78]. Taxol is an alcohol/Cremophor formulation that can cause local irritation and severe histamine-mediated hypersensitivity reactions [79-81]. PEG-derivatized phospholipid has been shown to be able to form simple micellar formulation with PTX, but has limited loading capacity (31-33). We also noticed a low PTX loading capacity with a similar system based on PEG₅₀₀₀-OA₂ conjugate (**Table 1**). Incorporation of Fmoc into this system led to a 3-fold increase in PTX loading capacity. In addition, the colloidal stability of PTX/PEG₅₀₀₀-(Fmoc-OA)₂ mixed micelles was significantly improved compared to that of PTX-loaded PEG₅₀₀₀-OA₂ micelles (**Table 1**). This is corroborated by the observation that PTX formulated in PEG₅₀₀₀-(Fmoc-OA)₂ micelles also demonstrated a much slower kinetics of PTX release compared to Taxol formulation and PEG₅₀₀₀-OA₂ micelles without Fmoc motifs (**Figure 11**). These improvements may attribute to the strengthened carrier/PTX interaction, of which the major one is likely Fmoc/PTX π - π stacking interaction. More studies are needed to be accomplished in the future to obtain a further understanding of mechanism of carrier/PTX interaction.

We have further demonstrated an improved antitumor activity for our micellar PTX compared to Taxol formulation both *in vitro* and *in vivo*. At an increased dosage (20 mg/kg) of PTX (**Figure 13**), which is beyond the maximum tolerated dose of Taxol [67], our micelle formulation showed a significantly enhanced tumor inhibitory effect and great safety with no animal death and apparent weight loss. The improved performance is likely due to an enhanced carrier/drug interaction and an improved stability of the PTX micelle formulation *in vivo*, which presumably lead to an effective delivery of PTX to tumors through the EPR effect.

In summary, we have shown that incorporation of Fmoc motifs into a PEG-lipopeptide

conjugate resulted in an improved nanocarrier that is effective in formulating eight model drugs of diverse structures. We have further shown that incorporation of PTX into our new formulation led to improved antitumor activity over Taxol in vitro and in vivo. Our study suggests that micelle-forming PEG-lipopeptide surfactants with interfacial Fmoc motifs may represent a promising drug formulation platform for a broad range of drugs with diverse structures. The following chapters are focused on more structure-activity relationship study to further improve this new formulation.

3.0 A PEG-FMOC CONJUGATE AS A NANOCARRIER FOR PACLITAXEL

3.1 BACKGROUND

Nanomedicine has been shown to dramatically improve the *in vivo* performance of various anticancer agents through modifying their physiochemical properties, pharmacokinetics, and distribution profiles [11-13, 19, 82, 83]. To date, a variety of polymer- and lipid-based systems have been developed and a few of them are currently being used in the clinic [10, 14, 20, 84, 85]. However, it remains a challenge to develop a simple, easy-to-scale up system that provides excellent drug loading capacity and formulation stability.

As a well-developed delivery system, micelles are attractive due to the ease of preparation, and small sizes that can contribute to a reduced rate of elimination from circulation and enhanced accumulation at solid tumors with leaky vasculature based on the enhanced penetration and retention (EPR) effect [15, 16]. Most of the current micellar systems are composed of two distinct domains, one being hydrophilic and the other hydrophobic, and drug loading is solely based on the interactions of their hydrophobic domains with the poorly water-soluble drugs [21, 32, 64]. While working well for highly hydrophobic/lipophilic agents, these systems exhibit limited effectiveness for drugs with moderate hydrophobicity due to limited drug-carrier compatibility.

Recent studies have highlighted the benefits of introducing other drug-interactive domains into the conventional micellar systems to improve the drug loading capacity and formulation stability through introduction of additional mechanisms of carrier/drug interactions. For example, some studies have demonstrated that inclusion of a hydrotropic domain or entire drug molecule such as doxorubicin can effectively improve the performance of several polymeric systems with respect to drug loading capacity and colloidal stability of drug-loaded micelles [48, 50, 53, 54, 86].

We have recently developed a new concept that introduction of a drug-interactive domain at the interfacial region represents an effective strategy to improve the compatibility between lipid-core micelles and the hydrophobic drugs. Among several drug-interactive domains tested, 9-Fluorenylmethoxycarbonyl (Fmoc) was shown to have an unusual propensity in interacting with many types of agents of diverse structure and water solubility [55]. After interfacially modified with Fmoc groups, polyethylene glycol (PEG)-lipopeptides are active in formulating a panel of dissimilar drugs, ranging from paclitaxel (PTX), steroids, xanthene- and porphyrin-based photodynamic agents, to hydrophobic peptide drugs, with significant improvements in both drug loading capacity and drug retention [58]. These data strongly suggest that Fmoc qualifies as a “formulation chemophor”, exhibiting a potent activity in interacting with various pharmaceutical agents and thus a capability of improving carrier-drug compatibility.

In general, it is believed that a large hydrophobic domain such as a lipid chain or hydrophobic polymer is necessary to construct micelle-forming surfactants, and indeed, Fmoc-containing PEG-lipid conjugates were more effective than the counterparts without a lipid motif in formulating a number of hydrophobic agents. Interestingly, a PEG-Fmoc conjugate without a lipid motif, PEG₅₀₀₀-lysyl-(α -Fmoc- ϵ -t-Boc-lysine)₂ (PEG-Fmoc), was found to be highly

effective in solubilizing PTX. More surprising is the finding that PEG-Fmoc was significantly more effective than the counterpart with a lipid motif in formulating PTX. This study is focused on characterization of PEG-Fmoc as a simple and effective micellar formulation for PTX. The potential mechanism involved in the drug/carrier interaction between PEG-Fmoc and PTX is also investigated, which may shed insights into the future development of further improved nanocarrier for therapeutic agents.

3.2 METHODS

3.2.1 Materials

Paclitaxel (PTX, >99%) was purchased from TSZ Chem (MA, USA). Docetaxel (DTX, >99%) was obtained from LC Laboratories (MA, USA). α -Fmoc- ϵ -Boc-lysine, di-Boc-lysine, N, N'-dicyclohexylcarbodiimide (DCC), N-hydroxysuccinimide (NHS), trifluoroacetic acid (TFA), and triethylamine (TEA) were obtained from Acros Organic (NJ, USA). Monomethoxy PEG₅₀₀₀, monomethoxy PEG₅₅₀, cholesterol (CHOL), 4-dimethylaminopyridine (DMAP), ninhydrin, and other unspecified chemicals were all purchased from Sigma-Aldrich (MO, USA). Dulbecco's phosphate buffered saline (DPBS), Dulbecco's Modified Eagle's Medium (DMEM), fetal bovine serum (FBS), 100X penicillin-streptomycin solution were all purchased from Invitrogen (NY, USA). All solvents used in this study were HPLC grade.

3.2.2 Synthesis of PEG₅₀₀₀-lysyl-(α -Fmoc- ϵ -t-Boc-lysine)₂ (PEG-Fmoc)

PEG-Fmoc was synthesized largely following our published method [58]. Briefly, 1 equiv. of monomethoxy PEG₅₀₀₀ was mixed with excess amount of di-Boc-lysine and DCC in dichloromethane (DCM) with addition of DMAP, and the reaction was allowed at room temperature for 48 h. The mixture was filtered and precipitated in ice-cold ether, followed by washes with cold ethanol and ether to obtain purified PEG₅₀₀₀-di-Boc-lysine. The PEG derivative was then treated with DCM/TFA (1:1, v/v) for 2 h at room temperature, followed by removal of the solvent, precipitation in cold ether, and washes with cold ethanol and ether. Finally, the deprotected PEG₅₀₀₀-lysine-NH₂ was mixed with excess amount of α -Fmoc- ϵ -Boc-lysine that was pre-activated with NHS, DCC, and small amount of DMAP in DCM at 37°C for 4 h. The reaction was allowed at 37 °C till the ninhydrin test became negative, indicating the absence of free amino groups. The reaction mixture was filtered and precipitated by ice-cold ether, followed by washes with cold ethanol and ether. The obtained material was dissolved in water and filtered through a 450 nm filter, followed by lyophilization to yield the powder of purified PEG₅₀₀₀-lysyl-(α -Fmoc- ϵ -t-Boc-lysine)₂.

3.2.3 Preparation and biophysical characterization of PTX/PEG-Fmoc mixed micelles

Thin-film hydration method was utilized for preparation of PTX/PEG-Fmoc mixed nanomicelles. PEG-Fmoc and PTX in chloroform were well mixed in a glass tube at designated molar ratios. A thin film of carrier/drug mixture was generated through removal of the organic solvent by a gentle stream of nitrogen. The trace amount of solvent was further removed via

vacuum for 2 h. Then the film was hydrated and suspended in DPBS by vortex to obtain a clear solution of PTX/PEG-Fmoc mixed nanomicelles. Any non-entrapped drug was removed by filtration through 450 nm PVDF syringe filter.

The size distribution of PTX/PEG-Fmoc mixed nanomicelles was examined by dynamic light scattering (DLS), and the zeta potential was measured via a Malvern *Zeta Nanosizer*. The morphology was observed by transmission electron microscopy (TEM) after negative staining. The CMC measurement was performed as reported before with pyrene as a fluorescence probe [58]. To quantify PTX in the micelles, PTX was extracted by methanol, and detected by Waters Alliance 2695-2998 high-performance liquid chromatography (HPLC) system with a RP-18 column (250 mm × 4.6 mm) equipped with a UV detector at 227 nm at room temperature. A mixture of methanol/water (80:20, v/v) was used as mobile phase at a flow rate at 0.8 mL/min. The drug loading capacity (DLC) and efficiency (DLE) were calculated using the formula:

$$\text{Drug loading capacity\%} = \frac{\text{weight of drug}}{\text{weight of polymer} + \text{weight of drug}} \times 100\%$$

$$\text{Drug loading efficiency\%} = \frac{\text{weight of drug loaded into micelles}}{\text{weight of drug used}} \times 100\%$$

3.2.4 Effect of lyophilization/reconstitution on particle sizes

One mL of PTX/PEG-Fmoc in DPBS was prepared as described above and the PTX concentration was kept at 1 mg/mL. The clear solution was frozen and lyophilized overnight to obtain white powder. The powder was then reconstituted with 1 mL of distilled water to obtain a clear solution. Particle sizes of the PTX-loaded micelles before and after lyophilization/reconstitution were recorded via DLS using a Zetasizer.

3.2.5 Differential scanning calorimetry (DSC) analysis

A Mettler Toledo DSC was used for DSC analysis. Samples (PTX, PEG-Fmoc/PTX, and drug-free PEG-Fmoc) were accurately weighed and placed in aluminum crucibles, which were sealed using a Mettler Toledo sealer. An empty crucible was used as a reference. The temperature range was set from 25 °C to 285 °C with a rate at 10 °C/min using nitrogen (50 mL/min) as segment gas.

3.2.6 Fluorescence quenching

PEG₅₀₀₀-lysyl-(α -Fmoc- ϵ -oleic acid-lysine)₂ (PEG-Fmoc-OA) was synthesized as reported [58]. PTX/PEG-Fmoc and PTX/PEG-Fmoc-OA mixed micelles of various PTX/carrier molar ratios were prepared in DPBS as described above, and the molar concentrations of PEG-Fmoc and PEG-Fmoc-OA carrier were kept constant for comparison. The samples were placed into a 96-well plate, and examined for the fluorescence intensity at the excitation wavelength of 270 nm and emission wavelength of 300-460 nm using a Synergy H1 Hybrid Multi-Mode Microplate Reader.

3.2.7 *In vitro* drug release kinetics

Two mL of PTX/PEG-Fmoc mixed micelles in DPBS (PH = 7.4) (1 mg PTX/mL) was prepared and placed into a dialysis bag (MWCO 12 kDa, Spectrum Laboratories) that was incubated in a tank containing 200 mL of DPBS with 0.5% (w/v) Tween 80 under gentle shaking at 37 °C. At

scheduled time points (0, 1, 2, 4, 8, 24, 48, and 72 h), the concentration of PTX remaining in the dialysis bag was measured by HPLC as described above. Taxol formulation (6 mg PTX/mL in Cremophor EL/ethanol, 1:1, v/v) was diluted with DPBS to a final PTX concentration of 1 mg/mL and utilized as a control.

3.2.8 Cell culture

4T1-2 is a mouse metastatic breast cancer cell line. PC-3 and DU145 are two androgen-independent human prostate cancer cell lines. They were all cultured at 37 °C in DMEM containing 10% FBS and 1% penicillin-streptomycin in a humidified environment with 5% CO₂.

3.2.9 *In vitro* cytotoxicity study

Mouse metastatic breast cancer cell line 4T1.2, and two human prostate cancer cell lines PC-3 and DU145 were utilized to evaluate the *in vitro* cytotoxicity of PTX/PEG-Fmoc. Cells were seeded in 96-well plates at 1000 (4T1.2), 2000 (DU145) and 3000 (PC-3) cells per well. Twenty-four h later, cells were treated with PTX/PEG-Fmoc or Taxol with PTX concentrations ranging from 6.25 to 200 ng/mL. Seventy-two h later, 20 µL of 3-(4, 5-dimethylthiazol-2-yl)-2,5-diphenyltetrazoliumbromide (MTT, 5 mg/mL) was added into each well. Following incubation for 4 h, the medium was removed and 150 µL of DMSO was added to each well to solubilize the formazan crystal. The absorbance of each well was detected at 550 nm with a reference wavelength at 630 nm using a microplate reader, and cell viability was calculated based on the formula below. Untreated cells were included as a control.

$$\% \text{ cytotoxicity} = [1 - (\text{OD}_{\text{treat}} - \text{OD}_{\text{blank}})/(\text{OD}_{\text{control}} - \text{OD}_{\text{blank}})] \times 100\%$$

3.2.10 Animals

Female BALB/c mice (6 to 8 weeks) were purchased from Charles River (Davis, CA), and male nude mice (6 to 8 weeks) were purchased from Harlan (Livermore, CA). All animals were housed under pathogen-free conditions according to AAALAC guidelines. All animal-related experiments were performed in full compliance with institutional guidelines and approved by the Animal Use and Care Administrative Advisory Committee at the University of Pittsburgh.

3.2.11 Maximum tolerated dose (MTD) study

BALB/c mice were randomly divided into seven groups (n=4) and i.v. administered with PTX/PEG-Fmoc (30, 50, 75, 100, and 120 mg PTX/kg) or Taxol (15, 20, and 25 mg PTX/kg). Mice were then followed for 10 days for survival and changes in body weight. The MTD was determined at a maximal dose of PTX that leads to neither animal death nor significant changes in the general appearance or greater than 15% of body weight loss over the entire experimental period.

3.2.12 Fluorescence optical imaging

Near infrared (NIR) fluorescence imaging was performed to investigate the *in vivo* biodistribution of PTX/PEG-Fmoc mixed nanomicelles using PTX labeled with Cy5.5, a near

infrared fluorescence dye. Two hundred μL of PTX-Cy5.5/PEG-Fmoc mixed nanomicelles (0.2 PTX-Cy5.5 mg/mL) were i.v. injected into SCID mice bearing PC-3 xenografts. At scheduled time points, the mice were anesthetized and scanned with a *Carestream Molecular Imaging's In-Vivo Imaging FX Pro*, using a 60 sec exposure time with the excitation at 630 nm and the emission at 700 nm. At the end of the imaging study, all the mice were sacrificed and the major organs and tumors were excised for ex vivo imaging.

3.2.13 *In vivo* therapeutic efficacy

A syngeneic mouse breast cancer model (4T1.2) was established via s.c. inoculation of 2×10^5 of 4T1.2 cells into the right flank of female BALB/c mice, and the treatments were initiated when the tumor size reached $\sim 50 \text{ mm}^3$. Mice were divided randomly into five groups (n=5) and received i.v. injection of saline, Taxol (10 mg PTX/kg), and PTX/PEG-Fmoc (10, 20, and 40 mg PTX/kg), respectively. Tumor volumes were measured by a caliper and calculated based on the formula: $(L \times W^2)/2$, where L is the longest and W is the shortest tumor diameters (mm). The data were presented as relative tumor volume (RTV, the tumor volume at a given time point divided by the tumor volume prior to first treatment). Mice were sacrificed when tumors developed ulceration. Changes in body weights of all mice were also monitored during the entire course of treatment to evaluate the potential toxicity of the formulations. Tumors were harvested at the completion of the experiment and tumor weights were measured. Tumor growth inhibition rate (IR) was calculated as: $1 - (\text{mean tumor weight of PTX treated group} / \text{mean tumor weight of saline treated group}) * 100\%$.

3.2.14 Statistical analysis

Statistical analysis was performed with two-tailed Student's t-test between two groups. $p < 0.05$ was considered statistically significant, and $p < 0.01$ was considered highly statistically significant. One-way ANOVA was conducted to assess significance among multiple groups.

3.3 RESULTS AND DISCUSSION

3.3.1 Design, preparation, and characterization of PEG-Fmoc/PTX mixed micelles

We previously developed a new lipid surfactant, PEG₅₀₀₀-lysyl-(α -Fmoc- ϵ -oleic acid-lysine)₂ (PEG-Fmoc-OA), and examined its utility in formulating a number of therapeutic agents of diverse structure including PTX [58]. Our data showed that PEG-Fmoc-OA was much more effective than the counterpart without Fmoc motifs (PEG₅₀₀₀-di-oleoyl lysine, PEG-OA) with respect to both drug loading capacity and formulation stability. However, little was known about the molecular basis of carrier-drug interaction for our new micellar system. Particularly, a mode of interaction between Fmoc/PTX and its contribution to the overall performance of the new lipidic vector is largely unknown.

To clearly address this issue, we have synthesized a PEG-Fmoc conjugate without OA motifs to rule out any influence from lipid motifs whose interaction with drug also contributes to the overall performance of the new lipidic surfactant. PEG-Fmoc was readily synthesized via three steps as depicted in **Figure 15**. ¹H-NMR spectrum of PEG-Fmoc shows signals at 3.63 ppm

attributed to the methylene protons of PEG backbone, the multiple Fmoc proton signals between 7.3-7.8 ppm, and the t-Boc signals at 1.44 ppm (**Figure 16**). The molecular weight from MALDI-TOF MS is similar to the theoretical value (6030) (**Figure 17**), indicating the successful synthesis of PEG-Fmoc conjugate.

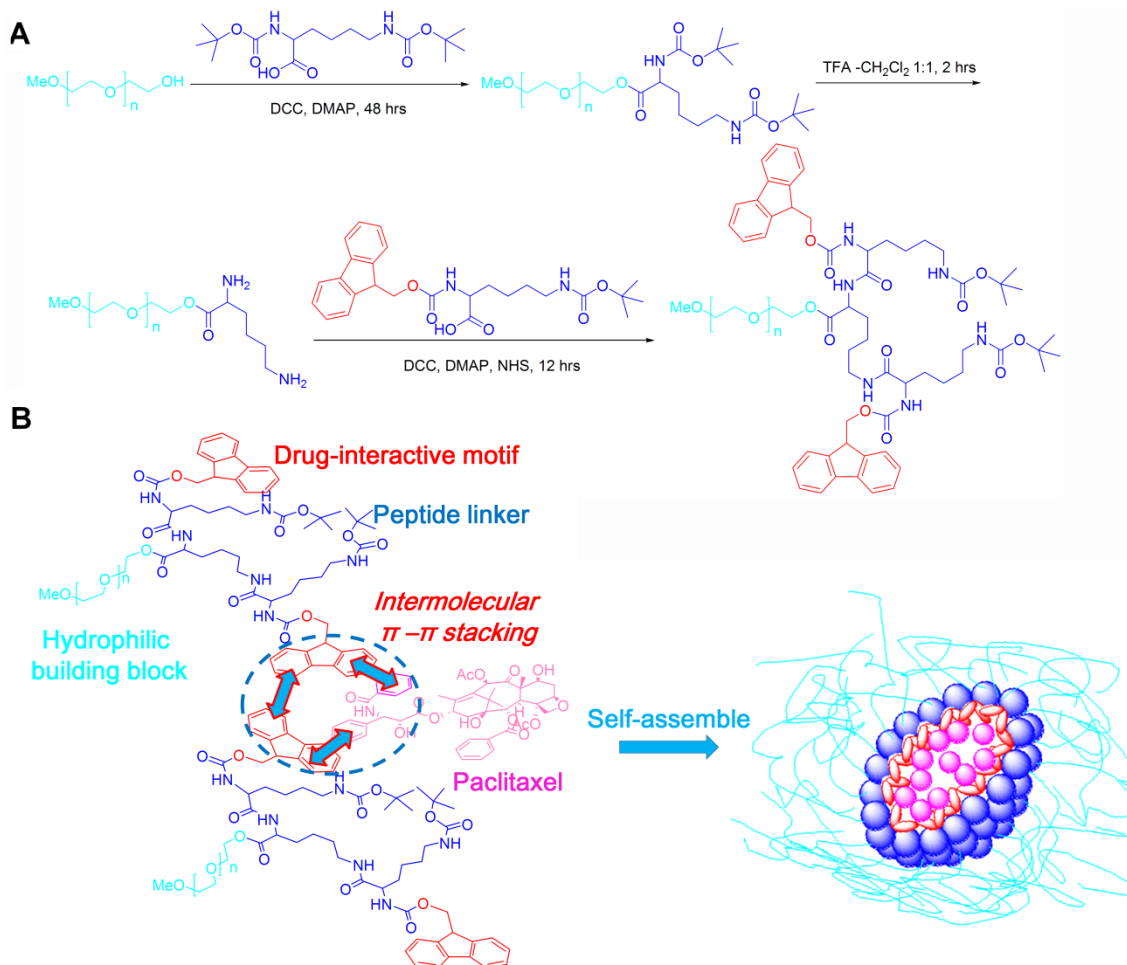


Figure 15. Synthetic route of PEG-Fmoc (A), and schematic representation of self-assembled PEG-Fmoc/PTX mixed micelle based on carrier/drug intermolecular $\pi-\pi$ stacking (B).

PEG-Fmoc readily formed small-sized (25~30 nm) micelles in aqueous solution. Negative-staining EM showed homogeneously distributed spherical particles (**Figure 18**). This is different from PEG-Fmoc-OA that showed tubular morphology on EM, suggesting formation of

filamentous micelles. PEG-OA was known to form spherical micelles [58]. Taken together, these data suggest that both Fmoc and lipid motifs contribute to the formation of the unique filamentous structure of PEG-Fmoc-OA.

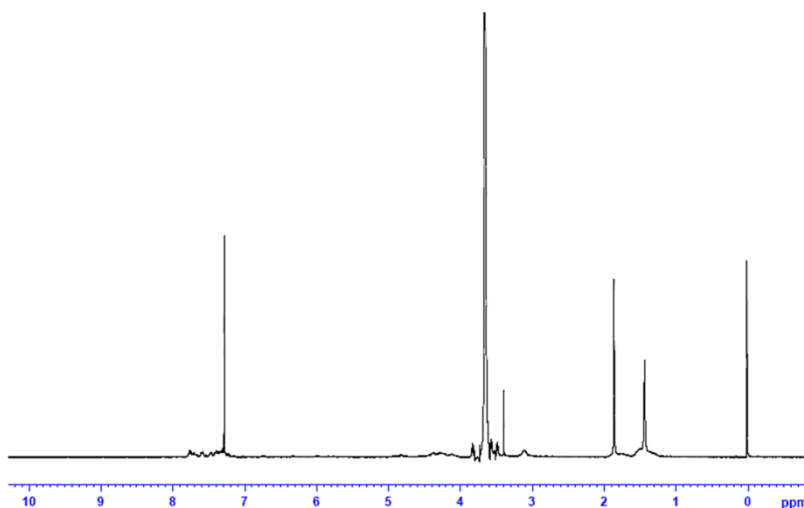


Figure 16. ^1H -NMR spectrum of PEG-Fmoc.

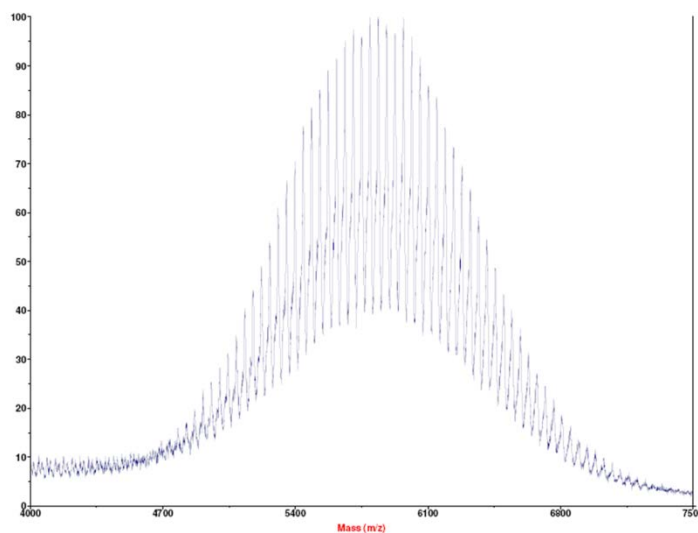


Figure 17. MALDI-TOF mass spectrum of PEG-Fmoc.

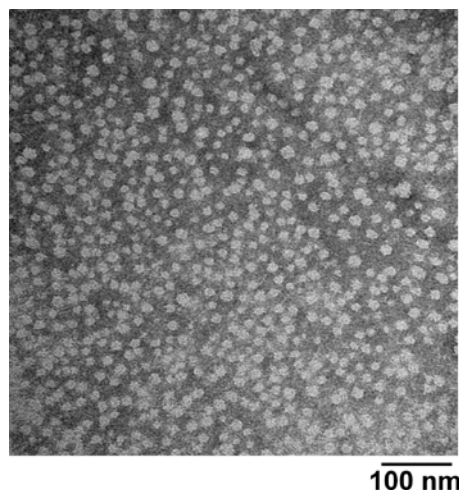


Figure 18. TEM image of PEG-Fmoc micelles at 5 mg/mL in DPBS using negative staining.

PEG-Fmoc readily formed mixed micelles with PTX and loading of PTX had minimal effect on the size of the particles as determined by DLS (**Figure 19A**). The small size and homogeneous distribution of the particles were further confirmed by negative-staining TEM as shown in **Figure 19B**. **Figure 19C** shows that the CMC value of PEG-Fmoc conjugate was 0.996 $\mu\text{mol/L}$. And $^1\text{H-NMR}$ spectrum analysis showed that the signals from both PEG-Fmoc and PTX were clearly detected when they were mixed in CDCl_3 (**Figure 20A**). In contrast, all of the proton signals of Fmoc and PTX were drastically suppressed in deuterated water, indicating a complete encapsulation of PTX inside the core area of the self-assembled particles in aqueous solution (**Figure 20B**).

Table 3 shows the drug loading capacity (DLC) at various PEG-Fmoc/PTX molar ratios. PEG-Fmoc/PTX mixed micelles could be prepared at a carrier/drug molar ratio as low as 0.25/1. At this ratio, the PTX loading capacity was $\sim 36\%$, which stands well among the reported PTX micellar formulations. Increasing the carrier/drug ratio was associated with an increase in drug loading efficiency (DLE) and an improvement in the colloidal stability of the mixed micelles in 50% FBS/PBS. Surprisingly, PEG-Fmoc was significantly more active than PEG-Fmoc-OA that

has a highest PTX loading capacity of 15.2% [58]. This is in contrast to solubilization and loading of several other drugs for which PEG-Fmoc-OA was more active than PEG-Fmoc.

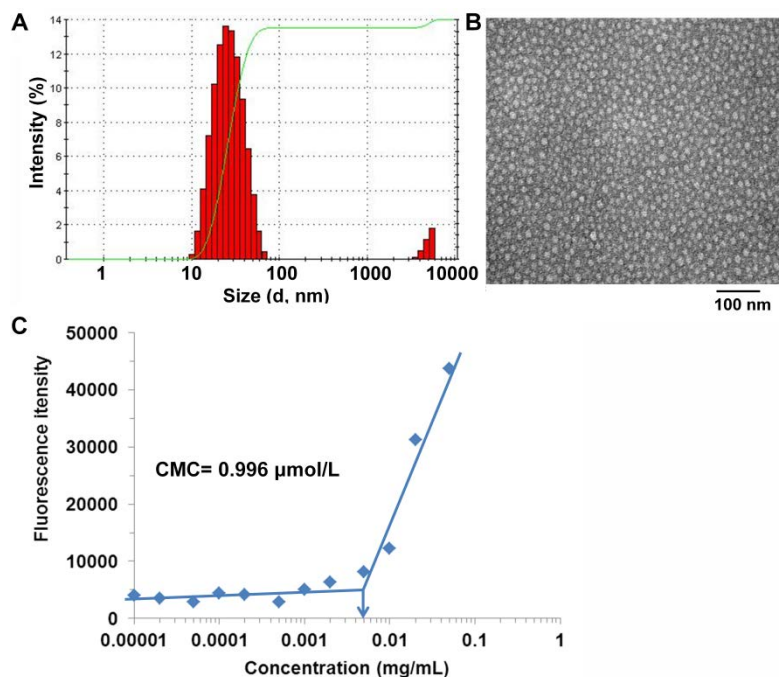


Figure 19. Biophysical characterization of PEG-Fmoc nanomicelles. (A) Particle size distribution of PEG-Fmoc/PTX nanomicelles at 1 mg PTX/mL in DPBS with a carrier/drug ratio of 0.75:1 (m/m) via DLS measurement; (B) TEM image of PEG-Fmoc/PTX nano-micelles with PTX concentration at 1 mg/mL using negative staining; (C) Critical micelle concentration (CMC) measurement of PEG-Fmoc using pyrene as a fluorescence probe.

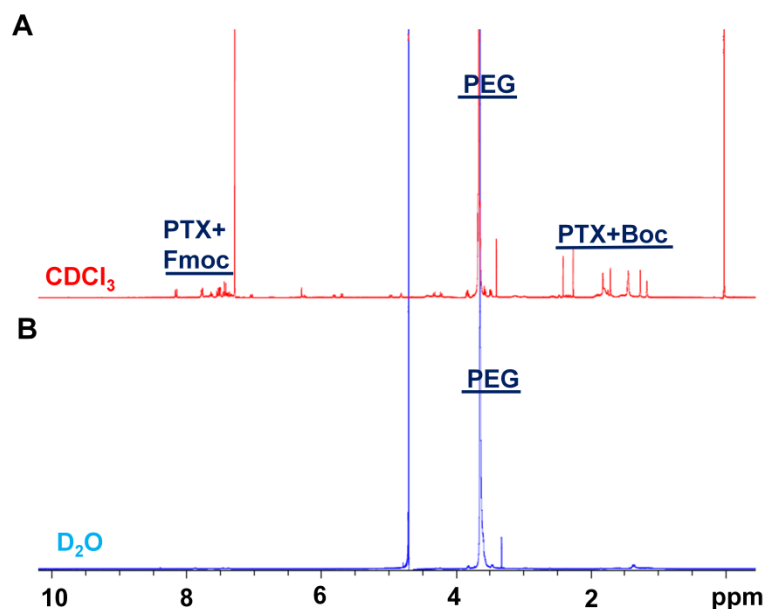


Figure 20. $^1\text{H-NMR}$ spectra of PEG-Fmoc/PTX in CDCl_3 and D_2O . The suppressed proton signals of Fmoc motifs and PTX in D_2O indicated the self-assembly of PEG-Fmoc micelles in aqueous solution and entrapment of PTX into the interior core of PEG-Fmoc micelles.

Table 3. Characterization of drug-free and PTX-loaded PEG-Fmoc nanomicelles.

| | Carrier/drug molar ratio | Particle size (d,nm) | ^a PDI | Zeta-potential (mV) | Zeta-potential | | ^d Stability in DPBS (h) | ^d Stability in 50% FBS (h) |
|---------------------------|-----------------------------|-------------------------|------------------|------------------------|-------------------|-------------------|---------------------------------------|--|
| | | | | | ^b DLC% | ^c DLE% | | |
| PEG-Fmoc | - | 28.55±0.27 | 0.488 | -1.024±0.127 | - | - | - | - |
| ^e PEG-Fmoc/PTX | 0.25:1 | 33.67 ±0.60 | 0.229 | -1.070±0.283 | 36.16 | 77.72 | 16 | 3 |
| | 0.5:1 | 27.51 ±0.92 | 0.264 | -0.996±0.424 | 22.07 | 86.49 | 42 | 8 |
| | 0.75:1 | 25.34 ±0.63 | 0.278 | -0.849±0.135 | 15.88 | 96.96 | 78 | 28 |

^aPDI, polydispersity index. ^bDLC, drug loading capacity. ^cDLE, drug loading efficiency. ^dStability indicates no noticeable drug precipitation or significant size change during the follow up time period. ^ePTX concentrations were kept at 1 mg/mL, drug-free nano-carrier concentration was 5 mg/mL.

3.3.2 Mechanism of carrier/drug interactions

Fmoc is known to have strong π - π stacking interaction with other molecules bearing aromatic rings [87-89], which is normally stronger than the van der Waals interaction. Fmoc is likely to promote the formation of stable PEG-Fmoc micelles through the Fmoc/Fmoc interaction. The fact that PTX could be loaded into PEG-Fmoc micelles at a high loading capacity suggests that Fmoc effectively interacts with PTX. An absence of PTX endothermic melting peak in PEG-Fmoc/PTX micelles was observed in differential scanning calorimetry (DSC) analysis, which indicated a loss of PTX crystallinity caused by a strong carrier-PTX interaction in PEG-Fmoc/PTX micelles (**Figure 21**). To further gain insight into the mechanism of drug-carrier interaction, fluorescence quenching study was conducted. As depicted in **Figure 22A**, a fluorescence maxima of PEG-Fmoc alone was recorded at 305 nm at an excitation wavelength of 270 nm. However, a dramatic fluorescence quenching was observed when PTX was loaded into the micelles, and the extent of decrease in fluorescence intensity was correlated to the amount of PTX loaded in micelles. This fluorescence quenching in the presence of PTX is likely due to the energy transfer caused by the intermolecular π - π stacking interaction [72] between Fmoc motifs and the aromatic rings of PTX, which may represent the major mechanism of carrier/drug interaction in PEG-Fmoc/PTX (**Figure 15B**). As a control, PTX alone did not show any fluorescence at the wavelength range examined.

To further demonstrate that π - π stacking plays a key role in the Fmoc/PTX interaction, the fluorescence quenching study was similarly conducted with two other hydrophobic molecules, DTX and CHOL (**Figure 23**). As depicted in **Figure 24**, DTX, an analog of PTX with one fewer aromatic ring, caused slightly less fluorescence quenching, which may be due to a relatively

weaker π - π stacking interaction between DTX and Fmoc. In addition, no significant fluorescence quenching was observed in the hydrophobic interaction between PEG-Fmoc and CHOL, a highly hydrophobic molecule that does not bear aromatic rings. Taking together, these data suggest π - π stacking as a major mechanism in the PTX/Fmoc interaction. However, hydrophobic interaction and hydrogen bonding may also contribute to the overall interaction between Fmoc and PTX.

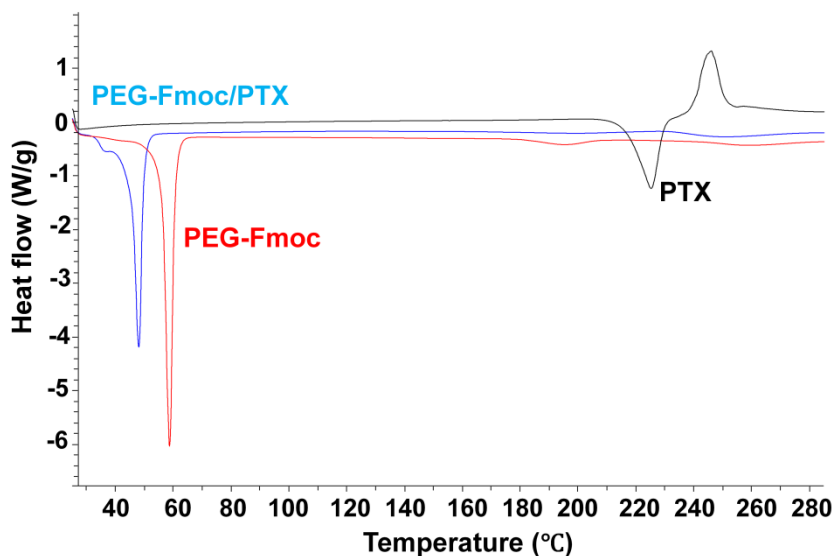


Figure 21. DSC thermograms of PTX alone, PEG-Fmoc/PTX mixed micelles, and drug-free PEG-Fmoc micelles.

Interestingly, PEG-Fmoc-OA exhibited remarkably reduced fluorescence intensity compared to its lipid-free counterpart, PEG-Fmoc, on equal molar basis (**Figure 22B**). This severe self-quenching is likely due to the extremely strong carrier-carrier π - π interaction. Incorporation of lipid chains brought changes to packing parameter and molecular arrangement of PEG-Fmoc-OA assemblies. Unlike PEG-Fmoc that forms spherical micelles, PEG-Fmoc-OA forms filamentous micelles of tubular structures [58]. This morphology alteration may facilitate an overwhelming Fmoc/Fmoc interaction between carriers, leading to an impaired π - π interaction between Fmoc and PTX. Loading of PTX into PEG-Fmoc-OA micelles may be largely mediated by hydrophobic/hydrophobic interaction. This is in agreement with the finding that loading of PTX

into PEG-Fmoc-OA micelles is not associated with dramatic quenching of Fmoc fluorescence. The different modes of drug/carrier interactions might play a major role in the drastic difference in PTX loading capacity between the two systems (PEG-Fmoc vs PEG-Fmoc-OA).

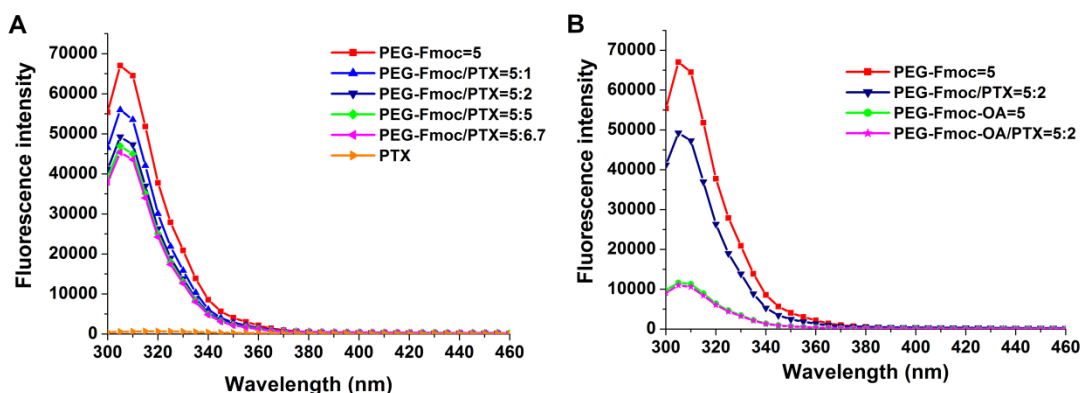


Figure 22. Fluorescence quenching study. Fluorescence intensity of PEG-Fmoc (A) at 300- 460 nm was recorded with an excitation wavelength at 270 nm, and compared with its lipid-bearing counterpart PEG-Fmoc-OA (B). Both PEG-Fmoc and PEG-Fmoc-OA were kept at 0.88 mM for comparison, and all carrier/drug ratios were reported as molar ratios.

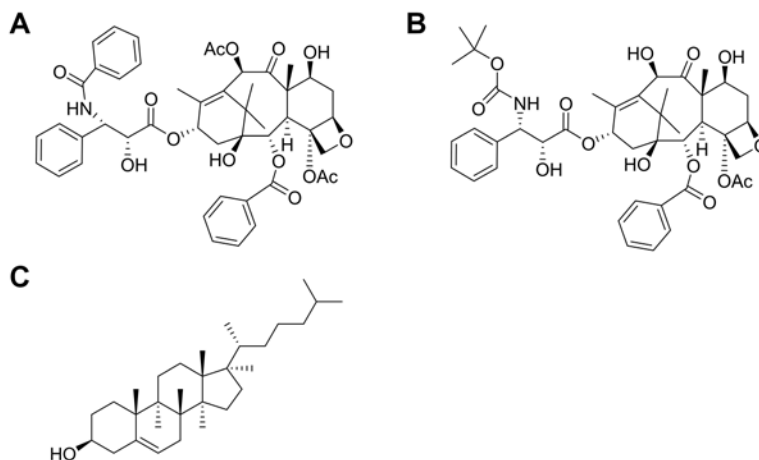


Figure 23. Chemical structures of paclitaxel (PTX) (A), docetaxel (DTX) (B), and cholesterol (CHOL) (C).

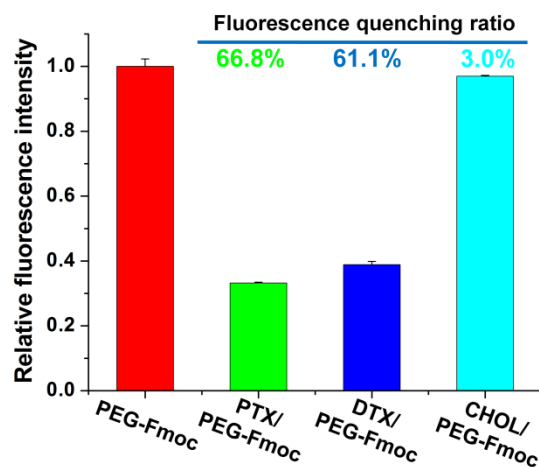


Figure 24. Fluorescence quenching caused by different hydrophobic molecules. PEG-Fmoc micelles loaded with different hydrophobic drugs (PTX, DTX, and CHOL) were prepared, respectively, at a carrier/drug molar ratio of 5:1 and PEG-Fmoc concentration of 1.17 mM, and the emission fluorescence intensity was detected at 305 nm. The fluorescence quenching ratio (%) was calculated as: $(1 - (\text{fluorescence intensity of drug-loaded PEG-Fmoc} / \text{fluorescence intensity of drug-free PEG-Fmoc})) \times 100\%$.

We further studied the Fmoc/PTX interaction via NMR. Shifts in ^{13}C -NMR spectra of PTX were recorded in the presence of varying concentrations of PEG-Fmoc. As shown in **Figure 25**, PEG-Fmoc caused significant signal shifts in all of the three aromatic rings of PTX, and these signal shifts occurred in an Fmoc concentration-dependent manner. It was also apparent that more dramatic shifts were observed in rings A and B than in ring C as indicated by the average shift index Δ that represents the average absolute value of the signal shifts of all the six carbon atoms in one aromatic ring. In general, a signal shift of greater than 0.02 in ^{13}C -NMR spectrum is believed to be significant and suggestive of intermolecular interaction. These data suggest a strong interaction between Fmoc and the aromatic rings of PTX, particularly rings A and B. A stronger interaction between Fmoc and rings A and B of PTX may be attributed to a higher flexibility of the two rings and a less steric hindrance imposed by the bulky core of PTX. The interaction of Fmoc with PTX was similarly demonstrated by NMR with a more simplified system, Fmoc-Lys (Boc)-OH as shown in **Figure 26**. The above data shed some insight into the

molecular interaction of PEG-Fmoc with PTX. However, more studies are needed to better understand the mechanism involved in the drastic difference between PEG-Fmoc-OA and PEG-Fmoc with respect to PTX loading capacity.

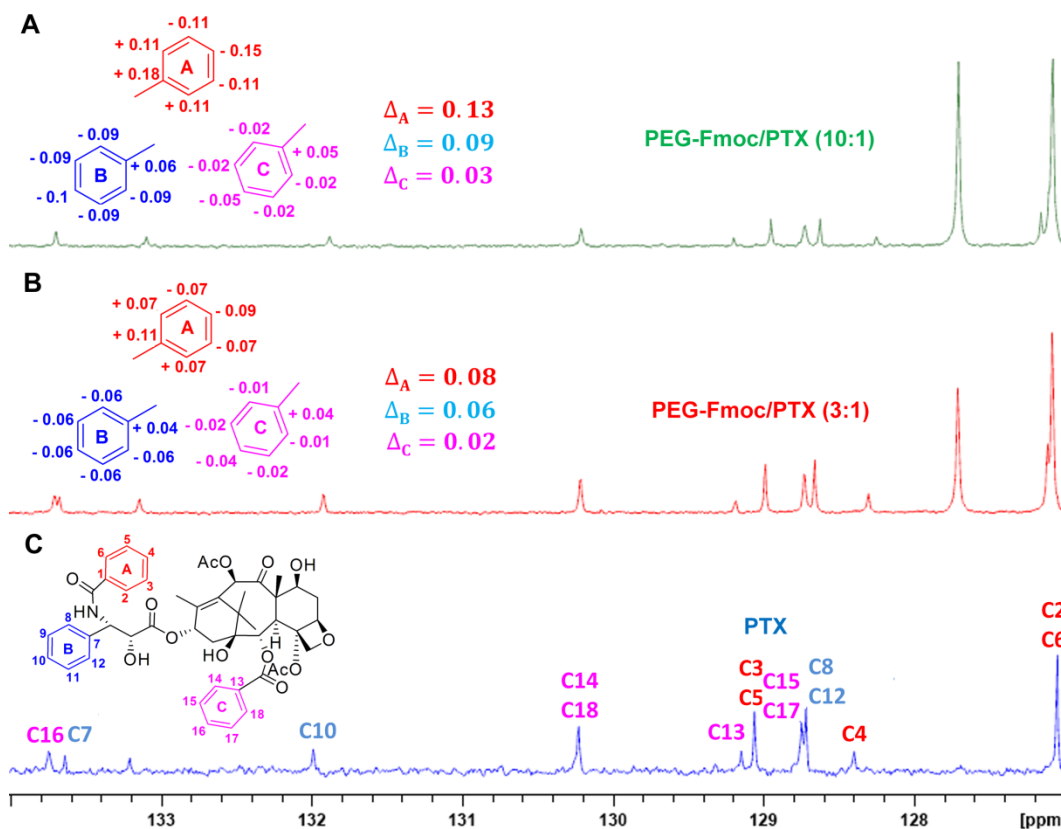


Figure 25. ^{13}C -NMR of carrier-mixed (A & B) and carrier-free PTX (C) in CDCl_3 . PTX was mixed with PEG_{550} - α -Fmoc- ϵ -t-Boc-lysine at a drug/carrier molar ratio of 1:10 (A) and 1:3 (B), respectively. Average shift index (Δ) was calculated as the average absolute value of chemical shift changes of all the six carbon atoms on the same aromatic ring compared with free PTX (C).

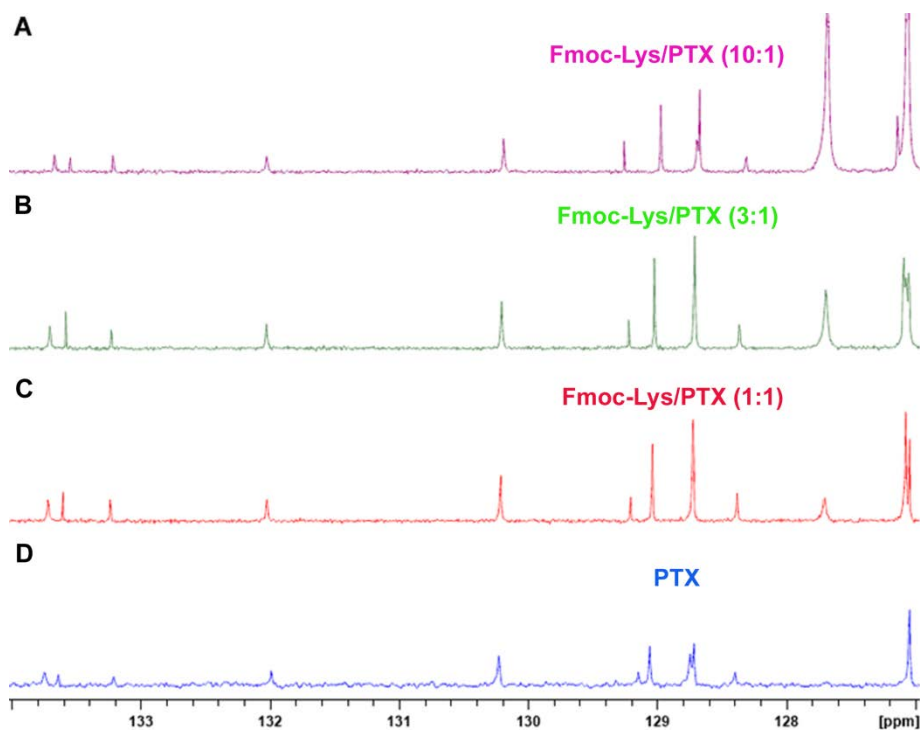


Figure 26. ^{13}C NMR of free PTX and PTX/Fmoc-Lys (Boc)-OH in CDCl_3 . PTX was mixed with Fmoc-Lys (Boc)-OH at a drug/carrier molar ratio of 1:10 (A), 1:3 (B) and 1:1 (C), and then subjected to ^{13}C NMR analysis. Free PTX (D) was used as a control.

3.3.3 Effect of lyophilization/reconstitution on PEG-Fmoc/PTX mixed micelles

The preliminary data suggest that PEG-Fmoc may represent as a simple and effective micellar system for delivery of PTX. Therefore, we went on to further characterize PEG-Fmoc/PTX mixed micelles with respect to their biophysical and biological properties. We first examined the effect of freezing and lyophilization on PEG-Fmoc/PTX mixed micelles since lyophilization is an important procedure for long-term storage in clinical practice. Our results showed that PEG-Fmoc/PTX mixed micelles could be lyophilized and then readily reconstituted in water without any addition of cryo-protectants. In addition, there were no major changes in size distribution following lyophilization and reconstitution (**Figure 27**). This property may help to facilitate the clinical investigation of this simple delivery system.

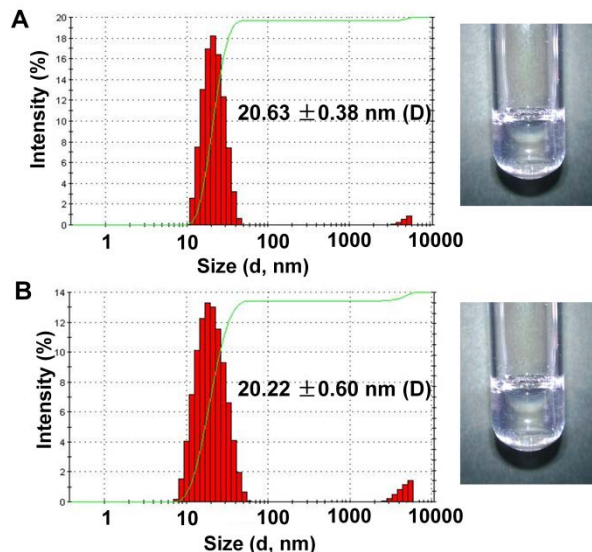


Figure 27. Size distribution of PEG-Fmoc/PTX mixed micelles with PTX concentration at 1 mg/mL before (A) and after (B) lyophilization/reconstitution.

3.3.4 Release kinetics of PTX from PEG-Fmoc/PTX mixed micelles

As an important indicator of formulation stability, release kinetics of PTX from PEG-Fmoc/PTX was evaluated via a dialysis method, and Taxol, a clinically used PTX formulation [90, 91] was employed as a comparison. As depicted in **Figure 28**, PEG-Fmoc/PTX mixed micelles exhibited a sustained release profile in PBS, pH 7.4 at 37 °C. After first 24 h, only 19.3% of entrapped PTX was released from PEG-Fmoc/PTX mixed micelles. Even after 72 h, only 23.5% of PTX was released from PEG-Fmoc/PTX mixed micelles. This compared favorably to Taxol formulation in which 40.4% of PTX was released during the 1st 24 h. The slow kinetics of PTX release is likely due to a strong carrier/drug interaction, which may help to facilitate the PTX delivery through minimizing its premature release from PEG-Fmoc/PTX mixed micelles before they reach the tumor site.

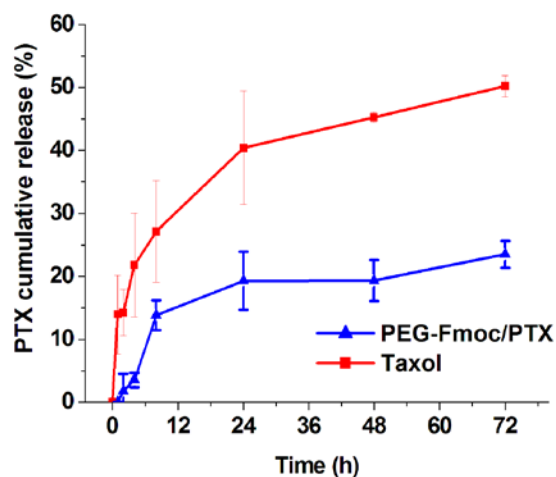


Figure 28. PTX release kinetics of PEG-Fmoc/PTX examined via a dialysis method. PTX concentrations in PEG-Fmoc/PTX and Taxol were kept at 1 mg/mL, and DPBS containing 0.5% (w/v) Tween 80 was utilized as release medium. PTX concentration was analyzed at 0, 1, 2, 4, 8, 24, 48 and 72 h using HPLC at 227 nm.

3.3.5 *In vitro* cytotoxicity of PEG-Fmoc/PTX

In vitro cytotoxicity of PEG-Fmoc/PTX was evaluated with several tumor cell lines including mouse metastatic breast cancer cell line, 4T1.2, and two human prostate cancer cell lines, PC-3 and DU145. As shown in **Figure 29**, PEG-Fmoc/PTX mixed micelles exhibited more potent cytotoxicity than Taxol in all the 3 cancer cell lines tested. The carrier alone did not show any significant toxicity to cells under the concentrations tested. This increased cytotoxicity may be attributed to a facilitated entry of PTX into tumor cells. It has been reported that nano-scale delivery systems enter cells through endocytosis [92-94]. This could help to bypass the efflux mediated by drug transporters such as P-glycoprotein, resulting in increased intracellular drug accumulation and improved cytotoxicity.

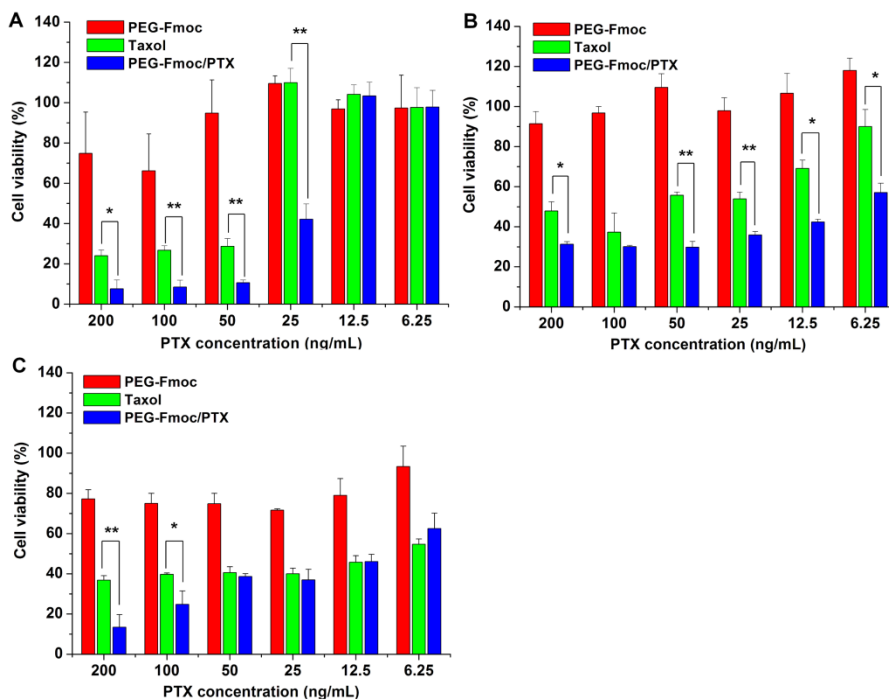


Figure 29. *In vitro* cytotoxicity of PEG-Fmoc/PTX. 4T1.2 mouse breast cancer cell line (A), human prostate cancer cell lines PC-3 (B), and DU145 (C) were treated with PEG-Fmoc/PTX, drug-free PEG-Fmoc and Taxol for 72 h, and tumor cell inhibition was determined by MTT assay. * $P < 0.05$ or ** $P < 0.01$ (PEG-Fmoc/PTX vs Taxol).

3.3.6 Biodistribution of PEG-Fmoc/PTX micelles through NIR fluorescent optical imaging

To investigate the *in vivo* fate of PEG-Fmoc/PTX, NIR fluorescence imaging was utilized to track the biodistribution of PTX in tumor-bearing mice after i.v. injection of PEG-Fmoc/PTX. Cy5.5, a near infrared fluorescent probe, was conjugated to PTX and SCID mice bearing human prostate cancer PC-3 xenografts were used. As shown in **Figure 30**, Cy5.5-PTX was largely found at tumor sites 24 h after i.v. administration of PEG-Fmoc/Cy5.5-PTX and substantial amounts of signal remained at tumor sites even 96 h later. Intravenous administration of free Cy5.5-PTX led to accumulation of the signals largely at the site of kidneys (data not shown). This is largely due to the increased hydrophilicity of PTX following conjugation with Cy5.5,

which led to its clearance from the kidneys. After completion of the whole body imaging study at 96 h post-injection, major organs and tumors were excised, and *ex vivo* imaging was performed. Strong NIR fluorescence signals of Cy5.5-PTX were found in tumor tissues. Moderate levels of signals were also found in lung and liver, which was due to the nonspecific uptake of nanoparticles by these organs, albeit at relatively low levels [95]. We also noticed significant levels of NIR signals in kidneys, which might be due to the clearance of the Cy5.5-PTX that became dissociated from PEG-Fmoc/Cy5.5-PTX mixed micelles. Very low NIR levels were found in heart and muscle. It should be noted that coupling of Cy5.5 to PTX led to significant changes in the overall size and other biophysical properties of PTX as reflected by both reduced loading capacity and slightly increased sizes for PEG-Fmoc/Cy5.5-PTX mixed micelles (data not shown). Thus, the targeting efficiency of PEG-Fmoc/PTX might be underestimated with the Cy5.5-PTX-based NIR imaging. The PK/PD study is currently ongoing to directly examine the distribution of PTX in tumors and other major organs/tissues. As a control, Cy5.5-PTX formulated in Cremophor EL yielded poor imaging of the tumor-bearing mice.

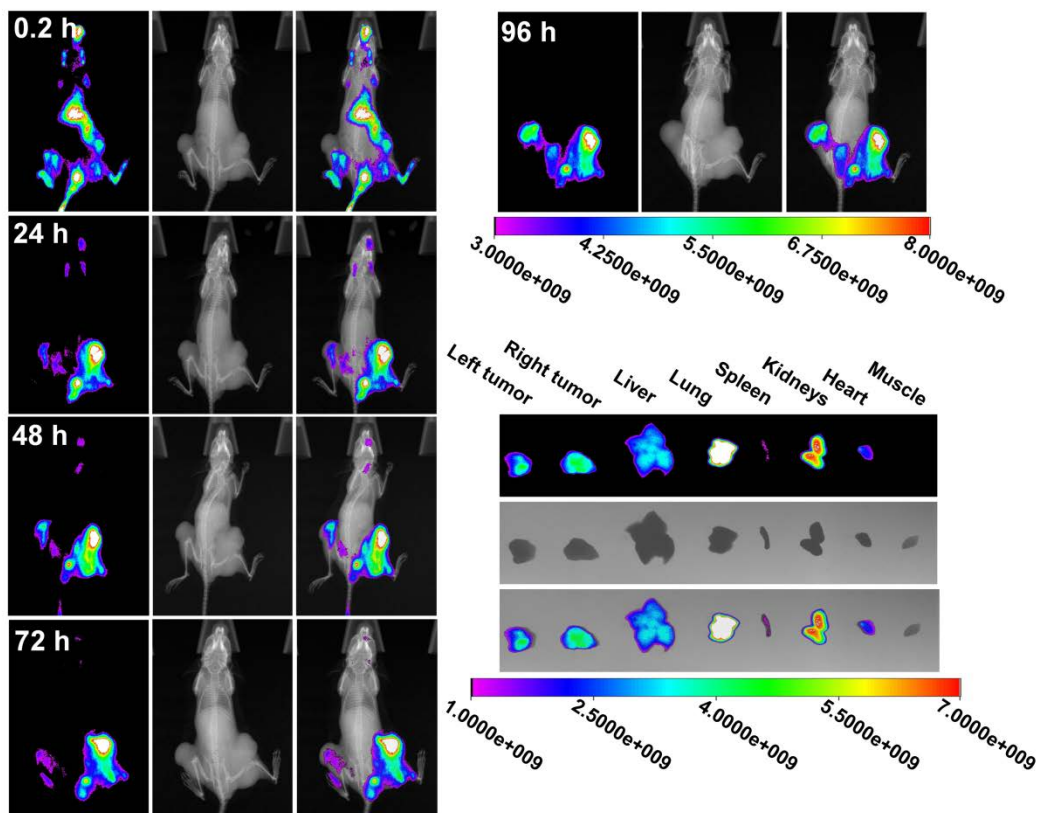


Figure 30. Biodistribution of PEG-Fmoc/Cy5.5-PTX in tumor-bearing mouse as examined by NIR fluorescence imaging. Mouse bearing PC-3 cancer xenograft was scanned at 0.2 h, 24 h, 48 h, 72 h, and 96 h after i.v. injection of PEG-Fmoc/Cy5.5-PTX; and ex vivo imaging of tumors and major organs was performed 96 h after injection.

3.3.7 Maximum tolerated dose (MTD) study

The maximum tolerated dose (MTD) of PEG-Fmoc/PTX was examined in tumor-free mice and compared to Taxol formulation. Five different doses of PEG-Fmoc/PTX and three doses of Taxol were tested in BALB/c mice through i.v. injection, followed by monitoring of body weight and other signs of toxicity of these animals. As shown in **Table 4**, Taxol could be tolerated at a maximum PTX dosage of 20 mg/kg. At this dose, no animal death occurred although several abnormal signs such as convulsion and retarded motion were noticed in most of the treated mice immediately after injection. Compared with Taxol, PEG-Fmoc/PTX exhibited a significantly

improved safety profile. Even at a dosage as high as 120 mg PTX/kg (6-fold higher than the MTD of Taxol), neither animal death nor significant weight loss was observed over the entire experiment period. The high MTD of PEG-Fmoc/PTX compares favorably to most of the reported PTX micellar formulations, and is consistent with its excellent formulation stability, slow release profile, and less tendency to accumulate in major organs as illustrated above, which shall provide a much broader therapeutic dosage window for enhanced therapeutic efficacy.

Table 4. Maximum tolerated dose of PEG-Fmoc/PTX and Taxol.

| Formulation | Dose (mg PTX/kg) | Mice death | Weight loss (%) |
|--------------|---------------------|------------|--------------------|
| Taxol | 15 | 0/4 | 0.49 |
| | 20 | 0/4 | -4.96 |
| | 25 | 1/4 | -4.35 |
| PEG-Fmoc/PTX | 30 | 0/4 | -2.77 |
| | 50 | 0/4 | -2.82 |
| | 75 | 0/4 | -5.99 |
| | 100 | 0/4 | -5.12 |
| | 120 | 0/4 | -9.49 |

3.3.8 *In vivo* therapeutic efficacy of PEG-Fmoc/PTX

The *in vivo* therapeutic efficacy of PEG-Fmoc/PTX was examined in a syngeneic mouse breast cancer model (4T1.2). 4T1.2 is known as a highly metastatic cancer cell line, and as demonstrated in **Figure 31A**, rapid tumor growth was observed in saline-treated group. Taxol

showed a modest effect in inhibiting the tumor growth at a PTX dose of 10 mg/kg. At the same dosage, PEG-Fmoc/PTX was significantly more effective than Taxol in inhibiting the tumor growth ($p < 0.05$). Increasing the PTX dosage was associated with a further enhancement in antitumor activity. At the PTX dosage of 20 and 40 mg/kg, the tumor growth inhibition rate (IR) was 60.6 and 69.7%, respectively (**Figure 31B**). All of the treatments were well tolerated except for a slight decrease of body weight (7-8%) that occurred following consecutive injections of PEG-Fmoc/PTX at the PTX dose of 40 mg/kg (**Figure 32**). The significantly enhanced antitumor activity and the excellent safety of PEG-Fmoc/PTX are consistent with its excellent biophysical properties and tumor-selective delivery.

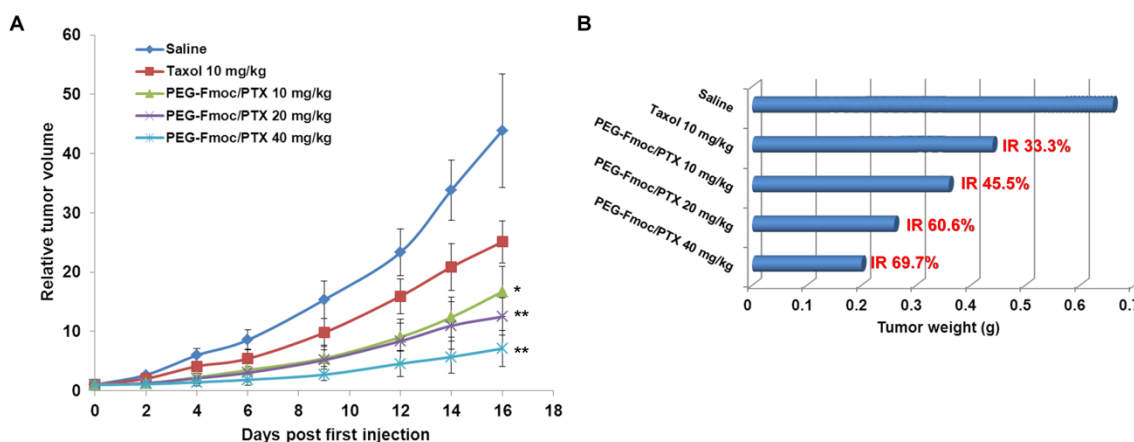


Figure 31. *In vivo* therapeutic efficacy of PEG-Fmoc/PTX. Groups of 5 BALB/c mice bearing 4T1.2 murine breast cancer grafts were injected with PEG-Fmoc/PTX (10, 20, or 40 mg PTX/kg body weight), Taxol (10 mg PTX/kg body weight) and saline on days 0, 2, 4, 7, 10 and 12, respectively. Tumor growth was monitored and plotted as relative tumor volume (A). * $P < 0.05$; ** $P < 0.01$ (vs Taxol). Tumor weights were measured after excision and plotted as average tumor weight, and tumor growth inhibition rate (IR) was calculated (B).

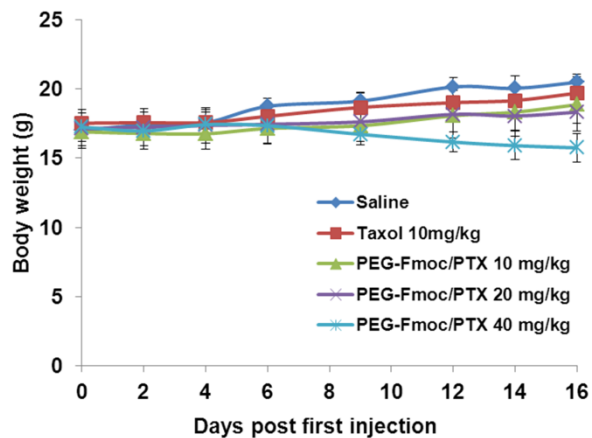


Figure 32. Changes of body weight in mice treated with PEG-Fmoc/PTX (10, 20, or 40 mg PTX/kg) or Taxol (10 mg PTX/kg).

3.3.9 Summary

In summary, a study of Fmoc/PTX molecular interaction has led to the discovery of PEG-Fmoc conjugate as an effective nanocarrier for PTX. This conjugate can be easily synthesized through a simple three-step route, and it readily forms small-sized (25-30 nm) micelles with PTX. A strong Fmoc/PTX π - π stacking interaction provides an excellent drug/carrier compatibility with a loading capacity (~36%) that stands well among the reported micellar formulations. PEG-Fmoc/PTX nanomicelles effectively and selectively accumulated at solid tumors and demonstrated an excellent safety profile with a MTD greater than 120 mg PTX/kg. Finally, PEG-Fmoc/PTX effectively inhibited the tumor growth in a murine breast cancer model, much more effectively than Taxol. Our PEG-Fmoc may hold promise as a simple, safe, and effective delivery system for PTX with a potential for rapid translation into clinical study.

4.0 PEGYLATED FMOC-AMINO ACID CONJUGATES AS EFFECTIVE NANOCARRIERS FOR IMPROVED DRUG DELIVERY

4.1 BACKGROUND

Among a variety of nano-scaled drug delivery systems developed in recent decades,[10, 13, 14, 84, 96, 97] micelles are attractive due to their unique properties, such as the ease in manipulation and small sizes usually under 100 nm, which can take the advantage of the well-known enhanced permeability and retention (EPR) effect to specifically accumulate at tumor site for improved therapy and reduced systemic toxicity.[15, 16] Generally, micelle-forming surfactants contain a highly hydrophilic chain, which is usually poly ethylene glycol (PEG), and one or several hydrophobic domains such as lipids or hydrophobic block co-polymers.[38, 65, 98-102] In aqueous phase, these amphipathic molecules would self-assemble into nano-scaled particles with a hydrophobic inner core, which can effectively encapsulate hydrophobic drugs.

Recently, efforts have been placed on rational design of micelle-forming surfactants, since it has been realized that insufficient compatibility between carriers and drug molecules is a major factor for limited drug loading capacity and formulation stability. For most of the micelle systems, drug encapsulation is solely based on carrier-drug hydrophobic interaction, which may not provide adequate compatibility for some drug molecules with moderate hydrophobicity. New strategies have been developed to equip conventional micelle-forming surfactants with functional

domains that provide additional mechanisms of drug-carrier interactions to enhance the compatibility of micelle systems with payload therapeutics. These domains include hydrotropic domains or entire drug molecules such as doxorubicin.[48, 49, 53, 54, 86, 103] Indeed, enhanced drug loading capacity and formulation stability were achieved after introduction of these functional motifs.

We have recently discovered that 9-Fluorenylmethoxycarbonyl (Fmoc) acts effectively as a drug-interactive domain exhibiting a potent propensity in interacting with a panel of drugs with diverse chemical structures and hydrophobicity.[55, 58] Interfacial decoration with Fmoc significantly improved the performance of PEG-lipopeptides (PEG₅₀₀₀-lysyl-di-oleic acid, PEG₅₀₀₀-OA₂) in formulating a variety of agents.[58] Interestingly, a PEG-Fmoc conjugate without lipid motifs (PEG₅₀₀₀-lysyl-(α -Fmoc- ϵ -t-Boc-lysine)₂, PEG₅₀₀₀-Fmoc₂) was more effective in solubilizing paclitaxel (PTX) than its counterpart with lipid motifs (PEG₅₀₀₀-(Fmoc-OA)₂).[59] However, this carrier was later found to have limited effectiveness in formulating many other anti-cancer agents including doxorubicin (data not shown). The underlying mechanism is not clearly understood at present. We hypothesized that this limitation might be resolved via further optimizing the neighboring structure of Fmoc motif.

In this study, a series of PEGylated Fmoc-amino acid conjugates (PFA) were developed as a simple model to conduct a structure-activity relationship (SAR) study to gain more insight into the role of neighboring motifs of Fmoc in the overall carrier-carrier and carrier-drug interactions. Amino acid derivatives with various side chains were utilized to generate PFA conjugates via a one-step synthetic route (two steps for PFA₈). The resulting conjugates were then subjected to extensive biophysical and biological characterizations.

4.2 METHODS

4.2.1 Materials

Paclitaxel (PTX, >99%) was purchased from TSZ Chem (MA, USA). α -Fmoc- ϵ -Boc-lysine, α -Fmoc- ϵ -Cbz-lysine, α -Fmoc- ϵ -Ac-lysine, Fmoc-tyrosine (tBu), Fmoc-phenylalanine, Fmoc-leucine, Fmoc-glycine were purchased from GL Biochem Ltd. (Shanghai, China). N, N'-dicyclohexylcarbodiimide (DCC), trifluoroacetic acid (TFA), griseofulvin and progesterone were obtained from Acros Organic (NJ, USA). Docetaxel, doxorubicin, imatinib and etoposide were obtained from LC Laboratories (MA, USA). Curcumin was purchased from TCI (OR, USA), and nifedipine was from Alfa Aesar (MA, USA). Monomethoxy PEG₂₀₀₀, 4-dimethylaminopyridine (DMAP), and other unspecified chemicals were all purchased from Sigma-Aldrich (MO, USA). Dulbecco's phosphate buffered saline (DPBS), Dulbecco's Modified Eagle's Medium (DMEM), fetal bovine serum (FBS), and 100 \times penicillin-streptomycin solution were purchased from Invitrogen (NY, USA). All solvents used in this study were HPLC grade.

4.2.2 Synthesis of PEG₂₀₀₀-Fmoc-amino acid conjugates (PFA)

For the synthesis of PEG₂₀₀₀-Fmoc-Lys (Boc) (PFA₁), monomethoxy PEG₂₀₀₀ was mixed with excess amount of Fmoc-lysine (Boc)-OH and DCC in dichloromethane (DCM) with addition of DMAP, and the reaction was allowed at room temperature for 48 h. The mixture was filtered and precipitated in ice-cold ether, followed by two washes with cold ethanol and ether. The obtained material was dissolved in distilled water and filtered through a 220 nm filter, followed by

lyophilization to yield the powder of purified PFA₁. PFA₂₋₇ were obtained with a similar procedure using different Fmoc-amino acid derivatives. PFA₈ was prepared by treating PFA₁ in TFA/DCM (1:1, v/v) for 2 h at room temperature, followed by precipitation in cold ether.

4.2.3 Preparation and biophysical characterization of PTX/PFA mixed micelles

Encapsulation of PTX into PFA micelles was performed via a thin-film hydration method. Briefly, PFA was well-mixed with PTX in chloroform at designated molar ratios, and a thin film was generated after removal of the organic solvent by a gentle stream of nitrogen, followed by vacuum for 2 h. The thin film of mixed PTX/PFA was hydrated in DPBS, and suspended by vortex to obtain a transparent solution of PTX-loaded PFA micelles. Any non-entrapped drug was removed by filtration through 450 nm PVDF syringe filter.

The morphology of formed micelles was observed by transmission electron microscopy (TEM) after negative staining. The size distribution was analyzed via dynamic light scattering (DLS), and the zeta-potential was detected by a Malvern Zeta Nanosizer. The critical micelle concentration (CMC) was determined using pyrene as a fluorescence probe.[58] The quantity of PTX in the micelles was measured after extraction by methanol by a Waters Alliance 2695-2998 high-performance liquid chromatography (HPLC) system with a RP-18 column (250 mm × 4.6 mm) equipped with a UV detector at 227 nm at room temperature. A mixture of methanol/water (80:20, v/v) was used as mobile phase at a flow rate at 0.8 mL/min.[59]

4.2.4 Fluorescence quenching

PTX/PFA micelles were prepared in DPBS as described above, in which the concentration of PFA was fixed at 1.17 mmol/L for comparison. The samples were placed into a 96-well plate, and examined for the fluorescence intensity at the excitation wavelength of 270 nm and emission wavelength of 300-460 nm using a Synergy H1 Hybrid Multi-Mode Microplate Reader.

4.2.5 Reconstituability of PTX/PFA mixed micelles following lyophilization

One mL of PTX/PFA₂ solution in DPBS was prepared as described above with a PTX concentration at 1 mg/mL, followed by freezing and lyophilization overnight to obtain white powder of the mixed micelles. The powder was then reconstituted with 1 mL of distilled water to obtain a transparent solution. Particle sizes of the PTX-loaded micelles before and after lyophilization/reconstitution were recorded through DLS.

4.2.6 PTX release kinetics

Two mL of PTX/PFA₂ micelles was prepared in DPBS (PH = 7.4) at a PTX concentration of 1 mg/mL. Taxol formulation (6 mg PTX/mL in Cremophor EL/ethanol, 1:1, v/v) was diluted with DPBS to a final PTX concentration of 1 mg/mL as a control. Samples were then transferred into a dialysis bag (MWCO 12 kDa, Spectrum Laboratories), and immersed into a release tank containing 200 mL of DPBS with addition of 0.5% (w/v) Tween 80 under gentle shaking at

37 °C. At designated time points (0, 1, 2, 4, 8, and 24 h), PTX concentration in the dialysis bag was detected by HPLC as the method described above.

4.2.7 Cell culture

4T1-2 is a mouse metastatic breast cancer cell line, PC-3 is an androgen-independent human prostate cancer cell line, HCT-116 is a human colonic carcinoma cell line, and A549 is a human lung adenocarcinoma cell line. The cells were all cultured at 37 °C in DMEM containing 10% FBS and 1% penicillin-streptomycin in a humidified environment with 5% CO₂.

4.2.8 *In vitro* cytotoxicity study

Four different cancer cell lines were utilized to evaluate the *in vitro* cytotoxicity of PTX-loaded PFA micelles. Cells were seeded in 96-well plates at 1×10^3 (4T1.2), 2×10^3 (HCT-116), and 3×10^3 (PC-3 and A549) cells per well 24 h prior to the treatment. Then the cells were treated with PTX/PFA₂ micelles or Taxol with a PTX concentration ranging from 0.1 to 1000 ng/mL in DMEM containing 10% FBS. After incubation for 72 h, 20 μ L of 3-(4, 5-dimethylthiazol-2-yl)-2,5-diphenyltetrazoliumbromide (MTT, 5 mg/mL) was added into each well, followed by incubation for another 4 h. The medium was then removed, and 150 μ L of DMSO was added to each well. The absorbance of each well was detected at 550 nm with a reference wavelength at 630 nm using a microplate reader, and cell viability was calculated based on the formula below. Untreated cells were included as a control.

$$\% \text{ cytotoxicity} = [1 - (\text{OD}_{\text{treat}} - \text{OD}_{\text{blank}}) / (\text{OD}_{\text{control}} - \text{OD}_{\text{blank}})] \times 100\%$$

4.2.9 Animals

Female BALB/c mice (6 to 8 weeks) were purchased from Charles River (Davis, CA). All animals were housed under pathogen-free conditions according to AAALAC guidelines. All animal-related experiments were performed in full compliance with institutional guidelines and approved by the Animal Use and Care Administrative Advisory Committee at the University of Pittsburgh.

4.2.10 Maximum tolerated dose (MTD) study

Female BALB/c mice were divided into nine groups randomly (n=4), and received i.v. injection of PTX/PFA₂ micelles (25, 50, 75, 100, and 125 mg PTX/kg) or Taxol (15, 20, 25 and 30 mg PTX/kg), respectively. Then the mice were monitored for survival and changes in body weight for 2 weeks. The MTD was determined at the maximal dose of PTX that leads to neither animal death nor significant changes in the general appearance or greater than 15% of body weight loss over the entire period.

4.2.11 *In vivo* therapeutic efficacy

A syngeneic mouse breast cancer model was established via s.c. inoculation of 2×10^5 of 4T1.2 cells into the right flank of female BALB/c mice. When the tumor size reached $\sim 50 \text{ mm}^3$, mice were randomly divided into four groups (n=5), and i.v. injected with saline, Taxol (10 mg PTX/kg), or PTX/PFA₂ micelles (10 and 25 mg PTX/kg), respectively, at designated time points.

Tumor volumes were measured by a caliper, calculated based on the formula: $(L \times W^2)/2$, in which L is the longest and W is the shortest tumor diameters (mm), and presented as relative tumor volume (RTV, the tumor volume at a given time point divided by the tumor volume prior to first treatment). Mice were sacrificed when tumors developed ulceration. Changes in body weights of all mice were also monitored during the entire course of treatment.

4.2.12 Statistical analysis

Statistical analysis was performed with two-tailed Student's t-test between two groups. $p < 0.05$ was considered statistically significant, and $p < 0.01$ was considered highly statistically significant. One-way ANOVA was conducted to assess significance among multiple groups, followed by Newman-Keuls test if $p < 0.05$.

4.3 RESULTS

4.3.1 Synthesis and characterization of PFA conjugates

Previously, we found that PEG₅₀₀₀-Fmoc₂, a PEG-Fmoc conjugate without lipid chain, exhibited remarkably enhanced compatibility with PTX compared to its counterpart with lipids.[59] However, this carrier showed limited effectiveness in formulating many other therapeutic agents. To gain insight into the SAR of the core-forming structure, a series of simple PEG-Fmoc conjugates with one PEG and one Fmoc-amino acid were developed and characterized. Our

initial attempt with such conjugates with PEG₅₀₀₀ did not work out as all of them were poor solubilizers of PTX. In contrast, the PEG₂₀₀₀-Fmoc series demonstrated varied levels of activity in encapsulating PTX. Therefore, a series of PEG₂₀₀₀-Fmoc conjugates were synthesized in this study and used as a simple model to better understand the impact of the Fmoc-neighboring motifs on carrier-drug interaction.

As illustrated in **Figure 33**, PFA conjugates were composed of three building blocks, one PEG₂₀₀₀ backbone, one Fmoc motif, and an amino acid derivative. All the PFA conjugates can be prepared through a simple, one-step synthetic route (PFA₁₋₇) except PFA₈ that requires an additional step for deprotection of t-Boc group. **Figure 34A** shows the ¹H NMR spectrum of PEG₂₀₀₀-Fmoc-ε-Cbz-lysine (PFA₂). Signal at 3.63 ppm is attributed to the methyl protons at the terminal of PEG₂₀₀₀ chain, and signals at 7.9-7.3 ppm are attributed to Fmoc and Cbz groups. The molecular weight of the PFA₂ conjugate detected by MALDI-TOF Mass Spectrum is close to the theoretical values (**Figure 35**). Taken together, these data indicate the successful synthesis of PFA₂ conjugate. Similarly, the structures of other PFA conjugates were also confirmed by ¹H NMR (**Figure 36**) and MALDI-TOF (**Figure 35**).

4.3.2 Effectiveness of PFA in formulating PTX

To investigate the effect of PFA structure on the carrier-drug interaction, we first examined the effectiveness of different PFA conjugates in encapsulating PTX in aqueous solution. Among the four lysine-based PFA conjugates, PFA₁ and PFA₂ could effectively formulate PTX at a respective carrier/drug ratio as low as 2:1 and 0.75:1, while PFA₃ and PFA₈ could not well solubilize PTX (**Table 5**). We then extended our screening to other amino acid derivatives with

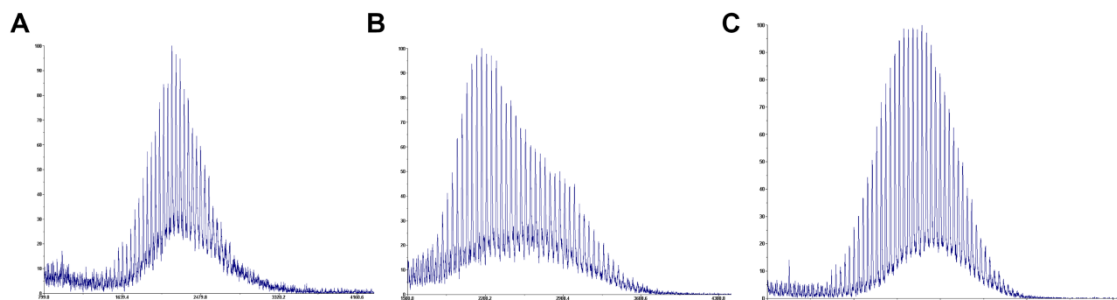


Figure 35. MALDI-TOF mass spectrum of PFA₁ (A), PFA₂ (B), and PFA₄ (C).

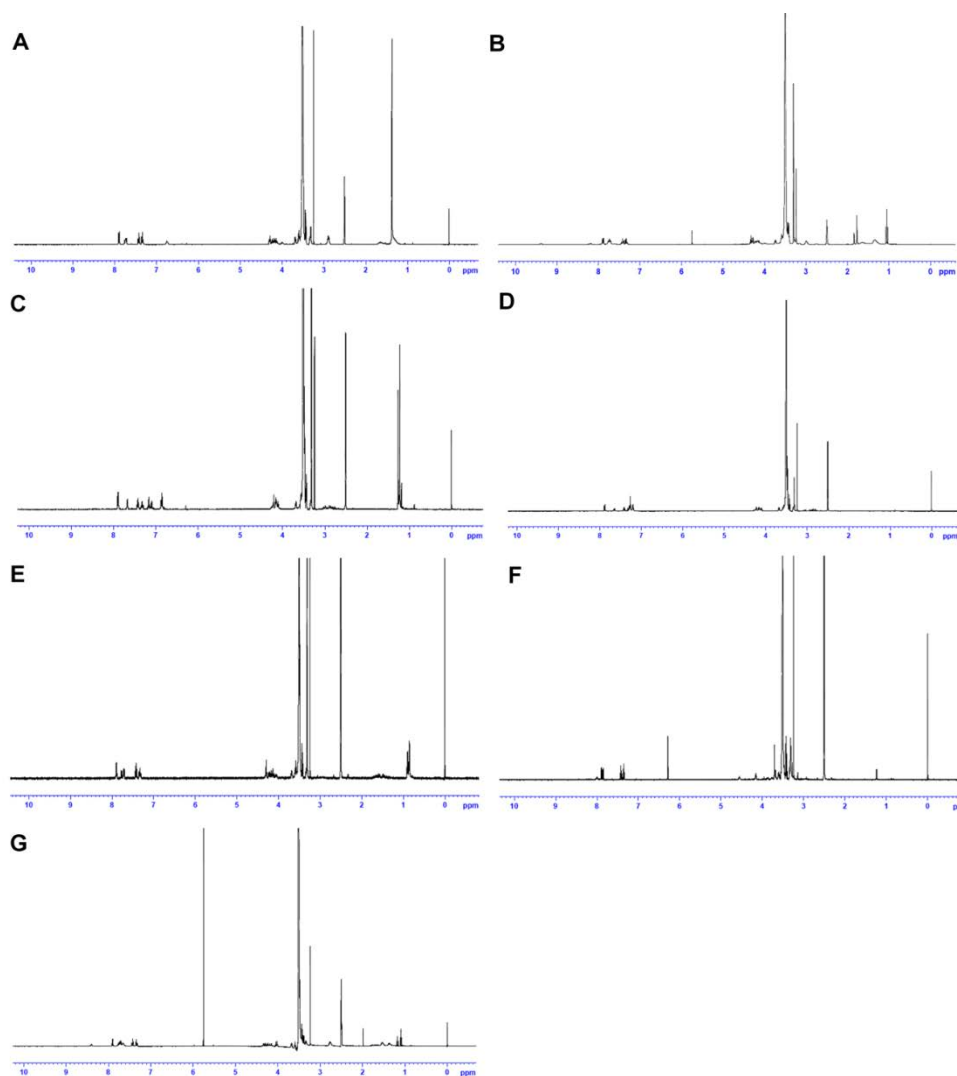


Figure 36. ¹H NMR spectrum of PFA₁ (A), PFA₃ (B), PFA₄ (C), PFA₅ (D), PFA₆ (E), PFA₇ (F), and PFA₈ (G).

different side chains. PFA₄ is a tyrosine derivative and showed a similar efficiency in formulating PTX as PFA₁, while PFA₅₋₇ performed poorly in solubilizing PTX at all carrier/drug ratios tested.

Table 5. Effectiveness of PFA conjugates in PTX encapsulation.

| Carrier | Building block (A) | PFA/PTX molar ratio | | |
|------------------|------------------------|---------------------|-----|-----|
| | | 0.75:1 | 1:1 | 2:1 |
| PFA ₁ | Lys (Boc) | M | M | C |
| PFA ₂ | Lys (Cbz) | C | C | C |
| PFA ₃ | Lys (Ac) | NS | NS | NS |
| PFA ₈ | Lys (NH ₂) | NS | NS | NS |
| PFA ₄ | Tyr (tBu) | NS | NS | C |
| PFA ₅ | Phe | NS | NS | M |
| PFA ₆ | Leu | NS | NS | M |
| PFA ₇ | Gly | NS | NS | NS |

C: clear solution obtained; M: milky solution obtained; NS: not soluble and large quantity of drug crystal observed in solution. PTX concentrations were kept at 1 mg/mL.

4.3.3 Further biophysical characterization of drug-free and PTX-loaded PFA micelles

We conducted further biophysical characterizations of PFA₁, PFA₂ and PFA₄ as these conjugates were capable of forming stable mixed micelles with PTX (**Table 5**). **Figure 37** showed the CMC values of PFA₁, PFA₂ and PFA₄ conjugates. PFA₂ exhibited a lowest CMC value of 0.0805 μmol/L, which is 80% and 90% lower than that of PFA₁ and PFA₄. **Table 6** shows that PFA₂ readily formed sub-nanosized (~60 nm) particles as determined by DLS, which is significantly smaller than PFA₁ and PFA₄ (~100 nm) micelles. PFA₁ and PFA₄ require a minimum carrier-drug ratio of 2:1 to load PTX, giving a PTX loading capacity of ~15%. In contrast, PFA₂ exhibited a dramatically enhanced DLC of ~30%. Negative-staining TEM

demonstrated a spherical morphology and homogeneous distribution of PFA micelles before and after PTX entrapment (**Figure 38**), and all the particles showed a neutral zeta-potential (**Table 6**).

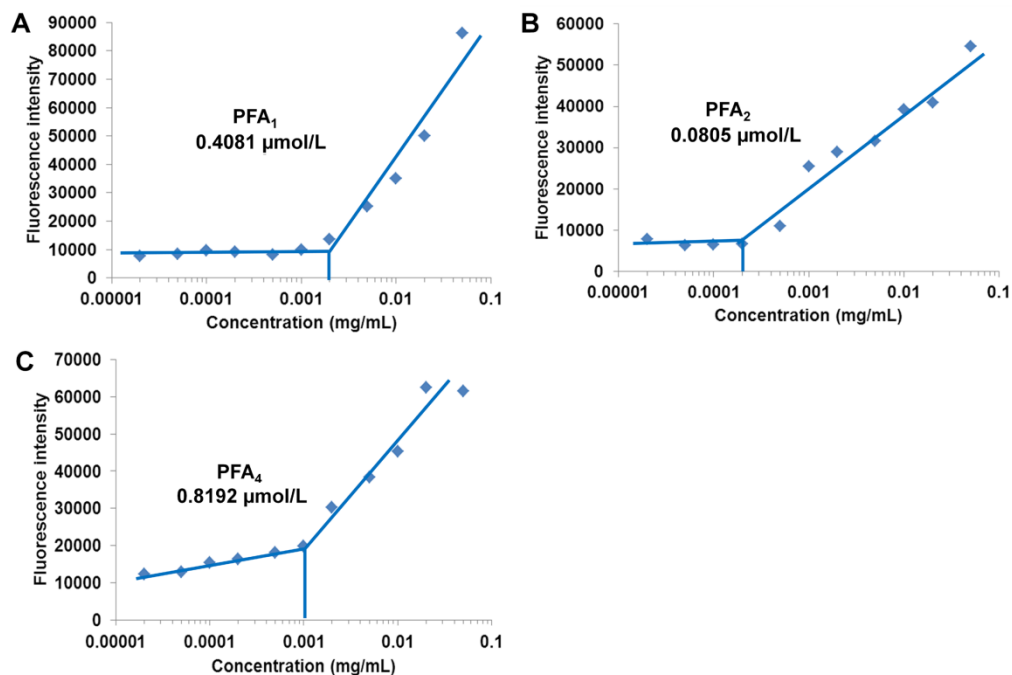


Figure 37. Critical micelle concentration (CMC) measurement of PFA₁ (A), PFA₂ (B), and PFA₄ (C) with pyrene as a fluorescence probe.

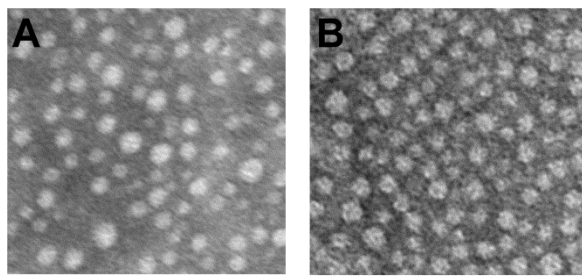


Figure 38. Negative staining TEM images of drug-free (A) and PTX-loaded (B) PFA₂ micelles. Scale bar is 100 nm.

Table 6. Characterization of drug-free and PTX-loaded PFA micelles.

| | ^a PFA/PTX molar ratio | Particle size (nm) | ^b PDI | Zeta-potential (mV) | ^c PTX content (w/w, %) | ^d Entrapment efficiency (%) |
|-----------------------|----------------------------------|--------------------|------------------|---------------------|-----------------------------------|--|
| PFA ₁ | - | 127±5 | 0.27 | -1.67±0.38 | - | - |
| PFA ₁ /PTX | 2:1 | 101±5 | 0.28 | -1.38±0.20 | 14.84 | 80.03 |
| PFA ₂ | - | 65±7 | 0.51 | -2.16±0.56 | - | - |
| PFA ₂ /PTX | 0.75:1 | 91±1 | 0.31 | -3.58±3.28 | 31.43 | 73.72 |
| | 1:1 | 84±9 | 0.41 | -1.87±1.72 | 25.58 | 86.06 |
| | 2:1 | 68±6 | 0.51 | -1.66±0.11 | 14.67 | 96.98 |
| PFA ₄ | - | 102±1 | 0.24 | -1.64±0.26 | - | - |
| PFA ₄ /PTX | 2:1 | 105±7 | 0.26 | -1.56±0.22 | 14.89 | 89.89 |

^aPTX concentrations were kept at 1 mg/mL. ^bPDI, polydispersity index. ^cPTX content was calculated as: weight of PTX/(weight of PFA + weight of PTX) × 100%. ^dEntrapment efficiency was calculated as: (weight of drug loaded into micelles/weight of drug used) × 100%.

Figure 34B shows the ¹H NMR spectrum of PTX/PFA₂ mixture in CDCl₃. All of the proton signals from PFA₂ and PTX were clearly visualized. In contrast, a drastic suppression of proton signals was observed for Fmoc, Cbz, and PTX when PFA₂ and PTX were mixed in D₂O (**Figure 34C**), suggesting the self-assembly of micelles in aqueous solution and a complete encapsulation of PTX into the inner hydrophobic core.

4.3.4 Effect of PFA structure on the carrier-drug and carrier-carrier interactions

The above data showed that PFA₂ exhibited a lowest CMC value, smallest particle size distribution, and highest PTX loading capacity among the three PFA conjugates that effectively encapsulated PTX. In order to delineate the correlation between structures of PFA and their biophysical properties, carrier-carrier and carrier-drug interactions were investigated via fluorescence quenching study and ¹³C NMR.

Figure 39A shows the fluorescence maxima of PFA conjugates detected at 305 nm upon excitation at 270 nm, which are consistent with the reported fluorescence spectrum of Fmoc motif.[58, 59, 104] The fluorescence intensity of the 3 PFA conjugates follows the order of $PFA_1 \gg PFA_2 > PFA_4$. Incorporation of PTX led to drastic fluorescence quenching for all the three PTX/PFA mixed micelles and this quenching occurred in a PTX-concentration dependent manner (**Figure 39B**). PFA_2 showed a fluorescence quenching of 49.8% after loading PTX, which is about twice as much as that for PFA_4 (**Figure 39C**). PFA_1 showed the least fluorescence quenching of 14% (**Figure 39C**).

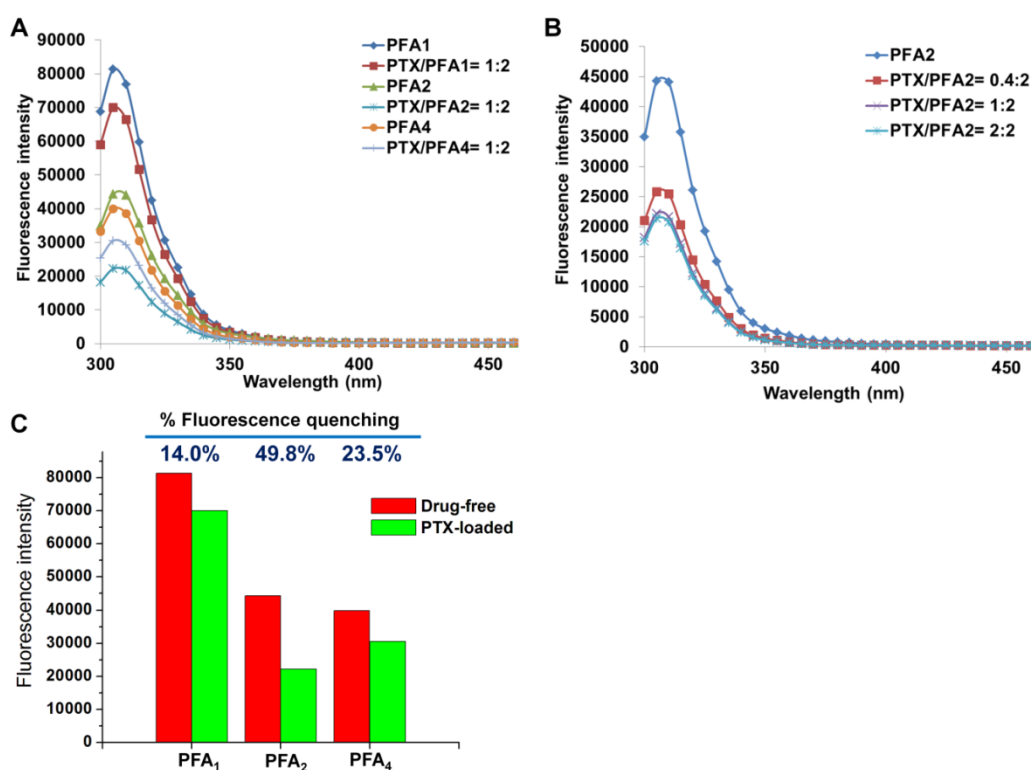


Figure 39. Fluorescence quenching study. Drug-free and PTX/PFA mixed micelles were prepared at a fixed PFA concentration of 1.17 mmol/L. PTX/PFA ratios were reported as molar ratios. The samples were excited at 270 nm and the fluorescence intensity at 300 to 460 nm was recorded. % Fluorescence quenching was calculated as: $(1 - \text{fluorescence intensity of PTX/PFA} / \text{fluorescence intensity of drug-free PFA}) \times 100\%$.

Figure 40 shows the signal shift of aromatic rings of PTX in ^{13}C NMR spectrum, which is caused by interaction with different conjugates. It is believed that a signal shift of greater than 0.02 in ^{13}C NMR spectrum is indicative of significant intermolecular interaction.[59] These data suggest a strongest interaction of the aromatic rings of PTX with Fmoc-Lys (Cbz), followed by Fmoc-Tyr (tBu) and Fmoc-Lys (Boc), which is consistent with the data in fluorescence quenching study (**Figure 39**).

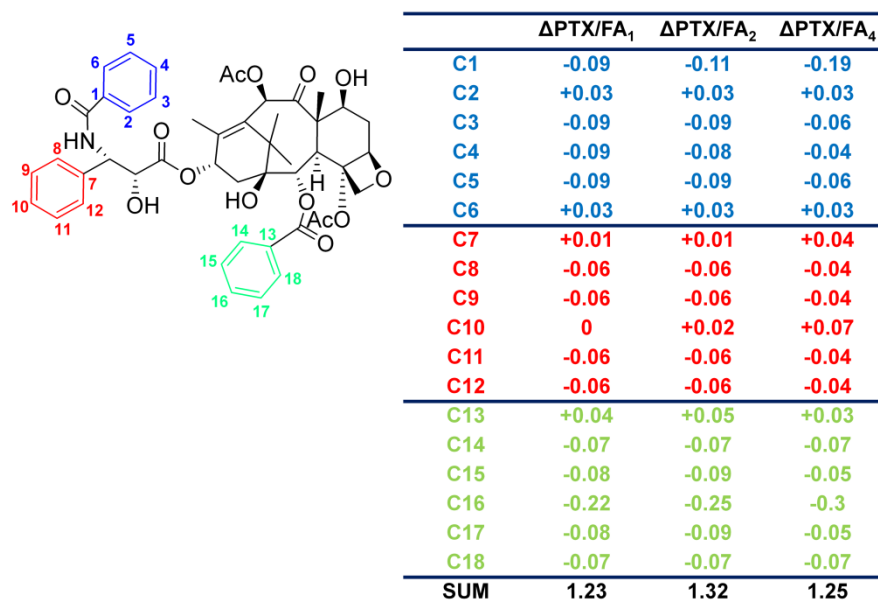


Figure 40. ^{13}C NMR of PTX mixed with FA_1 , FA_2 , and FA_4 in CDCl_3 . PTX was mixed with FA at a molar ratio of 1:5. Signal shift (Δ) indicates the signal shift of carbon atom on aromatic rings of PTX before and after mixing with FA, and SUM indicates a cumulative shift of all the atoms (absolute values).

4.3.5 Reconstituability of PTX/PFA mixed micelles following lyophilization

The above data demonstrated that PFA_2 was highly effective in formulating PTX. To further establish its potential as an effective nanocarrier, it was then subjected to additional *in vitro* and *in vivo* characterization as detailed below. **Figure 41** shows the reconstituability of PTX/ PFA_2 micelles following lyophilization. Without the use of any cryo-protectant, PTX-loaded PFA_2

micelles were readily reconstituted in water after lyophilization. No significant changes in particle size were noticed. In addition, 92% of PTX remain associated with the reconstituted micelles, suggesting that the integrity of the drug-loaded micelles was well retained during the lyophilization and reconstitution.

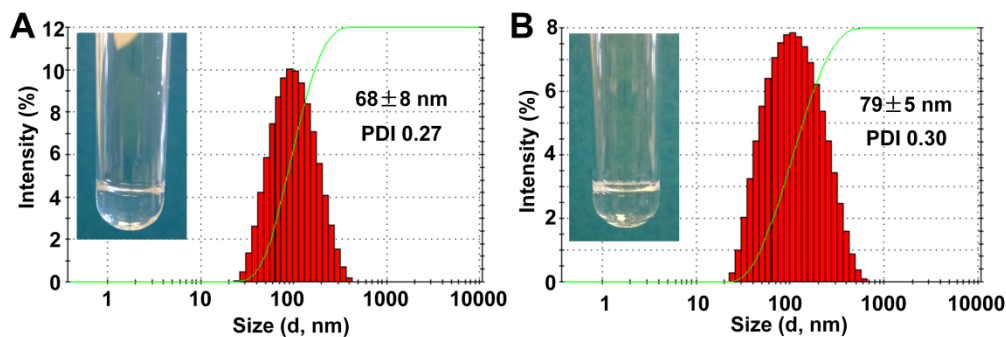


Figure 41. Size distribution of PTX/PFA₂ micelles before (A) and after (B) lyophilization/reconstitution. PTX concentration in the mixed micelles was kept at 1 mg/mL.

4.3.6 PTX release kinetics

The kinetics of PTX release from PTX/PFA₂ micelles was determined through a dialysis method and Taxol was used as a control. As depicted in **Figure 42**, Taxol formulation showed a burst release profile at the initial stage, and about 50% of PTX was released during the first 8 h. In contrast, PTX encapsulated in PFA₂ micelles showed a relatively slower rate of release, particularly at the early time points. After 8 h, less than 30% of entrapped PTX was escaped from micelles.

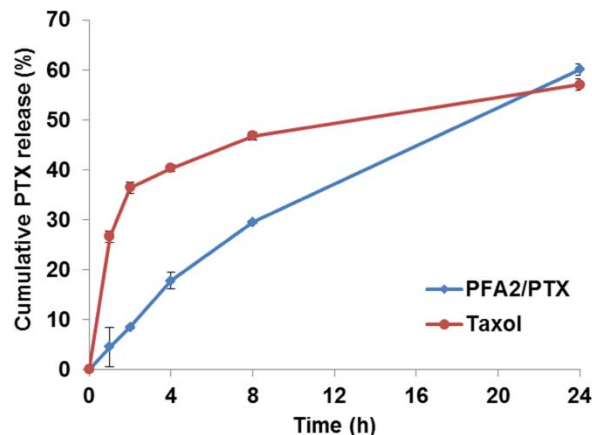


Figure 42. The kinetics of PTX release from PTX/PFA₂ as examined via a dialysis method. PTX concentration in PTX/PFA₂ and Taxol was kept at 1 mg/mL, and DPBS containing 0.5% (w/v) Tween 80 was used as release medium. PTX concentration was analyzed by HPLC at 0, 1, 2, 4, 8, and 24 h.

4.3.7 *In vitro* cytotoxicity

In vitro cytotoxicity of PTX/PFA₂ mixed micelles was evaluated with various cancer cell lines including human prostate cancer cell line, PC-3, mouse breast cancer cell line, 4T1.2, human colonic carcinoma cell line, HCT-116, and human lung adenocarcinoma cell line, A549. **Figure 43A** shows that PFA₂ micelles alone had minimal effect on the proliferation of PC-3 cells. Taxol, a clinically used formulation of PTX, inhibited the tumor cell growth in a dose-dependent manner. PTX/PFA₂ micelles were more effective than Taxol in inhibiting the tumor cell growth. Similar results were observed in other 3 tumor cell lines (**Figure 43 B~E**).

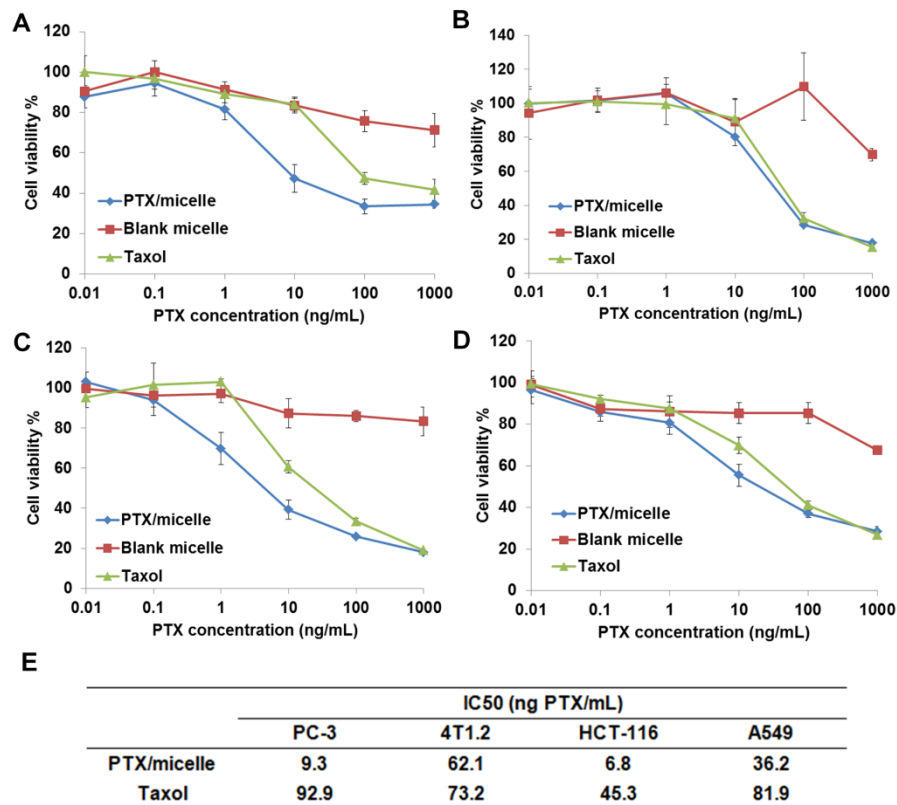


Figure 43. *In vitro* cytotoxicity. PC-3 androgen-independent human prostate cancer cells (A), 4T1-2 mouse metastatic breast cancer cells (B), HCT-116 human colonic carcinoma cells (C), and A549 human lung adenocarcinoma epithelial cells (D) were treated with PTX/PFA₂, drug-free PFA₂, and Taxol for 72 h, and cancer cell inhibition was determined by MTT assay. Panel E summarizes the IC₅₀ of PTX/PFA₂ and Taxol in different cell lines.

4.3.8 Maximum tolerated dose (MTD) study

Five different doses of PTX/PFA₂ micelles and three doses of Taxol were tested in the MTD study. Animal death, change of body weight, and other signs of toxicity in animals were followed during the entire period of experiment. As shown in **Table 7**, Taxol was well tolerated at a PTX dose of 20 mg/kg. Increasing the PTX dose to 25 mg/kg led to the death of 1 out of 4 treated mice, suggesting a MTD of ~20 mg/kg. However, PTX/PFA₂ micelles were well tolerated at a PTX dose of up to 100 mg/kg. The improved safety profile of PTX/PFA₂ mixed micelles is likely due to the enhanced formulation stability, resulting in slow release of PTX over a prolonged

period of time. The increased MTD of PTX/PFA₂ mixed micelles shall allow higher dosage of PTX to be administered to maximize the therapeutic effect.

Table 7. Maximum tolerated dose of PTX/PFA₂ micelles.

| | Dose of PTX (mg/kg) | Animal death | Weight change (%) |
|---------------------------------|------------------------|--------------|-------------------------|
| Taxol | 15 | 0/4 | 9.3±2.0 |
| | 20 | 0/4 | 9.8±1.4 |
| | 25 | 1/4 | N/A |
| | 30 | 3/4 | N/A |
| PTX/PFA ₂ micelle | 25 | 0/4 | 9.6±2.2 |
| | 50 | 0/4 | 11.2±2.1 |
| | 75 | 0/4 | 12.9±1.2 |
| | 100 | 0/4 | 10.5±1.7 |
| | 125 | 2/4 | N/A |

4.3.9 *In vivo* therapeutic efficacy

A highly aggressive mouse breast cancer model, 4T1.2, was established in BALB/c mice to evaluate the therapeutic efficacy of PTX/PFA₂ micelles *in vivo*. Tumors in saline-treated mice showed rapid uncontrolled growth. Taxol showed a modest effect in inhibiting the tumor growth at a dose of 10 mg PTX/kg. Delivery of PTX via PFA₂ micelles at the same dose led to a significantly enhanced antitumor activity ($p < 0.05$ vs. Taxol) (**Figure 44**). When the dosage was increased to 25 mg PTX/kg, a further improvement in tumor inhibition activity was achieved ($p < 0.01$ vs. Taxol). There were no obvious changes of animal body weight in all of the treatment groups.

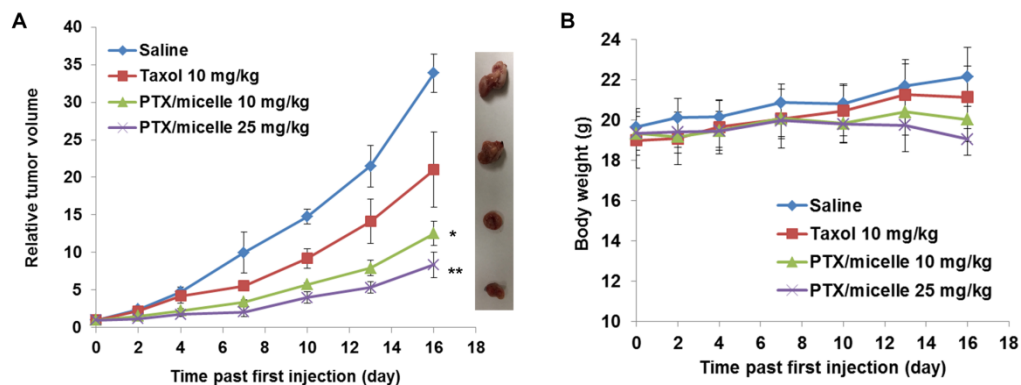


Figure 44. *In vivo* antitumor activity of PTX/PFA₂. BALB/c mice (n=5) bearing 4T1.2 murine breast cancer grafts were i.v. injected with PTX/PFA₂ (10 and 25 mg PTX/kg body weight), Taxol (10 mg PTX/kg body weight), and saline on days 0, 2, 4, 7, 10 and 13, respectively. Tumor growth was monitored and plotted as relative tumor volume (A). **P* < 0.05; ***P* < 0.01 (vs Taxol). No significant changes of body weight in mice were observed (B).

4.3.10 Effectiveness of PFA₂ micelles in formulating a broad variety of drug molecules

The broad utility of PFA₂ micelles was evaluated using eight model drugs with diverse structures and bioactivities, including curcumin, docetaxel, doxorubicin, etoposide, griseofulvin, nifedipine, imatinib and progesterone. As shown in **Table 8**, all the tested drugs can be effectively formulated by PFA₂ micelles at a concentration of 1 mg drug/mL, which represents an up to 1000-fold enhancement in solubility.

Table 8. Effectiveness of PFA₂ micelles in formulating various therapeutic agents.

| Model drug | Biologic activities | ^a MW (g/mol) | Number of aromatic rings | ^b Log P | ^b Original solubility (µg/mL) | Fold of increase in solubility | Particle size (nm) | ^c PDI |
|--------------|------------------------------------|-------------------------|--------------------------|--------------------|--|--------------------------------|--------------------|------------------|
| Curcumin | inflammatory response modulator | 368.4 | 2 | 3.1 | < 1 | >1000 | 34±1 | 0.58 |
| Docetaxel | antimitotic agent | 807.9 | 2 | 2.59 | 6 | 166.7 | 134±4 | 0.16 |
| Doxorubicin | cytotoxic anthracycline antibiotic | 543.5 | 2 | 1.27 | ^d N/A | N/A | 18±4 | 0.35 |
| Etoposide | topoisomerase inhibitor | 588.6 | 2 | 0.6 | 126 | 7.9 | 62±4 | 0.66 |
| Griseofulvin | antifungal agent | 352.8 | 1 | 2.0 | 14 | 71.4 | 29±8 | 0.53 |
| Nifedipine | Ca ²⁺ channel blocker. | 346.3 | 2 | 2.5 | 5 | 200 | 40±8 | 0.60 |
| Imatinib | tyrosine-kinase inhibitor | 493.6 | 4 | 1.99 | 50 | 20 | 83±7 | 0.44 |
| Progesterone | female hormone | 314.5 | 0 | 3.87 | 7 | 142.9 | 27±3 | 0.38 |

^aMW= molecular weight. ^bLog P and original solubility of listed drugs refer to references.[105-115] ^cPDI, polydispersity index. ^dN/A, data not available.

4.4 DISCUSSION

Incorporation of Fmoc into nanocarriers as interfacial drug-interactive motifs has recently been discovered as an effective strategy to improve carrier-drug compatibility of micellar system.[55, 58, 59] Intermolecular π - π stacking strengthens carrier/carrier and carrier/drug interaction, leading to more stable systems with significantly improved drug loading capacity and formulation stability. Our previous work showed that a Fmoc-decorated lipidic carrier (PEG₅₀₀₀-(Fmoc-OA)₂) was more effective in solubilizing PTX than its Fmoc-free counterpart (PEG₅₀₀₀-OA₂).[58] Interestingly, when the lipid chains of PEG₅₀₀₀-(Fmoc-OA)₂ were substituted with t-Boc motifs, the resulting system (PEG₅₀₀₀-Fmoc₂), although greatly simplified, showed drastic improvement in formulating PTX,[59] suggesting that the neighboring group of Fmoc also greatly impacts the overall drug-carrier interaction in these PEG-Fmoc conjugates.

To gain better insights into the SAR and further optimize this delivery system, a series of simple conjugates (PEG₂₀₀₀-Fmoc-amino acid) were developed that differ in the neighboring structures of Fmoc. All of these conjugates can be easily prepared via a one-step conjugation using the readily available Fmoc-decorated amino acids. PFA₁₋₃ and PFA₈ were lysine-based PFA conjugates with Cbz, Boc, Ac or free amino group substituted at the ϵ -position of lysine. Other amino acids as Tyr (tBu), Phe, Leu and Gly were also used to provide more diverse structures.

PFA₁ (PEG₂₀₀₀-Fmoc- ϵ -t-Boc-lysine) is a simplified model of our previously developed PEG₅₀₀₀-Fmoc₂ conjugate that formed small-sized (~30 nm) mixed micelles with PTX with a DLC greater than 30%.^[59] However, PFA₁ formed particles of significantly increased size (~100 nm) and decreased loading capacity of PTX (~15%), which may be attributed to a less tightly packed inner core of micelle due to weakened π - π stacking from fewer Fmoc motifs. Compared with PFA₁, PFA₂ exhibited much smaller particle size (~60 nm) and a DLC (~31%) that is comparable to that of PEG₅₀₀₀-Fmoc₂. Attachment of a Cbz group to the ϵ -position of lysine residue introduced additional π - π stacking interaction and hydrophobicity. This would likely strengthen carrier-carrier and carrier-drug interaction, leading to a more tightly packed core with a reduced size and increased DLC compared to PFA₁ with a t-Boc group. On the contrary, the ϵ -acetyl and amine group at PFA₃ and PFA₈ contribute little to the overall π - π stacking and hydrophobic interactions, which may explain, at least partially, why both conjugates are poor PTX solubilizers. Similarly, the different PTX loading capacity of PFA₄₋₇ may be explained by the degree to which the different Fmoc-neighboring motifs in these conjugates contribute to the overall π - π stacking and hydrophobic interaction.

Besides π - π stacking and hydrophobic interaction, hydrogen bonding may also impact the overall carrier-drug interaction. Although PFA₂, PFA₄ and PFA₅ are all equipped with an aromatic ring in the side chain of amino acid residue, they differ significantly in the DLC for PTX (**Table 5**). As shown in **Figure 33**, R₂ contains two hydrogen bonding donor/acceptor, which may form hydrogen bonds with PTX, leading to a more effective carrier-drug interaction, while R₄ is equipped with only one hydrogen bonding acceptor and none is found in R₅. The difference in the effectiveness of hydrogen-bonding of the different conjugates also contributes to the difference in their overall performance as a drug carrier.

In addition to the number and/or type of the drug-interacting groups, the steric hindrance imposed on them by the surroundings and thus their flexibility may further affect the carrier-drug interaction. A relatively long spacer between the benzene ring structure of Cbz and PEG backbone (10 atoms) in PFA₂ may facilitate its interaction with the drug molecules due to reduced steric hindrance and increased flexibility of Cbz. In contrast, a much shorter spacer in R₄ and R₅ (3 atoms) may have a weakened carrier-drug π - π interaction due to less accessibility of these benzene rings.

Since PFA₁, PFA₂ and PFA₄ can effectively formulate PTX, these three conjugates were selected for further studies of carrier-carrier and drug-carrier interaction. Fluorescence quenching has been widely utilized to study π - π stacking interaction. A reduction in fluorescence intensity of Fmoc at 305 nm usually indicates the occurrence of π - π stacking between Fmoc motifs and other aromatic rings, which is likely to cause intermolecular energy transfer.[72] The significant fluorescence quenching of PFA₂ and PFA₄ in comparison to PFA₁ is likely attributed to a more effective carrier-carrier interaction that involves the participation of Cbz (PFA₂) and Tyr (PFA₄) in π - π stacking. Further fluorescence quenching following incorporation of PTX encapsulation is

likely attributed to carrier-drug interaction. As discussed above, Cbz group in PFA₂ is likely to contribute significantly to PTX/PFA₂ π - π stacking considering its high flexibility and accessibility (**Figure 45**). Data from ¹³C NMR study (**Figure 40**) further support the notion of carrier-drug interaction.

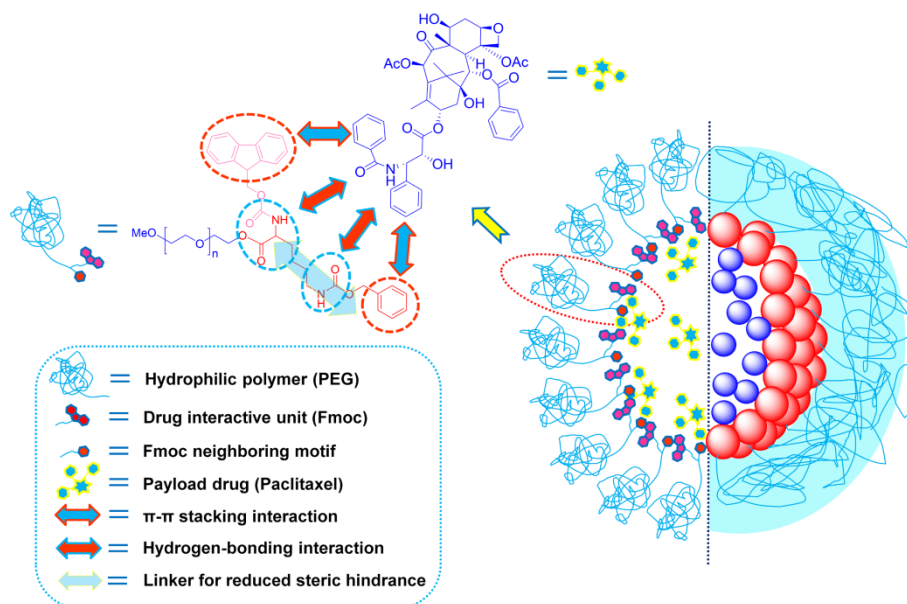


Figure 45. Schematic representation of proposed mechanisms of intermolecular interaction between PFA₂ conjugate and PTX.

The biophysical study sheds some insight into the SAR of the PFA series. It has also led to the discovery of PFA₂ as a potentially useful carrier for anticancer drug. We have demonstrated the utility of PFA₂ in anticancer drug delivery using PTX as a model drug. *In vitro*, PTX/PFA₂ micelles showed enhanced cytotoxicity in all of the cancer cell lines tested compared to Taxol. More importantly, a significantly improved tumor inhibitory activity and reduced toxicity were demonstrated *in vivo*. The improved performance of PTX/PFA₂ micelles over Taxol formulation is likely due to the effective carrier-drug interaction, leading to enhanced formulation stability and improved drug delivery to tumor.

Besides PTX, PFA₂ demonstrated a broad utility to formulate many other model drugs with diverse chemical structure, hydrophobicity, and biological activities. And furthermore, this simple conjugate can be easily synthesized and scaled-up for large-scale production. In addition, PFA₂ micelles can be lyophilized and reconstituted without change of size. These properties may facilitate its translation into clinical evaluation as a potential nanocarrier for improved drug delivery.

In summary, a SAR study based on a series of PFA conjugates was conducted to investigate the mechanism of carrier–drug interaction. Various modes of interactions are likely to contribute to the overall performance of the drug carrier including π – π stacking, hydrogen bonding, and hydrophobic interaction. The flexibility and accessibility of drug-interactive motifs may also play an important role. In addition, PFA₂ was identified to be a simple and effective drug carrier for PTX with small particle size, low CMC value, and high drug loading capacity. It also exhibited significantly improved effectiveness in delivering PTX in vitro and in vivo compared to Taxol formulation. Finally, PFA₂ demonstrated a broad application potential in formulating various therapeutic agents of diverse structures.

5.0 EFFECTIVE CO-DELIVERY OF DOXORUBICIN AND DASATINIB USING A PEG-FMOC NANOCARRIER FOR COMBINATION CANCER CHEMOTHERAPY

5.1 BACKGROUND

In previous sections, we have demonstrated the development of a variety of PEG-Fmoc conjugates that can effectively formulate a broad range of therapeutics as single agent. However, in clinical cancer therapy, due to the complex nature of cancer, simultaneous administration of multiple drugs with different mechanisms of action usually represents an attractive strategy over single drug treatment. This combination therapy can synergistically inhibit the tumor growth via modulating different signaling pathways. Such strategy shall help to maximize the therapeutic response of chemotherapy while minimizing the occurrence of multi-drug resistance [116-119].

One potent chemotherapeutic agent that is oftentimes utilized in combination chemotherapy is doxorubicin (DOX). DOX is a first-line chemotherapeutic agent in the treatment of a broad range of cancers including breast, ovary, bladder, cervix, prostate and lung cancers, and leukemias. DOX potently inhibits proliferation of cancer cells through binding to topoisomerase enzyme II or directly intercalating with DNA base pairs to suppress DNA replication and induce cell apoptosis[120-122]. In clinic, DOX is widely used in multi-drug regimens with other anti-cancer agents, such as cyclophosphamide, 5-fluorouracil, docetaxel, vinblastine, and bleomycin [123-125].

Recently, *in vitro* studies have clearly demonstrated significant synergistic effect between DOX and dasatinib (DAS) in inhibiting the proliferation, migration, and invasion of cancer cells [126]. DAS is a tyrosine kinase inhibitor that targets to various kinases such as Src, BCR-Abl, FAK, c-Kit, and others [127-132]. This distinct mechanism of action by DAS suggests its potential application in combination chemotherapy with other anti-cancer agents. For example, Pichot et. al. demonstrated that treatment of breast cancer cells with a combination of DOX and DAS led to significantly enhanced growth inhibition over each individual treatment [126]. Although this strong synergy may indicate a potential multi-agent regimen to enhance clinical therapeutic outcome of DOX, so far studies of this drug combination are only limited to *in vitro* investigation. One of the possible reasons lies in the difficulty in efficient co-delivery of the two agents to tumors due to their dissimilar physiochemical properties and pharmacokinetic profiles.

One of the most favored features of using nano-sized drug delivery system is its capability to encapsulate multi-agents of diverse chemical structures to achieve simultaneous delivery to target site [119, 133]. Several nano-sized delivery systems have been developed in recent decades [10, 11, 14, 84, 96]. Among them, micelles are one of the most attractive systems due to the simplicity in manipulation, high efficiency in solubilization of hydrophobic drugs, and small particle size that permits specific accumulation in solid tumor. Currently, various micellar systems have been intensively studied for their potential in target delivery of anti-cancer agents to tumor sites [20-22, 64, 134].

Previously, we developed a new type of micelles equipped with fluorenylmethyloxycarbonyl (Fmoc) as a highly effective drug interactive motif to facilitate carrier-drug interactions [55, 58, 59, 104, 135]. Compared with conventional micelles that simply entrap drugs through hydrophobic interactions, our micelles exhibited significantly improved compatibility with

payload drugs due to the additional mechanisms of carrier-drug interactions, such as π - π stacking and hydrogen bonding interaction. We have demonstrated that a simple PEG-Fmoc conjugate, PEG₅₀₀₀-lysyl-(α -Fmoc- ϵ -t-Boc-lysine)₂, exhibited excellent loading capacity and colloid stability in delivery of anti-cancer agent paclitaxel (PTX) [59]. However, this nanocarrier has limited utility for other hydrophobic agents. Subsequent studies on structure-activity relationship demonstrated that this problem can be solved through modulating neighboring groups of Fmoc. By replacing t-Boc motif with Cbz, the resulting system showed broadened utility in formulating a variety of anti-cancer agents including PTX, DOX, docetaxol, and imatinib [60].

In this study, a new nanocarrier, PEG₅₀₀₀-lysyl-(α -Fmoc- ϵ -Cbz-lysine)₂ (PLFCL), was developed for effective co-delivery of DOX and DAS for combination chemotherapy. In addition to comprehensive characterization of biophysical properties of this co-delivered nanomicelle formulation, synergistic chemotherapeutic efficacy was systemically evaluated in both cultured cancer cells and tumor-bearing animal models.

5.2 METHODS

5.2.1 Materials

DOX and DAS were purchased from LC Laboratories (MA, USA). α -Fmoc- ϵ -Cbz-lysine and di-Boc-lysine were purchased from GL Biochem Ltd. (Shanghai, China). N, N'-dicyclohexylcarbodiimide (DCC), N-hydroxysuccinimide (NHS), trifluoroacetic acid (TFA), and triethylamine (TEA) were obtained from Acros Organic (NJ, USA). Propylene glycol was

purchased from MP Biomedicals (OH, USA). Monomethoxy PEG₅₀₀₀, 4-dimethylaminopyridine (DMAP), ninhydrin, and other unspecified chemicals were all purchased from Sigma-Aldrich (MO, USA). Dulbecco's phosphate buffered saline (DPBS), Dulbecco's Modified Eagle's Medium (DMEM), fetal bovine serum (FBS), 100X penicillin-streptomycin solution were all purchased from Invitrogen (NY, USA). All solvents used in this study were HPLC grade.

5.2.2 Synthesis of PEG₅₀₀₀-lysyl-(α -Fmoc- ϵ -Cbz-lysine)₂ (PLFCL)

PLFCL was synthesized through a simple three-step synthesis route. Monomethoxy PEG₅₀₀₀ (1 equiv.) was dissolved in dried dichloromethane (DCM), and mixed with di-Boc-lysine (1.5 equiv.), DCC (1.8 equiv.) and DMAP (0.3 equiv.). The reaction was allowed at 37 °C for 48 h, followed by filtration twice to obtain clear filtrate. A large amount of white precipitate was obtained in cold ether, and washed twice with cold ethanol and ether. The obtained PEG₅₀₀₀-di-Boc-lysine was then treated with DCM/TFA (1:1, v/v) for 2 h at room temperature, followed by precipitation in ice-cold ether, and two washes with cold ethanol and ether.

In the last step, α -Fmoc- ϵ -Cbz-lysine (3 equiv.) was mixed with DCC (3.6 equiv.), NHS (3.6 equiv.), and DMAP (0.6 equiv.) in dried DCM, and allowed to react for 4 h at 37 °C. Then a mixture of PEG₅₀₀₀-lysine-NH₂ (1 equiv.) and TEA (3 equiv.) in DCM was added into the reaction. The conjugation was conducted at 37 °C till negative result was observed in ninhydrin test. Then the mixture was filtered twice, and precipitated in ice-cold ether, followed by two washes with cold ethanol and ether. The raw material was further purified by filtration through a 450 nm PVGF filter in distilled water, followed by lyophilization to yield white powder of PLFCL. The identity of obtained material was confirmed by ¹H NMR and MALDI-TOF.

5.2.3 Preparation and biophysical characterization of drug-free and drug-loaded PLFCL micelles

DOX&DAS co-encapsulated PLFCL micelles were prepared through a thin-film hydration method [59]. Briefly, designated molar ratios of DOX (5 mg/mL in 1:1 (v/v) of DCM/methanol), DAS (1 mg/mL in ethanol), and PLFCL (50 mg/mL in DCM) were mixed in a glass tube, and organic solvent was removed through a gentle stream of nitrogen, followed by drying in vacuum for overnight. The obtained thin-film of carrier/drug mixture was then hydrated in DPBS and suspended by vortex to obtain a clear solution of DOX&DAS/PLFCL micelles. DOX/PLFCL, DAS/PLFCL, and drug-free PLFCL micelles were prepared similarly. All drug-loaded micelles were filtered through a PVGF filter (450 nm) prior to characterization.

The critical micelle concentration of PLFCL was determined using pyrene as a fluorescence probe [58]. The size distribution and zeta potential of drug-free and drug-loaded micelles were detected through a Malvern Zeta Nanosizer. The morphology was observed by transmission electron microscopy (TEM) using negative staining method. The quantity of agents in micelles was detected through a Waters Alliance 2695 Separations Module with a Waters Symmetry RP-C18 column (250 mm × 4.6 mm) using acetonitrile: H₂O (52.5%:47.5%) containing 2.5 mM NH₄Ac and 0.05% CH₃COOH (pH 3.55) at a rate of 1 mL/min. DOX concentration was detected by a Waters 2475 Fluorescence Detector with excitation at 490 nm and emission at 590 nm. DAS concentration was measured through a Waters 2998 DAD Detector at 319 nm.

5.2.4 Fluorescence quenching

DOX&DAS/PLFCL, DOX/PLFCL, DAS/PLFCL, and drug-free PLFCL micelles were prepared as described above. Carrier/drug molar ratio was kept at 2:1, and concentrations of PLFCL, DOX and DAS were kept constant in different groups. The samples were placed into a 96-well plate. The fluorescence intensity of Fmoc was detected at the excitation wavelength of 270 nm and emission wavelength of 300-450 nm, and fluorescence of DOX was measured using an excitation wavelength of 480 nm and emission wavelength from 510-650 nm by a Synergy H1 Hybrid Multi-Mode Microplate Reader.

5.2.5 UV absorbance spectroscopy

DOX&DAS/PLFCL, DOX/PLFCL, DAS/PLFCL, and drug-free PLFCL micelles were prepared as described above, and the UV absorption spectra were scanned by a Varian Cary 50 Bio UV-Visible Spectrophotometer at a wavelength between 286 and 590 nm. All the samples were prepared at a carrier/drug molar ratio of 2:1, and all concentrations were kept constant between different groups for comparison. Blank aqueous solvent was used as the reference.

5.2.6 *In vitro* drug release kinetics

The release kinetics of DOX and DAS from PLFCL micelles was conducted through dialysis method using DPBS (PH = 7.4) containing 0.5% (w/v) Tween 80 as release medium. Free DAS solubilized in 50% propylene glycol (v/v), and free DOX were used as controls. Two mL of

sample solution was placed into a dialysis bag (MWCO 12 kDa, Spectrum Laboratories), and incubated in a tank containing 200 mL of release medium under gentle shaking at 37 °C. At scheduled time points (0, 1, 2, 4, 8, 24, and 48 h), the concentration of DOX and DAS remaining in the dialysis bag was measured by HPLC as described above.

5.2.7 Cell culture

Mouse metastatic breast cancer cell line 4T1.2, human prostate cancer cell line PC 3, and human colonic carcinoma cell line HCT-116 were used for *in vitro* evaluation. These cell lines were all cultured at 37 °C in DMEM containing 10% FBS and 1% penicillin-streptomycin in a humidified environment with 5% CO₂.

5.2.8 Intracellular trafficking

4T1.2 cells were seeded in glass bottom dishes (In Vitro Scientific, USA) at a density of 1×10^5 cells/dish. Following culture for 24 h, cells were treated with DOX&DAS/PLFCL, DOX/PLFCL, or free DOX in Opti-MEM (Life Technologies, USA) for 0.5, 2, and 4 h, respectively. The concentration of DOX or DAS was kept at 10 µmol/L. Then cells were stained with Hoechst 33342 (1 µg/mL) for 30 min, and LysoTracker Green DND-26 (50 nM) (Invitrogen, USA) for 5 min, followed by two washes with cold DPBS. The intracellular distribution of DOX of various formulations was observed under a confocal laser scanning microscope (CLSM, FluoView 1000, Olympus, Japan).

5.2.9 *In vitro* cytotoxicity study

4T1.2, PC 3 and HCT-116 cancer cell lines were used in *in vitro* cytotoxicity study. Cells were seeded in 96-well plates at a density of 1000 (4T1.2), 2000 (HCT-116) and 3000 (PC 3) cells per well 24 h prior to treatment. Then cells were treated by various concentrations of DOX and/or DAS in different formulations. Drug-free PLFCL micelles were dosed at equivalent concentrations as in corresponding drug-loaded groups. Cells were incubated for 72 h, and the cell viability was measured through MTT assay as reported before [30]. Untreated cells were included as a control.

5.2.10 Cell migration inhibition

Cell migration inhibition was conducted using murine 4T1.2 cell line through a wound healing assay. Briefly, 4T1.2 cells were seeded into a 6-well plate, and allowed 24 h to attach and grow to a confluence of 80%. Then cells were streaked with a sterile pipette tip, treated with media containing various formulations at each drug concentration of 100 nmol/L, and allowed 16 h to recover. Wound width before and after treatment was observed and quantified under a Nikon eclipse TE 300 microscope.

5.2.11 Animals

Female BALB/c mice (6 to 8 weeks) were purchased from Charles River (Davis, CA). All animals were housed under pathogen-free conditions according to AAALAC guidelines. All

animal-related experiments were performed in full compliance with institutional guidelines and approved by the Animal Use and Care Administrative Advisory Committee at the University of Pittsburgh.

5.2.12 *In vivo* therapeutic efficacy

Female BALB/c mice were s.c. inoculated with 4T1.2 cells (2×10^5 cells/mouse) at the right flank. When the tumor size reached $\sim 50 \text{ mm}^3$, mice were randomly divided into five groups (n=5) and administered with saline, DOX/PLFCL, DAS/PLFCL, DOX+DAS, and DOX&DAS/PLFCL, respectively, through tail vein on day 0, 3 and 6. The dosage of DOX or DAS was kept at 5 mg/kg. Tumor volumes were calculated according to the formula: $(L \times W^2)/2$, in which L is the longest and W is the shortest tumor diameter (mm), and presented as relative tumor volume (RTV, the tumor volume at a given time point divided by the tumor volume prior to first treatment). Mice were sacrificed and tumors were harvested at the completion of the experiment. Tumor weights were measured, and tumor growth inhibition ratio was calculated as: $1 - (\text{mean tumor weight of drug treated group} / \text{mean tumor weight of saline treated group}) * 100\%$. Changes in body weights of all mice were also monitored during the entire course of treatment.

In a separate experiment, groups of seven 4T1.2 tumor-bearing mice were similarly treated as described above to follow the animal survival. For humane reasons, the end point of survival study was set when the implanted tumor volume reached 1000 mm^3 . The survival rates are presented as Kaplan–Meier curves.

5.2.13 Histochemical staining

After completion of the *in vivo* therapy study, tumor tissues were excised and fixed in 4% formaldehyde in PBS, followed by embedment in paraffin. The paraffin-embedded tumor samples were sectioned into slices at 5 μm using a HM 325 Rotary Microtome. The slices were then stained with hematoxylin and eosin (H&E) for histopathological examination under a Zeiss Axiostar plus Microscope (PA, USA). In situ terminal deoxynucleotidyl transferase dUTP nick end labeling (TUNEL) assay was performed using an In Situ Cell Death Detection Kit (Roche, USA) according to the manufacturer's protocol. DAPI was used for nuclear staining. The stained tumor slides were observed by a Nikon eclipse TE 300 fluorescence microscope.

5.2.14 Statistical analysis

Statistical analysis was performed with two-tailed Student's t-test between two groups. $p < 0.05$ was considered statistically significant, and $p < 0.01$ was considered highly statistically significant. One-way ANOVA was conducted to assess significance among multiple groups, followed by Newman-Keuls test if $p < 0.05$.

5.3 RESULTS

5.3.1 Combinational effect of DOX&DAS on cancer cell proliferation

The combinational effect of DOX and DAS on cancer cells was firstly tested in human breast cancer cell lines by Pichot et. al [126]. To examine its potential broad application, we investigated the therapeutic efficacy of this drug combo in a variety of other cancer cell lines, including murine breast cancer cell line 4T1.2, human prostate cancer cell line PC 3, and human colon cancer cell line HCT-116. As shown in **Figure 46A**, 4T1.2 breast cancer cells were well responsive to each single treatment by DOX or DAS with an IC_{50} of 24.6 and 94.2 nM, respectively. Nonetheless, combination of the two agents led to a significant improvement in the inhibition of tumor cell growth. The combination of the two agents was also more active than each treatment alone in inhibiting the proliferation of PC 3 (**Figure 46B**) and HCT-116 (**Figure 46C**) tumor cells although these two cell lines were relatively more resistant than 4T1.2 cells to either DOX or DAS. **Figure 46D** summarizes the combination index from the above studies, in which $CI > 1$ indicates antagonism, $CI = 1$ indicates additivity, and $CI < 1$ indicates synergy. It is apparent that DOX and DAS show a significant synergy in inhibiting the growth of all 3 tumor cell lines tested.

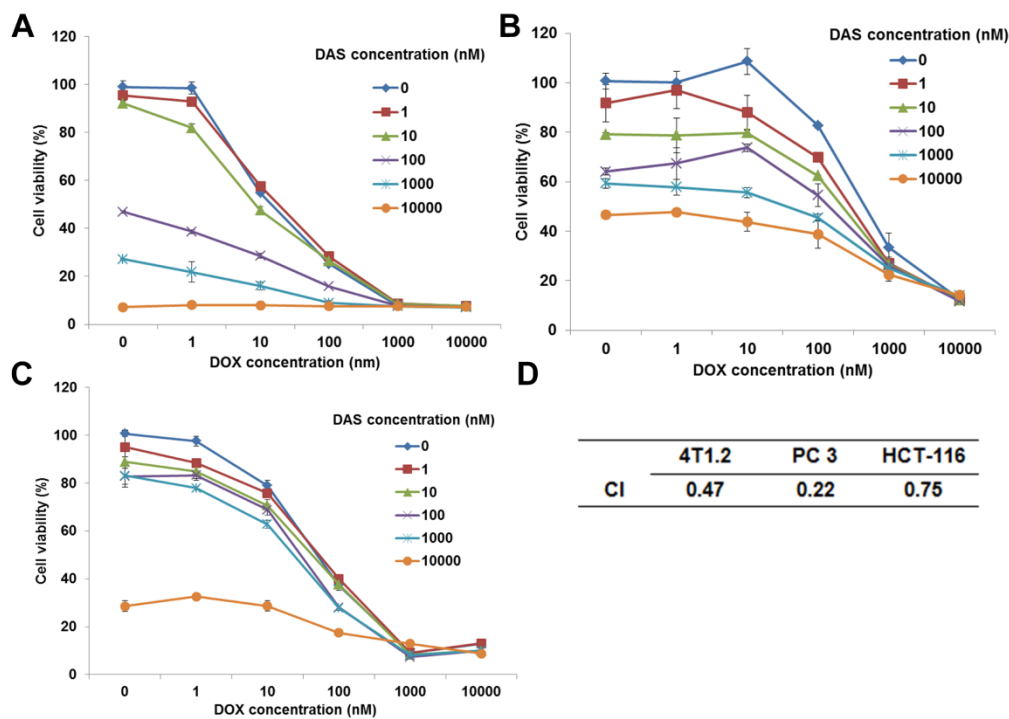


Figure 46. Proliferation inhibition of 4T1-2 mouse metastatic breast cancer cell line (A), PC 3 androgen-independent human prostate cancer cell line (B), and HCT-116 human colonic carcinoma cell line (C) treated with combination of DOX and DAS for 72 h. Synergy of DOX with DAS was indicated by combination index (CI) (D).

5.3.2 Design, synthesis, and characterization of PLFCL conjugate

We have previously developed a simple and effective nanomicellar carrier, PEG₅₀₀₀-lysyl-(α -Fmoc- ϵ -t-Boc-lysine)₂, that is highly effective in delivery of PTX to tumor cells *in vitro* and *in vivo* [59]. Drug loading into this carrier is largely achieved via the strong carrier and drug interactions including π - π stacking and hydrogen bonding. However, this carrier showed limited efficacy in formulating several other anticancer agents tested. Subsequent SAR studies showed that the neighboring structures of Fmoc also contributed significantly to the overall carrier/drug interaction. These studies have led to the development of PEG₂₀₀₀- α -Fmoc- ϵ -Cbz-lysine that was highly effective in formulating various therapeutic agents of diverse structures including PTX,

docetaxel, DOX, and imatinib [60]. This nanocarrier is a simple conjugate in which Boc was replaced by Cbz. It can be readily obtained by a one-step synthesis. Interestingly, despite the success of PEG₂₀₀₀- α -Fmoc- ϵ -Cbz-lysine in formulating various anticancer drugs as a single agent, DOX and DAS could not be effectively co-encapsulated into this single chain nanocarrier. This might be due to the limited size of drug-interacting pocket formed by PEG₂₀₀₀- α -Fmoc- ϵ -Cbz-lysine.

PLFCL is a PEG-peptidic conjugate that has two Fmoc/Cbz domains. We hypothesized that PLFCL will be more effective than PEG₂₀₀₀- α -Fmoc- ϵ -Cbz-lysine in co-delivery of DOX and DAS due to its increased number of drug-interactive motifs and its branched topology. The synthesis route of PLFCL conjugate was depicted in **Figure 47**. This simple nanocarrier was prepared through a three-step route with DCC/DMAP as coupling reagents that are routinely used in peptide synthesis. A short peptide consisting of three lysines was conjugated to the terminal of PEG chain to introduce a branched structure decorated with two Fmoc/Cbz domains. As shown in the ¹H NMR spectrum (**Figure 48A**), the proton signals of PEG backbone were located at 3.3-3.8 ppm with methylene protons at 3.26 ppm. The Fmoc and Cbz proton signals appeared at 7.2-7.8 ppm as multiple peaks and the protons at 1.4–1.8 ppm were attributed to lysine linker. The molecular weight of PLFCL detected by MALDI-TOF MS is close to the theoretical value (6098) (**Figure 49**). Taken together, these data indicate the successful synthesis of PLFCL conjugate.

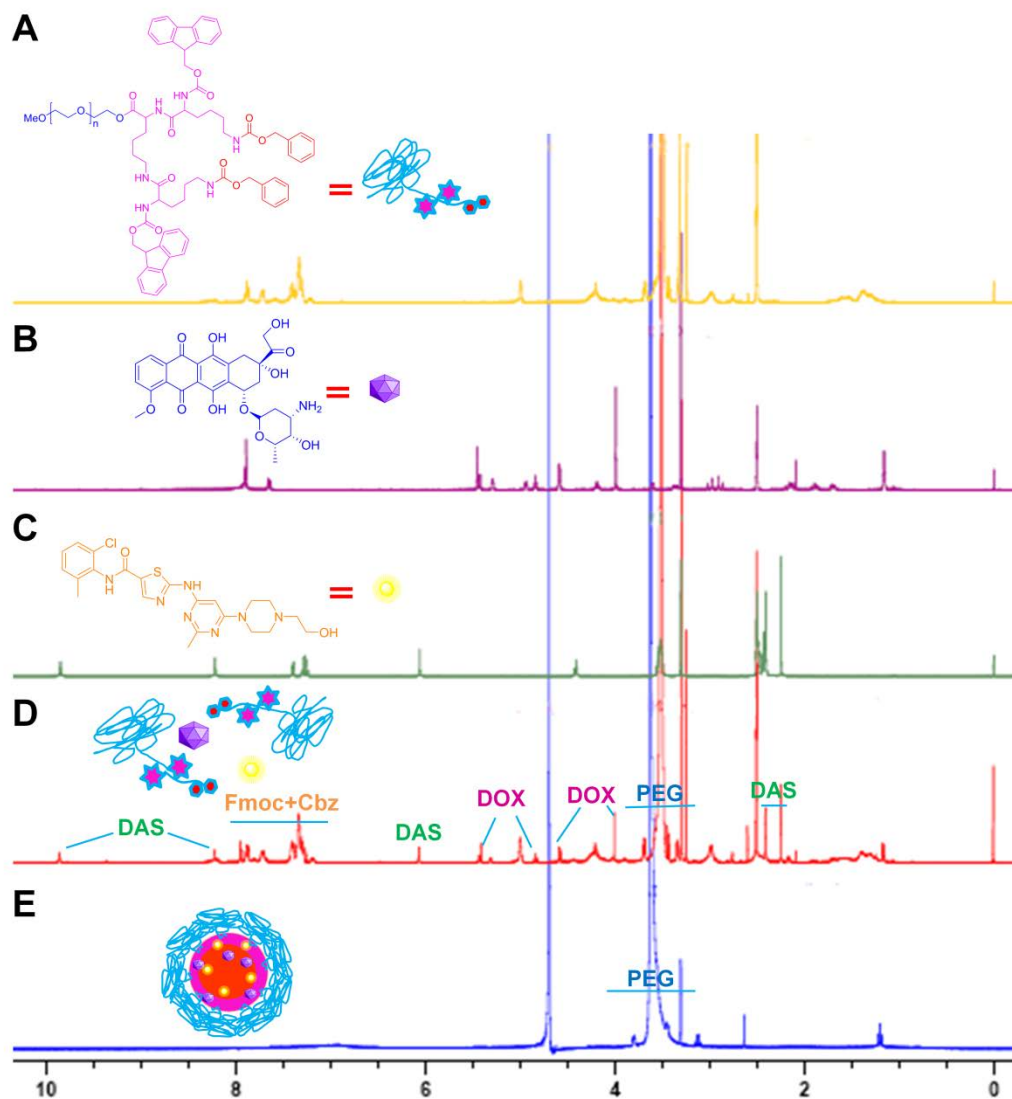


Figure 48. ¹H NMR spectra of PLFCL (A), DOX (B), DAS (C), DOX&DAS/PLFCL (D) in DMSO-*d*₆, and DOX&DAS/PLFCL in D₂O (E). The suppression of proton signals from Fmoc, Cbz, and both drug molecules in D₂O indicated the self-assembly of PLFCL micelles in aqueous medium and encapsulation of drug molecules into inner core of formed micelles.

5.3.3 Fabrication and biophysical characterization of PLFCL micelles for co-encapsulation of DOX&DAS

A simple thin-film hydration method was used in fabrication of PLFCL micelles. Upon exposure to aqueous environment, PLFCL was self-assembled into nano-sized micelles (**Figure 47**). The

measured CMC of PLFCL was 2.6 μM (**Figure 50**). This low CMC would contribute to a high stability of the micelle formulation upon dilution in blood stream after injection. The particle size of PLFCL micelles was ~ 30 nm, as determined by dynamic light scattering (DLS) (**Table 9**). TEM images using negative staining showed the spherical morphology of these self-assembled micelles (**Figure 51**).

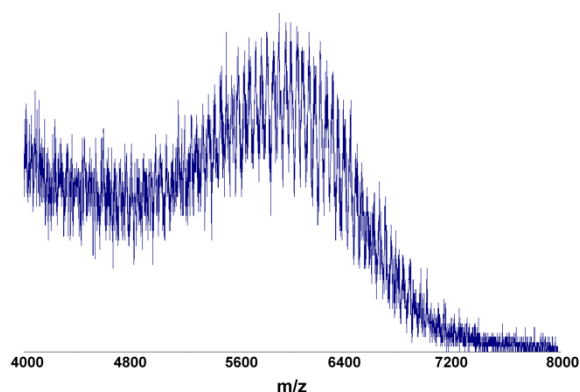


Figure 49. MALDI-TOF mass spectrum of PLFCL.

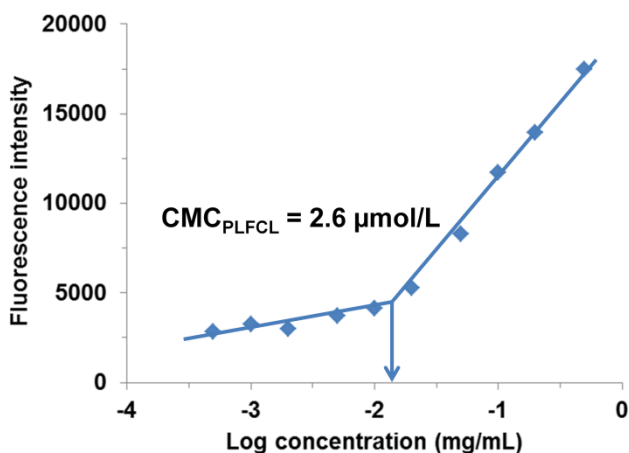


Figure 50. Critical micelle concentration (CMC) measurement of PLFCL using pyrene as a fluorescence probe.

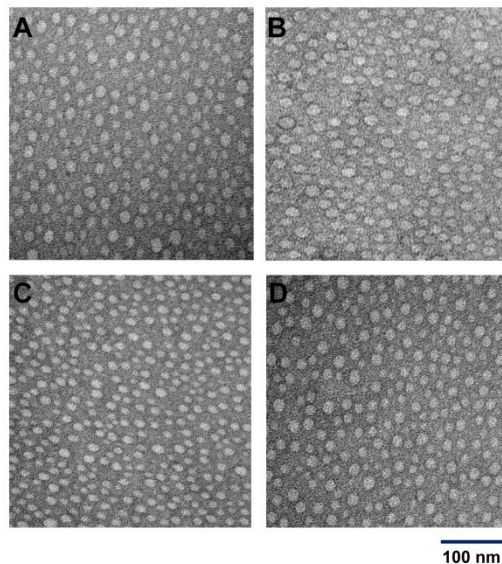


Figure 51. TEM images of drug-free (A), DOX-loaded (B), DAS-loaded (C), and DOX&DAS-loaded (D) PLFCL micelles using negative staining. Scale bar is 100 nm.

As an initial step to examine the potential of PLFCL in co-formulating DOX and DAS, a molar ratio of 1:1 between DOX and DAS was used. This ratio was chosen as DOX and DAS showed comparable cytotoxicity towards 4T1.2 cells and this cell line was used in the subsequent synergistic study both *in vitro* and *in vivo*. **Figure 48** shows the results of ^1H NMR study of drug-loaded PLFCL micelles. Since PLFCL is expected to be dispersed as monomers in organic solvent, the proton signals from PLFCL (**Figure 48A**), DOX (**Figure 48B**), and DAS (**Figure 48C**) were all clearly observed as expected when they were mixed in $\text{DMSO-}d_6$ (**Figure 48D**). However, the signals of Fmoc and Cbz were greatly suppressed in deuterated water (**Figure 48E**), indicating the self-assembly of nanomicelles in aqueous solution and the embedding of Fmoc/Cbz into inner core of formed micelles. Also, significant shielding of DOX and DAS protons was observed (**Figure 48E**). These data strongly suggest that both DOX and DAS were effectively loaded into the inner hydrophobic pocket formed by PLFCL.

5.3.4 Demonstration of carrier-drug intermolecular interaction

The effectiveness of PLFCL in co-encapsulation of DOX and DAS may largely attribute to the strong carrier-drug intermolecular interaction. We hypothesized that, in addition to the hydrophobic interaction, intermolecular π - π stacking may greatly contribute to the overall carrier-drug interaction. In order to verify this hypothesis, we used fluorescence and UV-absorbance studies to demonstrate π - π stacking interaction between carrier and drug molecules. As shown in **Figure 52A**, drug-free PLFCL micelles showed a maximum fluorescence emission at 305 nm at an excitation wavelength of 270 nm. This fluorescence emission is attributed to Fmoc motifs in PLFCL conjugates, which is consistent with previous studies [58, 59]. However, the Fmoc fluorescence was substantially quenched in DOX/PLFCL and DAS/PLFCL micelles, and a further fluorescence quenching was observed when both of the agents were co-loaded. This decreased fluorescence intensity of Fmoc in mixed micelles is due to the strong π - π stacking interaction of Fmoc motifs with payload DOX or/and DAS, both of which bear multiple aromatic ring structures (**Figure 53**). As controls, DOX and DAS alone did not show any fluorescence emission at this range of wavelength.

Figure 52B shows the fluorescence spectrum of DOX. With an excitation at 480 nm, free DOX exhibited fluorescence maxima at 600 nm. Compared with free DOX, a dramatically decreased fluorescence intensity of DOX was observed when it was formulated in PLFCL micelles. In addition, a red shift of DOX fluorescence spectrum was recorded in DOX/PLFCL micelles in comparison to free DOX. These data again indicate the π - π stacking of DOX with Fmoc and Cbz domains in PLFCL micelles. Compared with DOX, which has conjugated

aromatic ring structures, fluorescence emission of DAS was much weaker and partially overlapped with the strong Fmoc signals (data not shown).

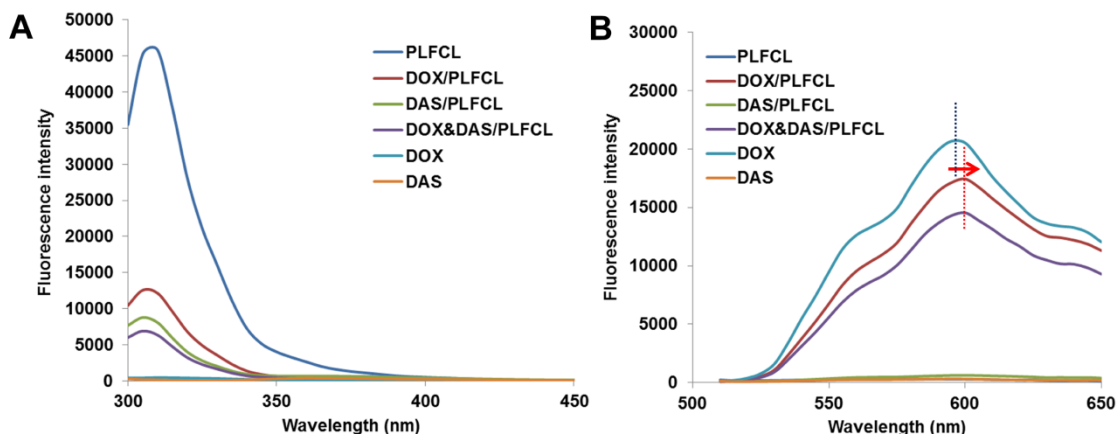


Figure 52. Fluorescence emission of Fmoc at 300-450 nm was recorded with an excitation wavelength at 270 nm (A). Fluorescence of DOX was measured using an excitation wavelength of 480 nm and emission wavelength from 510-650 nm (B). Both Fmoc and DOX showed significant fluorescence quenching in mixed micelles.

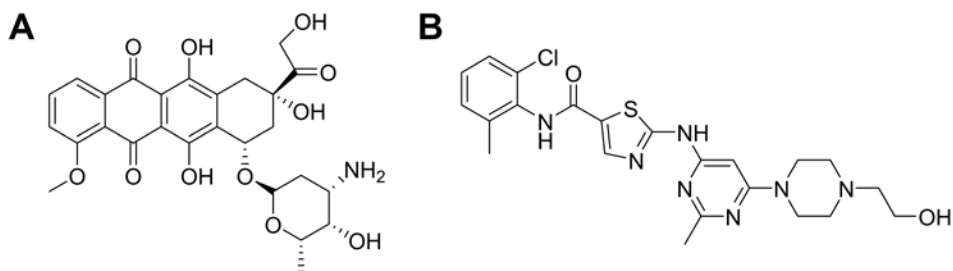


Figure 53. Chemical structures of (A) doxorubicin and (B) dasatinib.

The UV-absorbance spectra of DOX and DAS were also recorded as shown in **Figure 54**. After mixed with PLFCL conjugates, dramatic decrease in UV-absorbance of both DOX and DAS was observed compared with each free drug alone. Similarly, this is likely due to the π - π stacking of aromatic rings in payload drug molecules with Fmoc/Cbz in PLFCL carrier. Taken

together, these evidences strongly supported the carrier-drug intermolecular π - π stacking interaction, which may significantly contribute to the overall carrier-drug interactions.

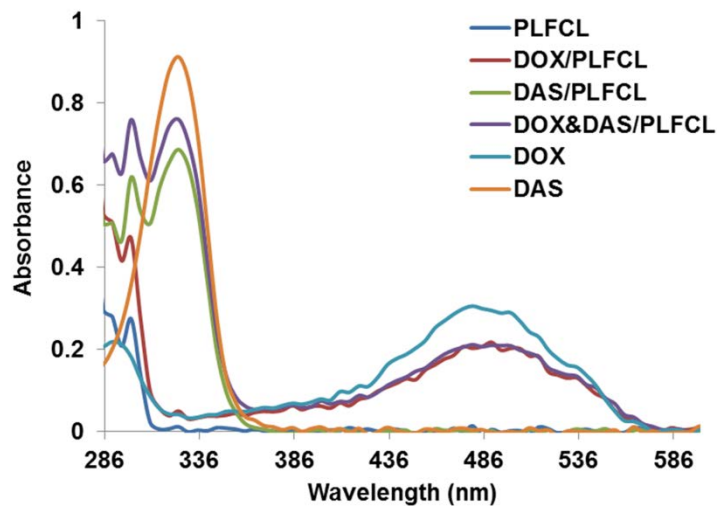


Figure 54. UV-spectrum of DOX and DAS before and after encapsulation into PLFCL micelles.

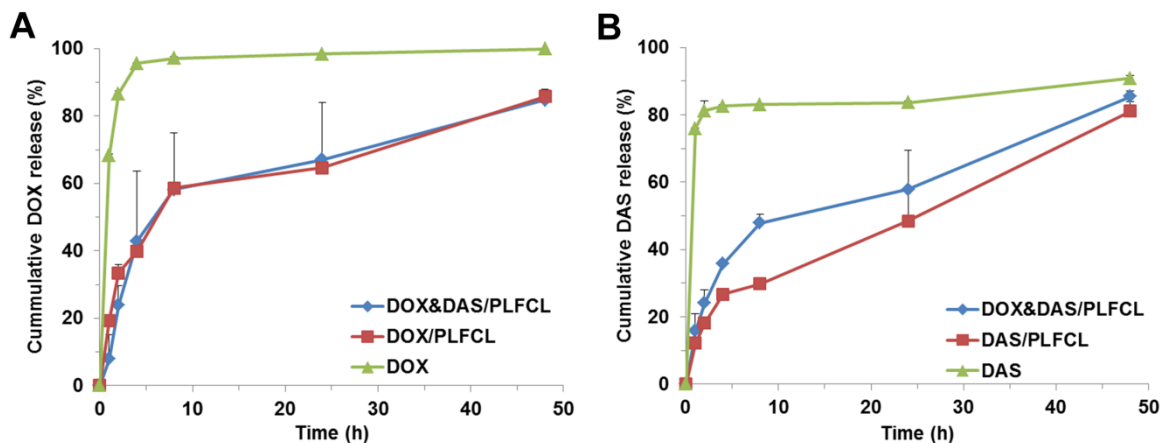


Figure 55. The kinetics of DOX (A) and DAS (B) release from DOX&DAS/PLFCL micelles as examined through a dialysis method. DPBS containing 0.5% (w/v) Tween 80 was used as release medium. Drug concentration was analyzed by HPLC at 0, 1, 2, 4, 8, 24 and 48 h.

5.3.5 Release kinetics of DOX & DAS from PLFCL micelles

Release kinetics of DOX and DAS from DOX&DAS/PLFCL micelles was evaluated through a dialysis method using DPBS (pH 7.4) as releasing medium at 37 °C. DOX or DAS loaded micelles and free drug were used as comparison. As depicted in **Figure 55**, free DOX and DAS showed a burst release with more than 80% of drugs released in the first 2 h. When encapsulated into PLFCL micelles, both agents exhibited significantly sustained release over free drugs. DOX release from DOX&DAS/PLFCL micelles was similar to that from DOX/PLFCL, while DAS release from DOX&DAS/PLFCL was slightly faster compared to the single agent formulation. This sustained drug release is likely due to the strong carrier-drug interaction between DOX/DAS and PLFCL conjugates. Importantly, DOX and DAS showed comparable release kinetics from DOX&DAS/PLFCL micelles. This release profile of DOX&DAS/PLFCL micelles shall favor the simultaneous delivery of these two agents to target site for combinational treatment.

5.3.6 Intracellular trafficking

Intracellular distribution of DOX&DAS/PLFCL micelles was followed by confocal laser scanning microscopy (CLSM) using DOX as a fluorescence probe. 4T1.2 cells were incubated with free DOX, DOX/PLFCL micelles, and DOX&DAS/PLFCL micelles for 0.5, 2, and 4 h, respectively. At 0.5 h, DOX was found to be distributed largely in perinuclear punctate pattern (**Figure 56A**). After 2 h, increasing amounts of signals appeared in nuclei (**Figure 56B&C**). This intracellular distribution suggests a cellular uptake largely through endocytosis, and a partial

release of entrapped DOX from endo/lysosomes to cytoplasm. Of note, compared with DOX delivered by PLFCL micelles, significantly greater amounts of DOX were found in the nuclei of cells treated with DOX&DAS/PLFCL as evidenced by co-localization of DOX and Hoechst (Figure 56B&C), suggesting a DAS-facilitated escape of DOX from endo/lysosomes inside cancer cells.

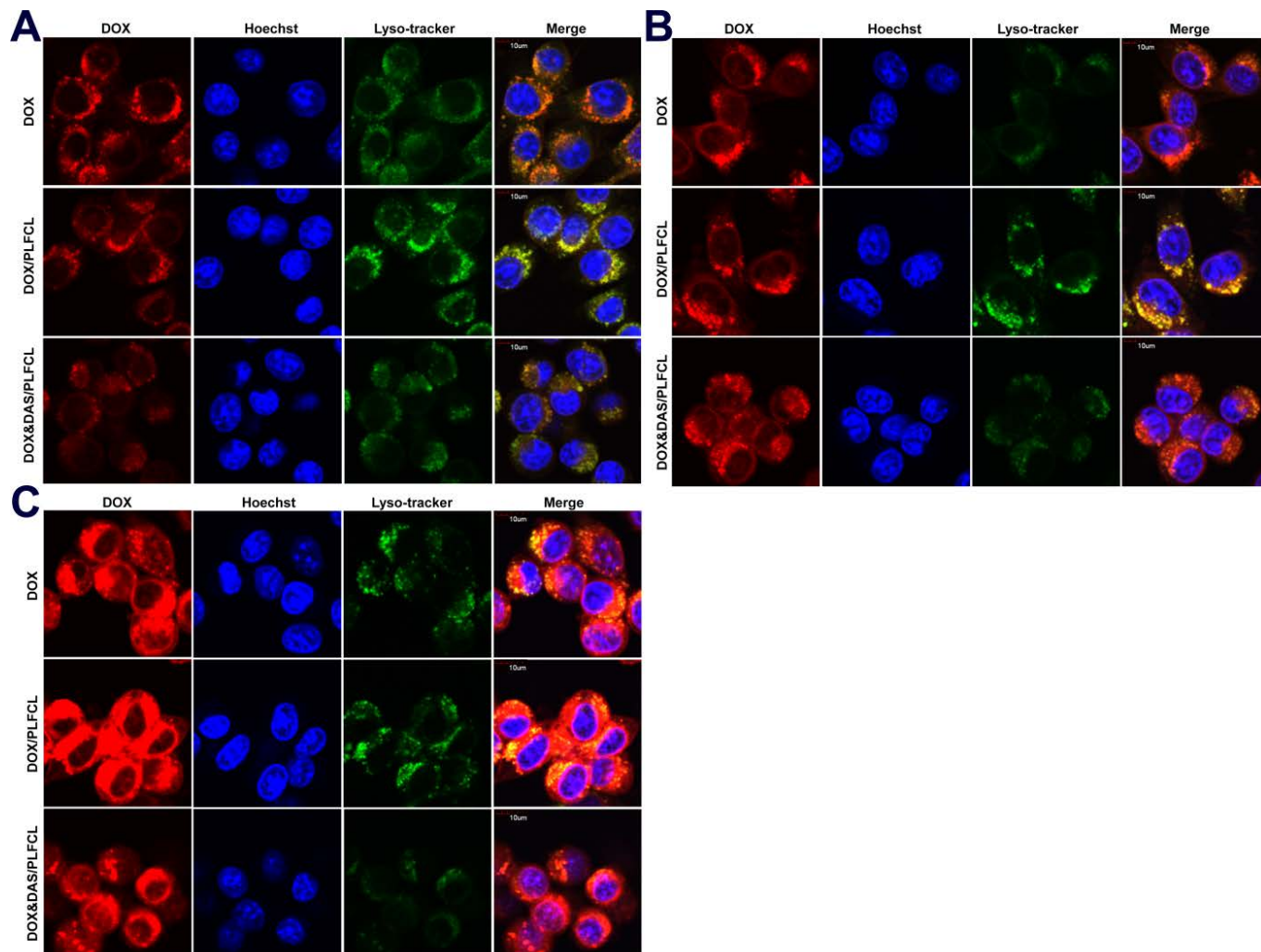


Figure 56. Intracellular trafficking of DOX in 4T1.2 cells. Cells were treated with DOX&DAS/PLFCL, DOX/PLFCL micelles, or free DOX at 10 $\mu\text{mol/L}$ for 0.5 h (A), 2 h (B), and 4 h (C). The nuclei were stained with Hoechst 33342, and endo/lysosomes were stained by LysoTracker DND-26. The intracellular distribution of DOX in various formulations was observed under a confocal laser scanning microscope (CLSM).

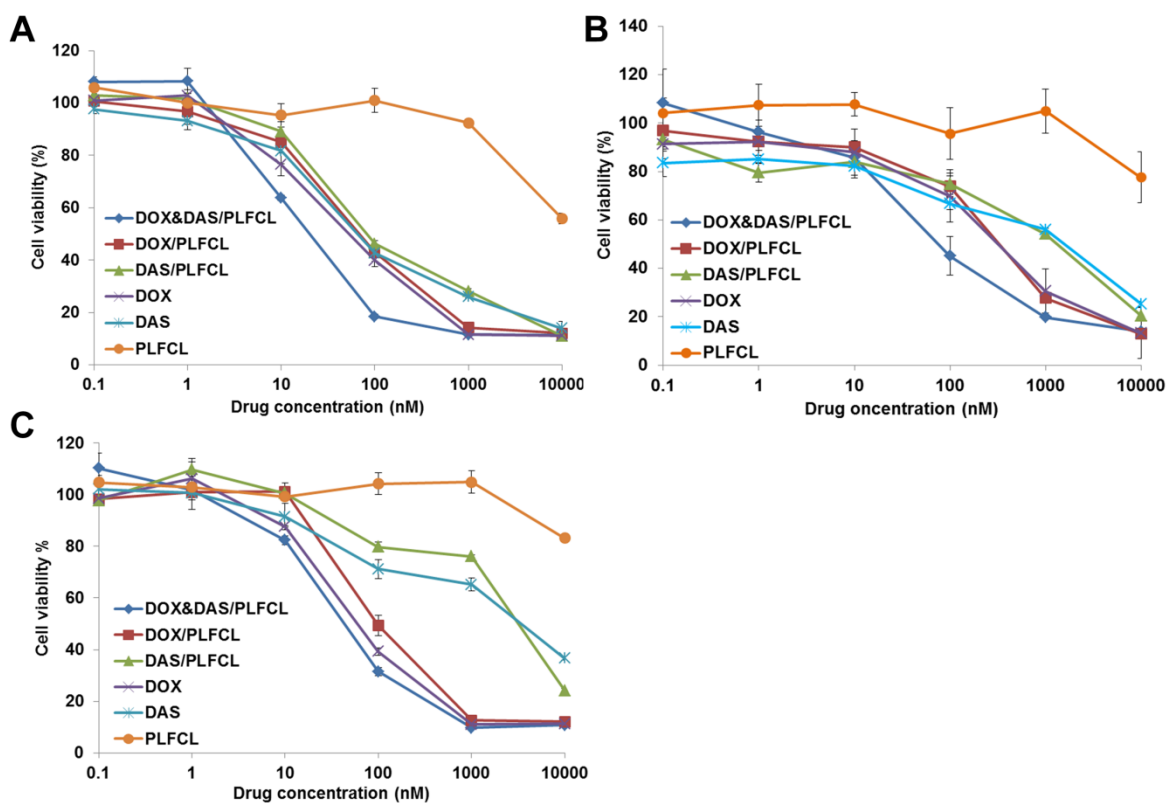


Figure 57. *In vitro* cytotoxicity. 4T1-2 mouse metastatic breast cancer cell line (A), PC 3 androgen-independent human prostate cancer cell line (B), and HCT-116 human colonic carcinoma cell line (C) were treated with different formulations for 72 h, and cancer cell inhibition was determined by MTT assay.

5.3.7 Inhibition of cancer cell proliferation and migration by DOX&DAS/PLFCL micelles

The effect of DOX&DAS/PLFCL micelles on cancer cell growth was tested with several cancer cell lines, including 4T1.2, PC 3, and HCT-116 cells. The cell survival was measured by MTT assay after a treatment of 72 h. As shown in **Figure 57**, drug-free PLFCL micelles did not show significant cytotoxic effect in all the tested cell lines. DOX/PLFCL or DAS/PLFCL showed a level of cytotoxicity that was comparable to that of free drug. In contrast, DOX&DAS/PLFCL exhibited dramatically enhanced inhibition on proliferation of all the tested cancer cells. This improved efficacy of DOX&DAS/PLFCL micelles was likely due to a strong synergy of

DOX&DAS as demonstrated in **Figure 46**. The DAS-facilitated drug release may also contribute to the enhanced combination effect.

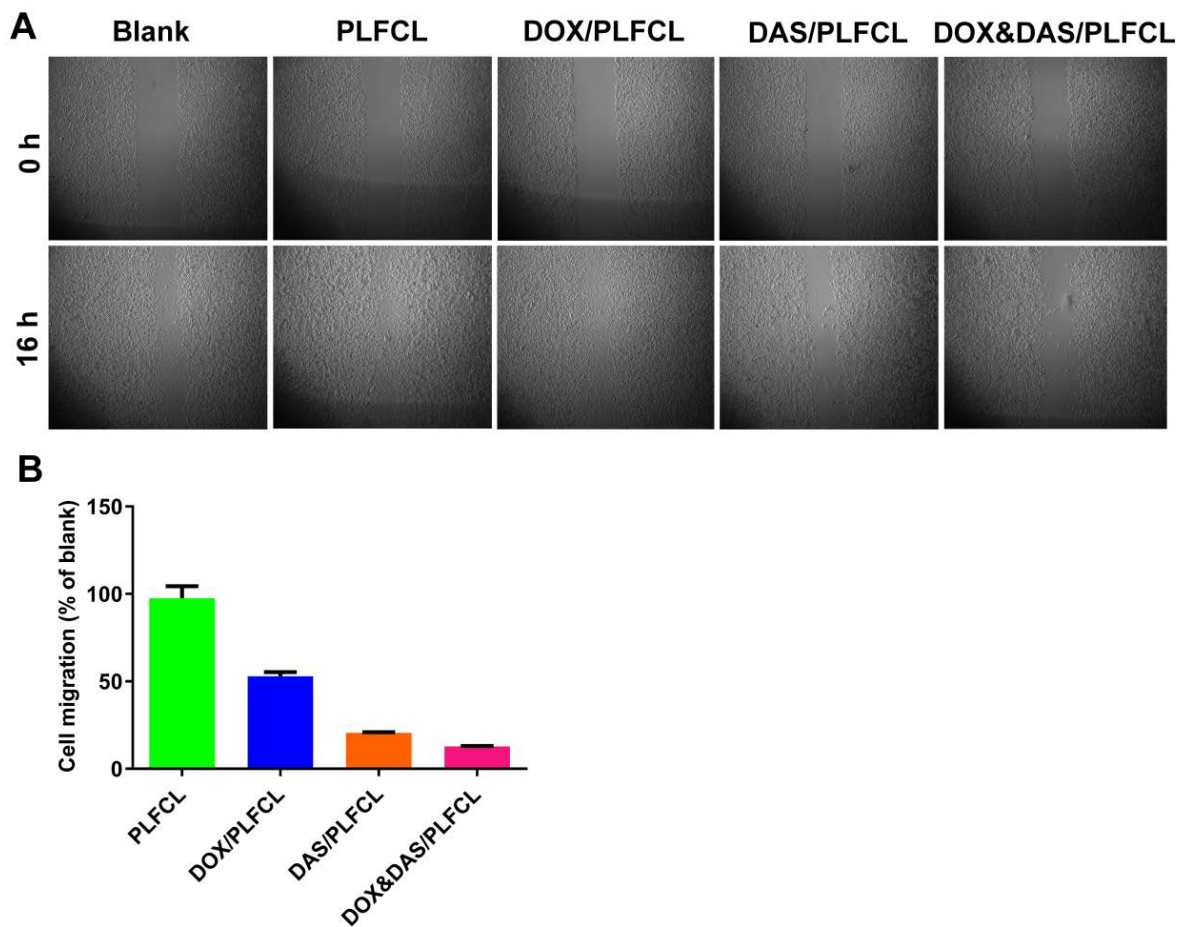


Figure 58. Wound healing assay of 4T1-2 mouse metastatic breast cancer cells 0 and 16 h after treated by drug-free or drug-loaded PLFCL micelles with each drug concentration at 100 nmol/L. Bright field images were obtained under microscope and relative cell migration was quantified using cells without treatment as control.

Following the demonstration of the enhanced inhibitory effect of DOX&DAS/PLFCL on the proliferation of cancer cells, a wound-healing assay was utilized to further evaluate its effect on cancer cell migration. A monolayer of 4T1.2, a highly aggressive cancer cell line, was intendedly streaked to generate a wound in cell culture. The ability of cell repopulation to the denuded area was measured after 16 h. As shown in **Figure 58A**, the wounded area was

substantially repopulated by 4T1.2 cancer cells in the group that either received no treatment or was treated with the carrier alone. DAS was more effective than DOX in inhibiting the migration on cancer cells. Nonetheless, the combination group was most effective in inhibiting the migration of cancer cells; the denuded area was well retained with only 12.9% of repopulated cells (**Figure 58B**). Taken together, DOX&DAS/PLFCL micelles exhibited synergistic effect in inhibition of both proliferation and migration of cultured cancer cells.

5.3.8 *In vivo* therapeutic efficacy and histochemical staining

In vivo therapeutic efficacy of DOX&DAS/PLFCL micelles was evaluated in BALB/c mice bearing 4T1.2 tumor. 4T1.2 is an aggressive cancer cell line with high proliferation rate, and saline-treated mice displayed a rapid increase in tumor size during the experiment (**Figure 59A**). DAS/PLFCL showed a modest anti-cancer activity with a tumor growth inhibition rate at 33% (**Figure 59B**), while a stronger therapeutic response was observed in DOX/PLFCL treated mice. Among all the groups, DOX&DAS/PLFCL exhibited the most potent anti-tumor activity. The tumor growth was almost completely inhibited (**Figure 59B**) with a tumor growth inhibition rate as high as 95% (**Figure 59C**). This high therapeutic efficacy is consistent with the strong synergy between DOX and DAS. The facilitated co-delivery of DOX and DAS by PLFCL also plays an important role as DOX&DAS/PLFCL was much more active than the free drug combination (DOX+DAS) in antitumor activity. All of the micellar formulations were well tolerated. In contrast, a decrease of body weight (**Figure 59D**) was noticed in free drug combo treated mice, which is likely due to the toxicity caused by free DOX and DAS distributed to normal organs.

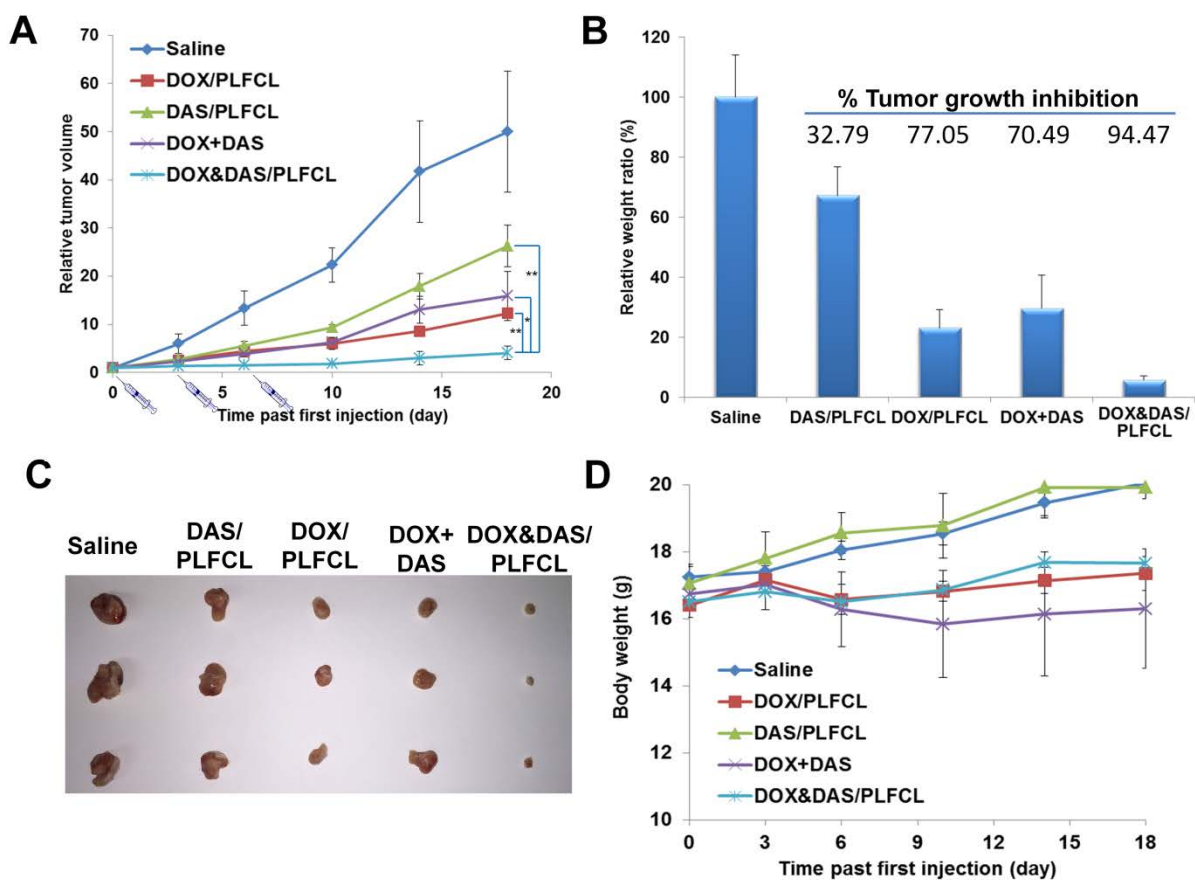


Figure 59. *In vivo* therapeutic efficacy of DOX&DAS/PLFCL micelles. Groups of 5 BALB/c mice bearing 4T1.2 murine breast cancer grafts were injected with DOX&DAS/PLFCL, DOX/PLFCL, DAS/PLFCL micelles (5 mg each agent/kg body weight) and saline on days 0, 3, and 6, respectively. Free DOX+DAS combination dissolved in 50% propylene glycol was used for comparison. Tumor growth was monitored and plotted as relative tumor volume (A). * $P < 0.05$; ** $P < 0.01$ (DOX&DAS/PLFCL micelles vs other treatment). Tumor weights were measured after excision and % tumor growth inhibition was calculated as: $1 - (\text{mean tumor weight of drug treated group} / \text{mean tumor weight of saline treated group}) * 100\%$ (B). Significant difference in tumor size was observed between groups (C), and changes of body weight in mice was also monitored (D).

We further conducted a similar study to follow the survival times of the mice that received different treatments. As shown in **Figure 60**, mice treated with saline had a short survival time of around 15 days. Prolongation in survival times was achieved in mice treated with DAS/PLFCL, DOX+DAS, and DOX/PLFCL with a median survival time of 18, 20, and 27 days, respectively. The longest survival time (36 days) was observed in mice treated with DOX&DAS/PLFCL.

The data on the tumor growth in this survival study were also collected and shown in **Figure 61**. They are consistent with the results shown in **Figure 59**, further confirming the improved therapeutic efficacy of DOX&DAS/PLFCL micelles over other formulations.

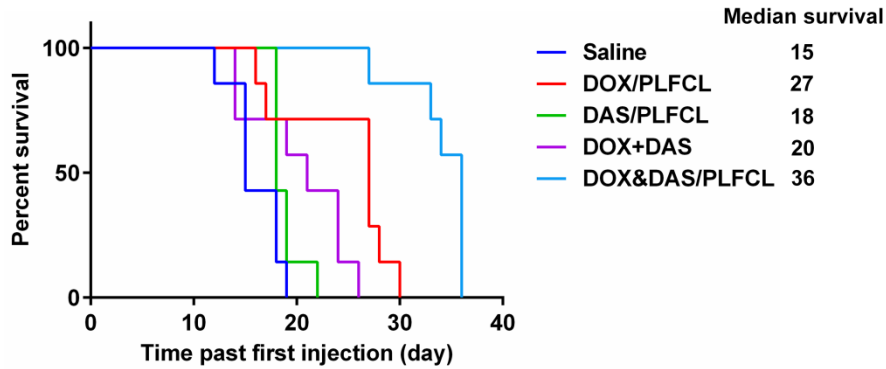


Figure 60. Kaplan-Meier survival curves for BALB/c mice (n=7) bearing 4T1.2 murine breast cancer grafts. Mice were treated with DOX&DAS/PLFCL, DOX/PLFCL, DAS/PLFCL micelles, free DOX+DAS combination (5 mg each agent/kg body weight), and saline on days 0, 3, and 6, respectively.

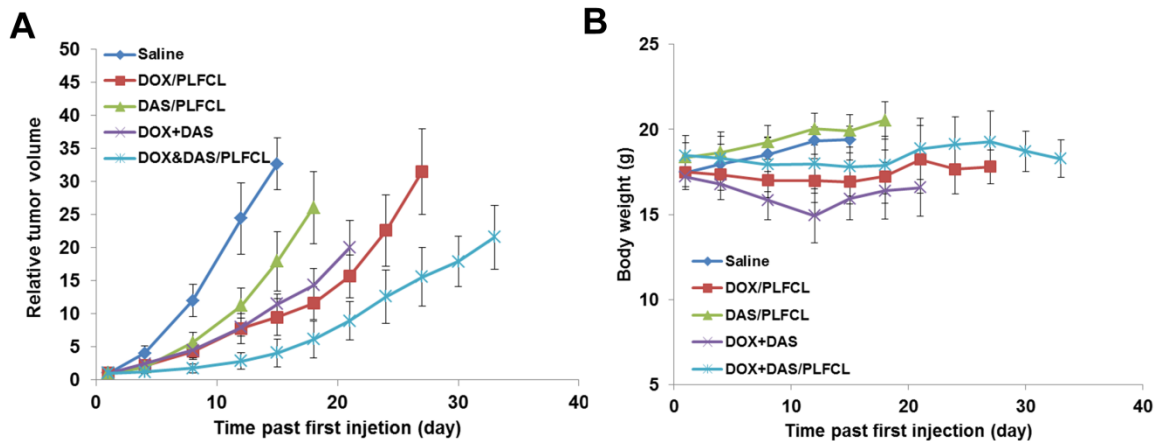


Figure 61. *In vivo* therapeutic efficacy of DOX&DAS/PLFCL micelles with long follow-up time. Groups of 7 BALB/c mice bearing 4T1.2 murine breast cancer grafts were injected with DOX&DAS/PLFCL, DOX/PLFCL, DAS/PLFCL micelles (5 mg each agent/kg body weight) and saline on days 0, 3, and 6, respectively. Free DOX+DAS combination dissolved in 50% propylene glycol was used for comparison. Tumor growth was monitored and plotted as relative tumor volume (A). Changes of body weight in mice was also monitored (B).

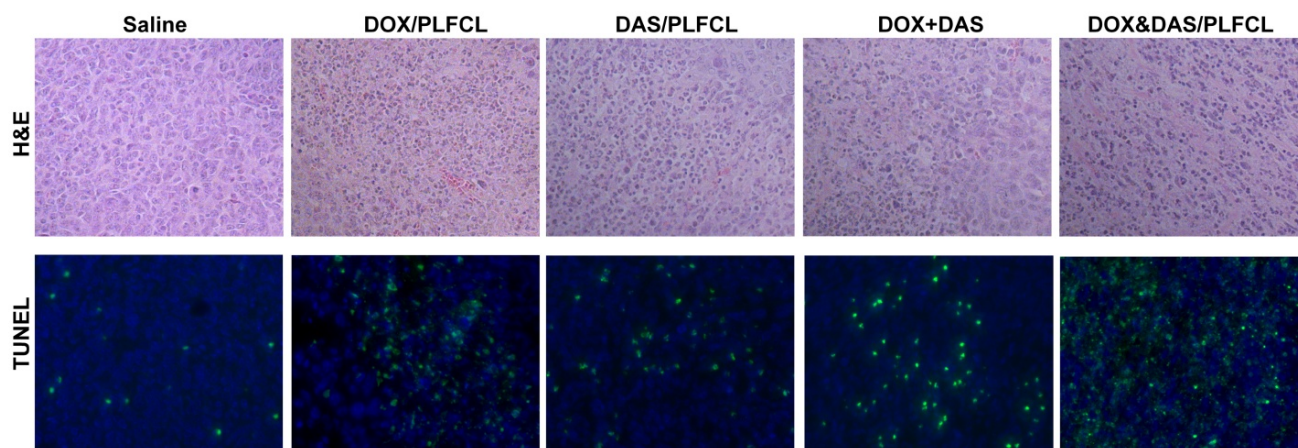


Figure 62. Histological analyses of tumor tissues using H&E staining and TUNEL assay.

Histological analysis was conducted to further evaluate the therapeutic efficacy of DOX&DAS/PLFCL micelles. Slices of fixed tumor tissues were stained with hematoxylin and eosin (H&E). As indicated in **Figure 62**, saline-treated tumors showed typical appearance of cancer cells with large nuclei due to high proliferation rate. In contrast, tumors that received other treatments showed altered morphology with shrunk nuclei and decreased tumor cell density. These changes in cell morphology suggested inhibition in proliferation of these treated cancer cells at tumor tissue. In addition, apoptotic cells were detected in tumor tissues by TUNEL assay (**Figure 62**). Among all the treatments, DOX&DAS/PLFCL micelles showed the most potent efficacy.

5.4 DISCUSSION

Combination chemotherapy represents one of the effective strategies in clinical cancer treatment. Simultaneous administration of multiple chemotherapeutics targeting to different signaling

pathways in cancer cells shall markedly maximize the anti-cancer activity whereas reducing the occurrence of MDR [116-119]. As a potent anti-cancer agent, DOX has been used in a variety of multi-drug regimens with other chemotherapeutics. Among them, DOX/DAS combination represents a unique regimen for targeted cancer therapy as DAS specifically acts on molecular targets that are overexpressed in various types of cancers. The effectiveness of this drug combo was firstly demonstrated by Pichot et al in breast cancer cells [126]. Our data further showed the synergistic action of DOX/DAS in several cancer cell lines (**Figure 46**). One unique aspect of codelivery of DAS with other chemotherapeutics via a nanocarrier is the DAS-facilitated drug release from endosomes following endocytosis (**Figure 56**). DAS bears two tertiary amines that can be protonated in acidic environment (**Figure 53**); therefore, it may act as “proton sponge” to induce rupture of endo/lysosomes to facilitate the escape of entrapped drugs to cytoplasm [136, 137]. The facilitated drug release from endosomes is likely to contribute to the overall antitumor effect both *in vitro* and *in vivo*.

Various carrier systems have been employed for co-delivery of DOX with other anti-cancer agents such as liposomes, double emulsions, and triblock copolymers [138-142]. The uniqueness of our PLFCL nanocarrier lies in its simplicity in both synthesis and fabrication. PLFCL can be readily synthesized through a simple three-step synthetic route, and self-assembled into nanomicelles with small particle size (~ 30 nm) via a simple thin film hydration method. These properties may greatly facilitate its scale-up production and rapid translation to clinical application. In addition to simplicity, our nanocarrier demonstrated high effectiveness in formulating anti-cancer agents with diverse physiochemical properties including DOX, DAS, paclitaxel, docetaxel, imatinib, gefitinib, etoposide, and curcumin (**Tables 9 & 10**). This is due to the effective carrier-drug interactions that are facilitated by π - π stacking, hydrogen bonding as

well as hydrophobic interaction (**Figure 52&54**). Although the application of PLFCL nanomicelles in codelivery of two drugs was demonstrated with DOX/DAS combo as a model system, its broad utility suggests it could serve as a platform that can be readily applied to other targeted combination therapies.

Table 10. Broad utility of PLFCL as a nanocarrer for a panel of chemotherapeutic agents.

| Drug candidate | Molecular target | Carrier/drug molar ratio | Drug content (w/w, %) | Particle size (nm) | ^a PDI | ^b Stability (h) |
|----------------|------------------|--------------------------|-----------------------|--------------------|------------------|----------------------------|
| Paclitaxel | tubulin | 0.25:1 | 35.90 | 24.9±0.4 | 0.332 | 16 |
| | | 1:1 | 12.28 | 28.8±0.3 | 0.421 | 90 |
| Docetaxel | tubulin | 0.25:1 | 34.64 | 44.4±0.6 | 0.523 | 24 |
| | | 1:1 | 11.70 | 37.5±0.8 | 0.498 | 72 |
| Imatinib | tyrosine kinase | 0.25:1 | 24.47 | 37.8±0.8 | 0.544 | 18 |
| | | 1:1 | 7.49 | 38.2±0.7 | 0.552 | 96 |
| Gefitinib | EGFR | 0.25:1 | 22.67 | 29.1±3.9 | 0.391 | 1 |
| | | 1:1 | 6.83 | 29.6±1.9 | 0.430 | 16 |
| Curcumin | NF-κB, Akt, etc. | 0.25:1 | 19.45 | 44.2±0.3 | 0.497 | 22 |
| | | 1:1 | 5.69 | 33.5±5.2 | 0.520 | 96 |
| Etoposide | topoisomerase II | 0.25:1 | 27.87 | 28.2±0.7 | 0.413 | 16 |
| | | 1:1 | 8.81 | 24.3±0.4 | 0.374 | 96 |

Drug concentrations were kept at 1 mg/mL in saline. ^aPDI, polydispersity index. ^bStability indicates no noticeable drug precipitation or significant size change during the follow up time period.

Synergistic action of DOX&DAS/PLFCL micelles was systemically assessed in cultured cancer cells and in a tumor-bearing animal model. Our data demonstrated an enhancement of DOX&DAS/PLFCL micelles in inhibition of proliferation and migration of cultured cancer cells over other treatments. *In vivo*, both DOX/PLFCL and DAS/PLFCL showed significant therapeutic effect against 4T1.2, a highly aggressive breast cancer model. This is likely due to the effective delivery of DOX or DAS to tumor by PLFCL via EPR effect. More importantly,

DOX&DAS/PLFCL micelles demonstrated further improvement in anti-tumor activity with regard to both tumor growth inhibition and animal survival.

In summary, a PEG-peptidic conjugate incorporated with Fmoc/Cbz domains was developed for effective co-delivery of DOX&DAS, two chemotherapeutic agents exhibiting potent synergistic anticancer activity. This PLFCL nanocarrier can be readily synthesized through a three-step route. DOX and DAS were efficiently co-loaded into PLFCL micelles with a small particle size. DOX&DAS/PLFCL nanomicelles demonstrated strong synergistic anti-cancer activity both in vitro and in vivo. Our nanocarrier may represent a simple and effective co-delivery system for improved combination chemotherapy.

6.0 SUMMARY AND PERSPECTIVES

Chemotherapy is one of the most effective strategies in the treatment of cancer, a leading cause of death over the world. During the past decades, enormous efforts have been put into the discovery and development of chemotherapeutic agents with improved therapeutic response in cancer patients. Some of the drug candidates, although, indeed demonstrated potent anti-cancer activity in the early stage of evaluation, few of them ultimately advanced to clinical application due to the ineffectiveness *in vivo*, or, oftentimes, severe systemic toxicity. These issues are largely attributed to the inefficient *in vivo* delivery of the cytotoxic agents to tumor site and unexpected toxicity to normal organs.

To address these issues in cancer chemotherapy, extensive investigations have been undertaken to achieve the tumor-specific distribution of chemotherapeutics. As an effective strategy without imposing changes on the original structure of anti-cancer agents, nanomedicine has drawn increasing attention since the middle of last century. Among a variety of nano-formulations, micellar system is unique and attractive due to its ease in manipulation, effectiveness in solubilizing poorly water-soluble agents, and small particle size that can take advantage of the EPR effect for tumor-specific delivery. For most of the micellar formulations, drug encapsulation is solely based on carrier-drug hydrophobic interactions. Although it is effective in formulating agents with high hydrophobicity, it oftentimes causes low compatibility of nanocarrier with a variety of drugs with moderate hydrophobicity. The insufficient carrier-

drug interaction is largely responsible for low drug loading capacity and poor colloid stability, two major issues in clinical application of micellar system.

During my graduate study, I worked on several cohesive projects with the aim to gain more insight into the molecular basis of carrier-drug interactions, and develop effective strategies to improve the compatibility of nanocarriers with payload therapeutics for more efficient *in vivo* delivery. My Ph.D. thesis work was specifically focused on the rational design of nanomicelles with improved carrier-drug interactions for enhanced cancer chemotherapy.

Firstly, we demonstrated that introduction of additional mechanisms of carrier-drug interaction is an effective strategy to improve drug loading and colloid stability of micellar system. Fmoc motifs were incorporated interfacially into micelle-forming PEG-lipids to provide extra modes of carrier-drug interactions, including π - π stacking and hydrogen bonding interactions. The resulting lipidic vector, PEG₅₀₀₀-(Fmoc-OA)₂, showed dramatically enhanced effectiveness in formulating paclitaxel (PTX) and several other hydrophobic drugs with diverse structures.

To clearly define the molecular basis of Fmoc/drug interaction for our system, a new model was established by using a simple PEG-Fmoc conjugate without lipid chains. Interestingly, this new nanomaterial without lipid core demonstrated a dramatic improvement in PTX encapsulation (36%, w/w), which stands well among all the micellar formulations of PTX. Fluorescence and ¹³C NMR spectra indicated a strong Fmoc/PTX intermolecular π - π stacking, which may play a major role in the overall carrier-drug interaction. We have further shown that this simple system is highly effective in delivery of PTX to tumor cells *in vitro* and *in vivo*.

Inspired by this discovery, we further conducted a SAR study with a library of nanomaterials to gain more insight into the impact of Fmoc neighboring group on the overall carrier-drug

interactions. Our data suggested that the biophysical properties and drug encapsulation of our micelles were significantly impacted by a number of factors, including the structures of the drug-interactive motifs and the steric hindrance. This SAR study led to the discovery of Cbz as a favored neighboring group of Fmoc for effective interaction with a broad range of drugs.

Based on the SAR study, we developed a nanocarrier with expanded interior volume and increased number of drug-interactive motifs for effective co-delivery of multiple agents for combination chemotherapy. Doxorubicin and dasatinib, two anti-cancer agents that showed significant synergy in inhibition of cancer cell proliferation, were efficiently co-encapsulated into this nanocarrier. Synergistic efficacy was systemically evaluated in both cultured cancer cells and tumor-bearing animal models. A dramatically enhanced tumor growth inhibition was achieved over single agent therapy.

In summary, our study demonstrated the drug loading and formulation stability of micellar system can be markedly improved through the incorporation of additional mechanisms of carrier-drug interaction. Our study shed some insights into the rational design of nanocarriers with improved compatibility with payload therapeutics, and this has led to the development of a series of simple nanocarriers that are effective in formulating single or multiple chemotherapeutic agents for improved therapeutic outcomes.

More studies are needed in the future to further improve micellar delivery system. One potential direction would be tailor-designed nanocarrier for a given drug molecule or drug combination. Instead of aiming to construct a nanocarrier that works “universally” for a wide range of payload agents, nanocarriers could be specifically designed for an agent of interest based on its unique physiochemical property. Besides that, simplicity could be another focus in the design of nanocarriers. Various new concepts of design have emerged for further

development of micellar system. Although these approaches are novel and could potentially further improve the performance of micellar system, they have an issue of overly sophisticated and complex. The complexity in structure of nanocarriers will not only cause concerns in stability and toxicity but also impose difficulties in scaled-up manufacture and quality controls in industry. The simplicity of newly developed nanocarriers can never be overemphasized for a rapid translation from bench to bedside.

BIBLIOGRAPHY

- [1] Anand P, Kunnumakkara AB, Sundaram C, Harikumar KB, Tharakan ST, Lai OS, et al. Cancer is a preventable disease that requires major lifestyle changes. *Pharmaceutical research*. 2008;25:2097-116.
- [2] Perera FP. Environment and cancer: who are susceptible? *Science*. 1997;278:1068-73.
- [3] Hanahan D, Weinberg RA. The hallmarks of cancer. *Cell*. 2000;100:57-70.
- [4] Malhotra V, Perry MC. Classical chemotherapy: mechanisms, toxicities and the therapeutic window. *Cancer biology & therapy*. 2003;2:S2-4.
- [5] Makin G, Hickman JA. Apoptosis and cancer chemotherapy. *Cell and tissue research*. 2000;301:143-52.
- [6] Rawat M, Singh D, Saraf S, Saraf S. Nanocarriers: promising vehicle for bioactive drugs. *Biological & pharmaceutical bulletin*. 2006;29:1790-8.
- [7] Lipinski CA, Lombardo F, Dominy BW, Feeney PJ. Experimental and computational approaches to estimate solubility and permeability in drug discovery and development settings. *Advanced drug delivery reviews*. 2001;46:3-26.
- [8] Gibson RJ, Keefe DM. Cancer chemotherapy-induced diarrhoea and constipation: mechanisms of damage and prevention strategies. *Supportive care in cancer*. 2006;14:890-900.
- [9] Groopman JE, Itri LM. Chemotherapy-induced anemia in adults: incidence and treatment. *Journal of the National Cancer Institute*. 1999;91:1616-34.
- [10] Wagner V, Dullaart A, Bock AK, Zweck A. The emerging nanomedicine landscape. *Nature biotechnology*. 2006;24:1211-7.
- [11] Ferrari M. Cancer nanotechnology: opportunities and challenges. *Nature reviews Cancer*. 2005;5:161-71.
- [12] Jain RK, Stylianopoulos T. Delivering nanomedicine to solid tumors. *Nature reviews Clinical oncology*. 2010;7:653-64.

- [13] Farokhzad OC, Langer R. Impact of nanotechnology on drug delivery. *ACS nano*. 2009;3:16-20.
- [14] Zhang L, Gu FX, Chan JM, Wang AZ, Langer RS, Farokhzad OC. Nanoparticles in medicine: therapeutic applications and developments. *Clinical pharmacology and therapeutics*. 2008;83:761-9.
- [15] Maeda H. The enhanced permeability and retention (EPR) effect in tumor vasculature: the key role of tumor-selective macromolecular drug targeting. *Advances in enzyme regulation*. 2001;41:189-207.
- [16] Maeda H, Wu J, Sawa T, Matsumura Y, Hori K. Tumor vascular permeability and the EPR effect in macromolecular therapeutics: a review. *Journal of controlled release*. 2000;65:271-84.
- [17] Lammers T, Kiessling F, Hennink WE, Storm G. Drug targeting to tumors: principles, pitfalls and (pre-) clinical progress. *Journal of controlled release*. 2012;161:175-87.
- [18] Bae YH, Park K. Targeted drug delivery to tumors: myths, reality and possibility. *Journal of controlled release*. 2011;153:198-205.
- [19] Bertrand N, Wu J, Xu X, Kamaly N, Farokhzad OC. Cancer nanotechnology: The impact of passive and active targeting in the era of modern cancer biology. *Advanced drug delivery reviews*. 2013.
- [20] Kedar U, Phutane P, Shidhaye S, Kadam V. Advances in polymeric micelles for drug delivery and tumor targeting. *Nanomedicine: nanotechnology, biology, and medicine*. 2010;6:714-29.
- [21] Torchilin VP. Structure and design of polymeric surfactant-based drug delivery systems. *Journal of controlled release*. 2001;73:137-72.
- [22] Kataoka K, Harada A, Nagasaki Y. Block copolymer micelles for drug delivery: design, characterization and biological significance. *Advanced drug delivery reviews*. 2012;64:37-48.
- [23] Knop K, Hoogenboom R, Fischer D, Schubert US. Poly(ethylene glycol) in drug delivery: pros and cons as well as potential alternatives. *Angewandte chemie*. 2010;49:6288-308.
- [24] Pasut G, Veronese FM. State of the art in PEGylation: the great versatility achieved after forty years of research. *Journal of controlled release*. 2012;161:461-72.
- [25] Greenwald RB. PEG drugs: an overview. *Journal of controlled release*. 2001;74:159-71.
- [26] Torchilin VP, Lukyanov AN. Peptide and protein drug delivery to and into tumors: challenges and solutions. *Drug discovery today*. 2003;8:259-66.

- [27] Nagasaki Y, Okada T, Scholz C, Iijima M, Kato M, Kataoka K. The reactive polymeric micelle based on an aldehyde-ended poly(ethylene glycol)/poly(lactide) block copolymer. *Macromolecules*. 1998;31:1473-9.
- [28] Jeong B, Bae YH, Kim SW. Biodegradable thermosensitive micelles of PEG-PLGA-PEG triblock copolymers. *Colloid Surface B*. 1999;16:185-93.
- [29] Deng JZ, Gao NN, Wang YA, Yi HQ, Fang ST, Ma YF, et al. Self-assembled cationic micelles based on PEG-PLL-PLLeu hybrid polypeptides as highly effective gene vectors. *Biomacromolecules*. 2012;13:3795-804.
- [30] Ashjari M, Khoee S, Mahdavian AR, Rahmatolahzadeh R. Self-assembled nanomicelles using PLGA-PEG amphiphilic block copolymer for insulin delivery: a physicochemical investigation and determination of CMC values. *Journal of materials science: Materials in medicine*. 2012;23:943-53.
- [31] Trubetskoy VS, Torchilin VP. Use of polyoxyethylene-lipid conjugates as long-circulating carriers for delivery of therapeutic and diagnostic agents. *Advanced drug delivery reviews*. 1995;16:311-20.
- [32] Lukyanov AN, Torchilin VP. Micelles from lipid derivatives of water-soluble polymers as delivery systems for poorly soluble drugs. *Advanced drug delivery reviews*. 2004;56:1273-89.
- [33] Lukyanov AN, Gao Z, Mazzola L, Torchilin VP. Polyethylene glycol-diacyllipid micelles demonstrate increased accumulation in subcutaneous tumors in mice. *Pharmaceutical research*. 2002;19:1424-9.
- [34] Gao ZG, Lukyanov AN, Singhal A, Torchilin VP. Diacyllipid-polymer micelles as nanocarriers for poorly soluble anticancer drugs. *Nano letters*. 2002;2:979-82.
- [35] Musacchio T, Laquintana V, Latrofa A, Trapani G, Torchilin VP. PEG-PE micelles loaded with paclitaxel and surface-modified by a PBR-ligand: synergistic anticancer effect. *Molecular pharmaceutics*. 2009;6:468-79.
- [36] Dabholkar RD, Sawant RM, Mongayt DA, Devarajan PV, Torchilin VP. Polyethylene glycol-phosphatidylethanolamine conjugate (PEG-PE)-based mixed micelles: some properties, loading with paclitaxel, and modulation of P-glycoprotein-mediated efflux. *International journal of pharmaceutics*. 2006;315:148-57.
- [37] Mu L, Elbayoumi TA, Torchilin VP. Mixed micelles made of poly(ethylene glycol)-phosphatidylethanolamine conjugate and d-alpha-tocopheryl polyethylene glycol 1000 succinate as pharmaceutical nanocarriers for camptothecin. *International journal of pharmaceutics*. 2005;306:142-9.

- [38] Luo J, Xiao K, Li Y, Lee JS, Shi L, Tan YH, et al. Well-defined, size-tunable, multifunctional micelles for efficient paclitaxel delivery for cancer treatment. *Bioconjugate chemistry*. 2010;21:1216-24.
- [39] Zhu XX, Nichifor M. Polymeric materials containing bile acids. *Accounts of chemical research*. 2002;35:539-46.
- [40] Janout V, Regen SL. Bioconjugate-based molecular umbrellas. *Bioconjugate chemistry*. 2009;20:183-92.
- [41] Zhao Y. Facial amphiphiles in molecular recognition: From unusual aggregates to solvophobic driven foldamers. *Current opinion in colloid & interface science*. 2007;12:92-7.
- [42] Li Y, Xiao K, Luo J, Xiao W, Lee JS, Gonik AM, et al. Well-defined, reversible disulfide cross-linked micelles for on-demand paclitaxel delivery. *Biomaterials*. 2011;32:6633-45.
- [43] Li Y, Xiao K, Luo J, Lee J, Pan S, Lam KS. A novel size-tunable nanocarrier system for targeted anticancer drug delivery. *Journal of controlled release*. 2010;144:314-23.
- [44] Li Y, Xiao W, Xiao K, Berti L, Luo J, Tseng HP, et al. Well-defined, reversible boronate crosslinked nanocarriers for targeted drug delivery in response to acidic pH values and cis-diols. *Angewandte chemie*. 2012;51:2864-9.
- [45] Xiao K, Li Y, Lee JS, Gonik AM, Dong T, Fung G, et al. "OA02" peptide facilitates the precise targeting of paclitaxel-loaded micellar nanoparticles to ovarian cancer in vivo. *Cancer research*. 2012;72:2100-10.
- [46] Xiao K, Li Y, Luo J, Lee JS, Xiao W, Gonik AM, et al. The effect of surface charge on in vivo biodistribution of PEG-oligocholic acid based micellar nanoparticles. *Biomaterials*. 2011;32:3435-46.
- [47] Xiao K, Luo J, Li Y, Lee JS, Fung G, Lam KS. PEG-oligocholic acid telodendrimer micelles for the targeted delivery of doxorubicin to B-cell lymphoma. *Journal of controlled release*. 2011;155:272-81.
- [48] Kim JY, Kim S, Pinal R, Park K. Hydrotropic polymer micelles as versatile vehicles for delivery of poorly water-soluble drugs. *Journal of controlled release*. 2011;152:13-20.
- [49] Lee J, Lee SC, Acharya G, Chang CJ, Park K. Hydrotropic solubilization of paclitaxel: analysis of chemical structures for hydrotropic property. *Pharmaceutical research*. 2003;20:1022-30.
- [50] Yoon HY, Saravanakumar G, Heo R, Choi SH, Song IC, Han MH, et al. Hydrotropic magnetic micelles for combined magnetic resonance imaging and cancer therapy. *Journal of controlled release*. 2012;160:692-8.

- [51] Kim JY, Kim S, Papp M, Park K, Pinal R. Hydrotropic solubilization of poorly water-soluble drugs. *Journal of pharmaceutical sciences*. 2010;99:3953-65.
- [52] Lee SC, Huh KM, Lee J, Cho YW, Galinsky RE, Park K. Hydrotropic polymeric micelles for enhanced paclitaxel solubility: In vitro and in vivo characterization. *Biomacromolecules*. 2007;8:202-8.
- [53] Yoo HS, Park TG. Folate-receptor-targeted delivery of doxorubicin nano-aggregates stabilized by doxorubicin-PEG-folate conjugate. *Journal of controlled release*. 2004;100:247-56.
- [54] Yoo HS, Park TG. Folate receptor targeted biodegradable polymeric doxorubicin micelles. *Journal of controlled release*. 2004;96:273-83.
- [55] Gao X, Huang Y, Makhov AM, Epperly M, Lu J, Grab S, et al. Nanoassembly of surfactants with interfacial drug-interactive motifs as tailor-designed drug carriers. *Molecular pharmaceutics*. 2013;10:187-98.
- [56] Jiang J, Belikova NA, Hoyer AT, Zhao Q, Epperly MW, Greenberger JS, et al. A mitochondria-targeted nitroxide/hemigramicidin S conjugate protects mouse embryonic cells against gamma irradiation. *International journal of radiation oncology, biology, physics*. 2008;70:816-25.
- [57] Rajagopalan MS, Gupta K, Epperly MW, Franicola D, Zhang X, Wang H, et al. The mitochondria-targeted nitroxide JP4-039 augments potentially lethal irradiation damage repair. *In vivo*. 2009;23:717-26.
- [58] Zhang P, Lu J, Huang Y, Zhao W, Zhang Y, Zhang X, et al. Design and evaluation of a PEGylated lipopeptide equipped with drug-interactive motifs as an improved drug carrier. *The AAPS journal*. 2014;16:114-24.
- [59] Zhang P, Huang Y, Liu H, Marquez RT, Lu J, Zhao W, et al. A PEG-Fmoc conjugate as a nanocarrier for paclitaxel. *Biomaterials*. 2014;35:7146-56.
- [60] Zhang P, Huang Y, Kwon YT, Li S. PEGylated Fmoc-amino acid conjugates as effective nanocarriers for improved drug delivery. *Molecular pharmaceutics*. 2015;12:1680-90.
- [61] Zhang P, Li J, Ghazwani M, Zhao W, Huang Y, Zhang X, et al. Effective co-delivery of doxorubicin and dasatinib using a PEG-Fmoc nanocarrier for combination cancer chemotherapy. *Biomaterials*. 2015;67:104-14.
- [62] Serajuddin AT. Salt formation to improve drug solubility. *Advanced drug delivery reviews*. 2007;59:603-16.

- [63] Matsumura Y. Poly (amino acid) micelle nanocarriers in preclinical and clinical studies. *Advanced drug delivery reviews*. 2008;60:899-914.
- [64] Gaucher G, Dufresne MH, Sant VP, Kang N, Maysinger D, Leroux JC. Block copolymer micelles: preparation, characterization and application in drug delivery. *Journal of controlled release*. 2005;109:169-88.
- [65] Mi Y, Liu Y, Feng SS. Formulation of Docetaxel by folic acid-conjugated d-alpha-tocopheryl polyethylene glycol succinate 2000 (Vitamin E TPGS(2k)) micelles for targeted and synergistic chemotherapy. *Biomaterials*. 2011;32:4058-66.
- [66] Zhang Z, Tan S, Feng SS. Vitamin E TPGS as a molecular biomaterial for drug delivery. *Biomaterials*. 2012;33:4889-906.
- [67] Lu J, Huang Y, Zhao W, Marquez RT, Meng X, Li J, et al. PEG-derivatized embelin as a nanomicellar carrier for delivery of paclitaxel to breast and prostate cancers. *Biomaterials*. 2013;34:1591-600.
- [68] Zhang X, Lu J, Huang Y, Zhao W, Chen Y, Li J, et al. PEG-farnesylthiosalicylate conjugate as a nanomicellar carrier for delivery of paclitaxel. *Bioconjugate chemistry*. 2013;24:464-72.
- [69] Kang N, Leroux JC. Triblock and star-block copolymers of N-(2-hydroxypropyl)methacrylamide or N-vinyl-2-pyrrolidone and D,L-lactide: synthesis and self-assembling properties in water. *Polymer*. 2004;45:8967-80.
- [70] Lavasanifar A, Samuel J, Kwon GS. The effect of alkyl core structure on micellar properties of poly(ethylene oxide)-block-poly(L-aspartamide) derivatives. *Colloid Surface B*. 2001;22:115-26.
- [71] Kwon G, Naito M, Yokoyama M, Okano T, Sakurai Y, Kataoka K. Micelles based on ab block copolymers of poly(ethylene oxide) and poly(beta-benzyl L-aspartate). *Langmuir*. 1993;9:945-9.
- [72] Shirai K, Matsuoka M, Fukunishi K. Fluorescence quenching by intermolecular pi-pi interactions of 2,5-bis(N,N-dialkylamino)-3,6-dicyanopyrazines. *Dyes pigments*. 1999;42:95-101.
- [73] Zhou M, Smith AM, Das AK, Hodson NW, Collins RF, Ulijn RV, et al. Self-assembled peptide-based hydrogels as scaffolds for anchorage-dependent cells. *Biomaterials*. 2009;30:2523-30.
- [74] Geng Y, Dalhaimer P, Cai S, Tsai R, Tewari M, Minko T, et al. Shape effects of filaments versus spherical particles in flow and drug delivery. *Nature nanotechnology*. 2007;2:249-55.
- [75] Goldspiel BR. Clinical overview of the taxanes. *Pharmacotherapy*. 1997;17:S110-S25.

- [76] Rowinsky EK, Cazenave LA, Donehower RC. Taxol: a novel investigational antimicrotubule agent. *Journal of the National Cancer Institute*. 1990;82:1247-59.
- [77] Spencer CM, Faulds D. Paclitaxel. A review of its pharmacodynamic and pharmacokinetic properties and therapeutic potential in the treatment of cancer. *Drugs*. 1994;48:794-847.
- [78] Sollott SJ, Cheng L, Pauly RR, Jenkins GM, Monticone RE, Kuzuya M, et al. Taxol inhibits neointimal smooth muscle cell accumulation after angioplasty in the rat. *The Journal of clinical investigation*. 1995;95:1869-76.
- [79] Gelderblom H, Verweij J, Nooter K, Sparreboom A. Cremophor EL: the drawbacks and advantages of vehicle selection for drug formulation. *European journal of cancer*. 2001;37:1590-8.
- [80] Weiss RB, Donehower RC, Wiernik PH, Ohnuma T, Gralla RJ, Trump DL, et al. Hypersensitivity reactions from taxol. *Journal of clinical oncology*. 1990;8:1263-8.
- [81] Kloover JS, den Bakker MA, Gelderblom H, van Meerbeeck JP. Fatal outcome of a hypersensitivity reaction to paclitaxel: a critical review of premedication regimens. *British journal of cancer*. 2004;90:304-5.
- [82] Moghimi SM, Hunter AC, Murray JC. Long-circulating and target-specific nanoparticles: theory to practice. *Pharmacological reviews*. 2001;53:283-318.
- [83] Riehemann K, Schneider SW, Luger TA, Godin B, Ferrari M, Fuchs H. Nanomedicine--challenge and perspectives. *Angewandte chemie*. 2009;48:872-97.
- [84] Duncan R. Polymer conjugates as anticancer nanomedicines. *Nature reviews cancer*. 2006;6:688-701.
- [85] Torchilin VP. Recent advances with liposomes as pharmaceutical carriers. *Nature reviews drug discov*. 2005;4:145-60.
- [86] Huh KM, Lee SC, Cho YW, Lee J, Jeong JH, Park K. Hydrotropic polymer micelle system for delivery of paclitaxel. *Journal of controlled release*. 2005;101:59-68.
- [87] Zhang Y, Gu H, Yang Z, Xu B. Supramolecular hydrogels respond to ligand-receptor interaction. *Journal of the American Chemical Society*. 2003;125:13680-1.
- [88] Castelletto V, Moulton CM, Cheng G, Hamley IW, Hicks MR, Rodger A, et al. Self-assembly of Fmoc-tetrapeptides based on the RGDS cell adhesion motif. *Soft matter*. 2011;7:11405-15.
- [89] Jayawarna V, Ali M, Jowitt TA, Miller AE, Saiani A, Gough JE, et al. Nanostructured hydrogels for three-dimensional cell culture through self-assembly of fluorenylmethoxycarbonyl-dipeptides. *Advanced materials*. 2006;18:611-+.

- [90] Rowinsky EK, Donehower RC. Drug-Therapy - Paclitaxel (Taxol). *New England journal of medicine*. 1995;332:1004-14.
- [91] Singla AK, Garg A, Aggarwal D. Paclitaxel and its formulations. *International journal of pharmaceutics*. 2002;235:179-92.
- [92] Vasir JK, Labhasetwar V. Biodegradable nanoparticles for cytosolic delivery of therapeutics. *Advanced drug delivery reviews*. 2007;59:718-28.
- [93] Bareford LM, Swaan PW. Endocytic mechanisms for targeted drug delivery. *Advanced drug delivery reviews*. 2007;59:748-58.
- [94] Sahay G, Alakhova DY, Kabanov AV. Endocytosis of nanomedicines. *Journal of controlled release*. 2010;145:182-95.
- [95] Bertrand N, Leroux JC. The journey of a drug-carrier in the body: an anatomo-physiological perspective. *Journal of controlled release*. 2012;161:152-63.
- [96] Torchilin VP. Multifunctional nanocarriers. *Advanced drug delivery reviews*. 2006;58:1532-55.
- [97] Davis ME, Chen ZG, Shin DM. Nanoparticle therapeutics: an emerging treatment modality for cancer. *Nature review drug discovery*. 2008;7:771-82.
- [98] Krishnamurthy S, Ng VW, Gao S, Tan MH, Yang YY. Phenformin-loaded polymeric micelles for targeting both cancer cells and cancer stem cells in vitro and in vivo. *Biomaterials*. 2014;35:9177-86.
- [99] Wu H, Zhu L, Torchilin VP. pH-sensitive poly(histidine)-PEG/DSPE-PEG co-polymer micelles for cytosolic drug delivery. *Biomaterials*. 2013;34:1213-22.
- [100] Shao Y, Shi C, Xu G, Guo D, Luo J. Photo and redox dual responsive reversibly cross-linked nanocarrier for efficient tumor-targeted drug delivery. *ACS applied materials & interfaces*. 2014;6:10381-92.
- [101] Zhang C, Jin S, Li S, Xue X, Liu J, Huang Y, et al. Imaging intracellular anticancer drug delivery by self-assembly micelles with aggregation-induced emission (AIE micelles). *ACS applied materials & interfaces*. 2014;6:5212-20.
- [102] Nasongkla N, Bey E, Ren J, Ai H, Khemtong C, Guthi JS, et al. Multifunctional polymeric micelles as cancer-targeted, MRI-ultrasensitive drug delivery systems. *Nano letters*. 2006;6:2427-30.

- [103] Saravanakumar G, Choi KY, Yoon HY, Kim K, Park JH, Kwon IC, et al. Hydrotropic hyaluronic acid conjugates: Synthesis, characterization, and implications as a carrier of paclitaxel. *International journal of pharmaceutics*. 2010;394:154-61.
- [104] Zhang Y, Huang Y, Zhao W, Lu J, Zhang P, Zhang X, et al. Fmoc-conjugated PEG-vitamin E micelles for tumor-targeted delivery of paclitaxel: enhanced drug-carrier interaction and loading capacity. *The AAPS journal*. 2014.
- [105] Aditya NP, Shim M, Lee I, Lee Y, Im MH, Ko S. Curcumin and genistein coloaded nanostructured lipid carriers: in vitro digestion and antiprostata cancer activity. *Journal of agricultural and food chemistry*. 2013;61:1878-83.
- [106] Avaji PG, Jadhav VB, Cui JX, Jun YJ, Lee HJ, Sohn YS. Synthesis and physicochemical properties of new tripodal amphiphiles bearing fatty acids as a hydrophobic group. *Bioorganic & medicinal chemistry letters*. 2013;23:1763-7.
- [107] Vyas DM, Wong H, Crosswell AR, Casazza AM, Knipe JO, Mamber SW, et al. Synthesis and antitumor evaluation of water-soluble taxol phosphates. *Bioorganic & medicinal chemistry letters*. 1993;3:1357-60.
- [108] Shah JC, Chen JR, Chow D. Preformulation study of etoposide: identification of physicochemical characteristics responsible for the low and erratic oral bioavailability of etoposide. *Pharmaceutical research*. 1989;6:408-12.
- [109] Alvarez Nunez FA, Yalkowsky SH. Correlation between log P and ClogP for some steroids. *Journal of pharmaceutical sciences*. 1997;86:1187-9.
- [110] Nandi I, Bateson M, Bari M, Joshi HN. Synergistic effect of PEG-400 and cyclodextrin to enhance solubility of progesterone. *AAPS PharmSciTech*. 2003;4:E1.
- [111] Novalbos J, Abad-Santos F, Zapater P, Cano-Abad MF, Moradiellos J, Sanchez-Garcia P, et al. Effects of dotarizine and flunarizine on chromaffin cell viability and cytosolic Ca²⁺. *European journal of pharmacology*. 1999;366:309-17.
- [112] Yang W, de Villiers MM. The solubilization of the poorly water soluble drug nifedipine by water soluble 4-sulphonic calix[n]arenes. *European journal of pharmaceutics and biopharmaceutics*. 2004;58:629-36.
- [113] Mithani SD, Bakatselou V, TenHoor CN, Dressman JB. Estimation of the increase in solubility of drugs as a function of bile salt concentration. *Pharmaceutical research*. 1996;13:163-7.
- [114] Gramatte T. Griseofulvin absorption from different sites in the human small intestine. *Biopharmaceutics & drug disposition*. 1994;15:747-59.

- [115] Peng B, Lloyd P, Schran H. Clinical pharmacokinetics of imatinib. *Clinical pharmacokinetics*. 2005;44:879-94.
- [116] Greco F, Vicent MJ. Combination therapy: opportunities and challenges for polymer-drug conjugates as anticancer nanomedicines. *Advanced drug delivery reviews*. 2009;61:1203-13.
- [117] Broxterman HJ, Georgopapadakou NH. Anticancer therapeutics: "Addictive" targets, multi-targeted drugs, new drug combinations. *Drug resistance updates: reviews and commentaries in antimicrobial and anticancer chemotherapy*. 2005;8:183-97.
- [118] Al-Lazikani B, Banerji U, Workman P. Combinatorial drug therapy for cancer in the post-genomic era. *Nature biotechnology*. 2012;30:679-92.
- [119] Jhaveri A, Deshpande P, Torchilin V. Stimuli-sensitive nanopreparations for combination cancer therapy. *Journal of controlled release*. 2014;190:352-70.
- [120] Momparler RL, Karon M, Siegel SE, Avila F. Effect of adriamycin on DNA, RNA, and protein synthesis in cell-free systems and intact cells. *Cancer research*. 1976;36:2891-5.
- [121] Tacar O, Sriamornsak P, Dass CR. Doxorubicin: an update on anticancer molecular action, toxicity and novel drug delivery systems. *The Journal of pharmacy and pharmacology*. 2013;65:157-70.
- [122] Pommier Y, Leo E, Zhang H, Marchand C. DNA topoisomerases and their poisoning by anticancer and antibacterial drugs. *Chemistry & biology*. 2010;17:421-33.
- [123] Hortobagyi GN, Gutterman JU, Blumenschein GR, Tashima CK, Burgess MA, Einhorn L, et al. Combination chemoimmunotherapy of metastatic breast cancer with 5-fluorouracil, adriamycin, cyclophosphamide, and BCG. *Cancer*. 1979;44:1955-62.
- [124] Nabholz JM, Mackey JR, Smylie M, Paterson A, Noel DR, Al-Tweigeri T, et al. Phase II study of docetaxel, doxorubicin, and cyclophosphamide as first-line chemotherapy for metastatic breast cancer. *Journal of clinical oncology*. 2001;19:314-21.
- [125] Santoro A, Bonadonna G, Valagussa P, Zucali R, Viviani S, Villani F, et al. Long-term results of combined chemotherapy-radiotherapy approach in Hodgkin's disease: superiority of ABVD plus radiotherapy versus MOPP plus radiotherapy. *Journal of clinical oncology*. 1987;5:27-37.
- [126] Pichot CS, Hartig SM, Xia L, Arvanitis C, Monisvais D, Lee FY, et al. Dasatinib synergizes with doxorubicin to block growth, migration, and invasion of breast cancer cells. *British journal of cancer*. 2009;101:38-47.
- [127] Lombardo LJ, Lee FY, Chen P, Norris D, Barrish JC, Behnia K, et al. Discovery of N-(2-chloro-6-methyl-phenyl)-2-(6-(4-(2-hydroxyethyl)-piperazin-1-yl)-2-methylpyrimidin-4-

- ylamino)thiazole-5-carboxamide (BMS-354825), a dual Src/Abl kinase inhibitor with potent antitumor activity in preclinical assays. *Journal of medicinal chemistry*. 2004;47:6658-61.
- [128] Nautiyal J, Majumder P, Patel BB, Lee FY, Majumdar AP. Src inhibitor dasatinib inhibits growth of breast cancer cells by modulating EGFR signaling. *Cancer letters*. 2009;283:143-51.
- [129] Araujo J, Logothetis C. Dasatinib: a potent SRC inhibitor in clinical development for the treatment of solid tumors. *Cancer treatment reviews*. 2010;36:492-500.
- [130] Shor AC, Keschman EA, Lee FY, Muro-Cacho C, Letson GD, Trent JC, et al. Dasatinib inhibits migration and invasion in diverse human sarcoma cell lines and induces apoptosis in bone sarcoma cells dependent on SRC kinase for survival. *Cancer research*. 2007;67:2800-8.
- [131] Dos Santos C, McDonald T, Ho YW, Liu H, Lin A, Forman SJ, et al. The Src and c-Kit kinase inhibitor dasatinib enhances p53-mediated targeting of human acute myeloid leukemia stem cells by chemotherapeutic agents. *Blood*. 2013;122:1900-13.
- [132] Schittenhelm MM, Shiraga S, Schroeder A, Corbin AS, Griffith D, Lee FY, et al. Dasatinib (BMS-354825), a dual SRC/ABL kinase inhibitor, inhibits the kinase activity of wild-type, juxtamembrane, and activation loop mutant KIT isoforms associated with human malignancies. *Cancer research*. 2006;66:473-81.
- [133] Hu CM, Aryal S, Zhang L. Nanoparticle-assisted combination therapies for effective cancer treatment. *Therapeutic delivery*. 2010;1:323-34.
- [134] Croy SR, Kwon GS. Polymeric micelles for drug delivery. *Current pharmaceutical design*. 2006;12:4669-84.
- [135] Zhang X, Huang Y, Zhao W, Liu H, Marquez R, Lu J, et al. Targeted delivery of anticancer agents via a dual function nanocarrier with an interfacial drug-interactive motif. *Biomacromolecules*. 2014;15:4326-35.
- [136] Pack DW, Hoffman AS, Pun S, Stayton PS. Design and development of polymers for gene delivery. *Nature review drug discovery*. 2005;4:581-93.
- [137] Behr JP. The proton sponge: A trick to enter cells the viruses did not exploit. *Chimia*. 1997;51:34-6.
- [138] Zhao X, Chen Q, Liu W, Li Y, Tang H, Liu X, et al. Codelivery of doxorubicin and curcumin with lipid nanoparticles results in improved efficacy of chemotherapy in liver cancer. *International journal of nanomedicine*. 2015;10:257-70.

- [139] Liu Y, Fang J, Kim YJ, Wong MK, Wang P. Codelivery of doxorubicin and paclitaxel by cross-linked multilamellar liposome enables synergistic antitumor activity. *Molecular pharmaceutics*. 2014;11:1651-61.
- [140] Lv S, Tang Z, Li M, Lin J, Song W, Liu H, et al. Co-delivery of doxorubicin and paclitaxel by PEG-polypeptide nanovehicle for the treatment of non-small cell lung cancer. *Biomaterials*. 2014;35:6118-29.
- [141] Ke XY, Lin Ng VW, Gao SJ, Tong YW, Hedrick JL, Yang YY. Co-delivery of thioridazine and doxorubicin using polymeric micelles for targeting both cancer cells and cancer stem cells. *Biomaterials*. 2014;35:1096-108.
- [142] Wang H, Zhao Y, Wu Y, Hu YL, Nan K, Nie G, et al. Enhanced anti-tumor efficacy by co-delivery of doxorubicin and paclitaxel with amphiphilic methoxy PEG-PLGA copolymer nanoparticles. *Biomaterials*. 2011;32:8281-90.